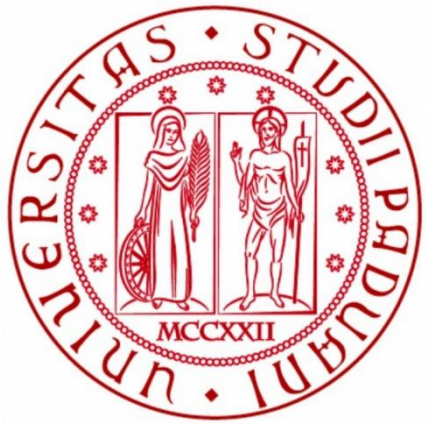

Ciemat
Centro de Investigaciones
Energéticas, Medioambientales
y Tecnológicas

UNIVERSITÀ DEGLI STUDI DI PADOVA

Department of Industrial Engineering

Master Degree in Energy Engineering

Reduction of power oscillations in Wave Energy Converters using prediction techniques based on Autoregressive Models

Supervisor at UNIPD: Anna Stoppato

Supervisor at CIEMAT: Marcos Lafoz

Co-Supervisor at CIEMAT: Pablo Moreno-Torres

Majoring: Michele Pasquotto

1061588

Academic Year 2015/2016

Preface

This master thesis is the result of my experience of five months at the Spanish research center CIEMAT (Centro de Investigaciones Energéticas, Medioambientales y Tecnológicas), in Madrid, Spain.

First of all, I would like to thank my supervisor Anna Stoppato, without whom I wouldn’t have had this precious opportunity.

A special thanks goes to Marcos Lafoz, who accepted immediately to host me at the CIEMAT and gave me an incredible support during my time there, not only educational but also human, and I really appreciated it.

I want to say thank also to Pablo for his essential help, his patience, and for the courage and the precious advices that he gave me in the most difficult moments of this work.

Finally, a big thanks goes to all the other guys of the CIEMAT research group (Gus, Marquitos, Mariano, Jorge, Jesus, Carlos) and all the people working there, they all welcomed me and made me feel home.

Michele

Abstract

One of the main issues of wave energy nowadays is the oscillation of the generated power, which is due to the oscillating nature of the waves. These power fluctuations may have an important undesired impact on the electrical grid. In order to compensate the power oscillations, the research group of CIEMAT proposed a Power Smoothing System (PSS) consisting in the use of a supercapacitor-based energy storage. The control system of this PSS works with real time measurements, which means that it doesn't see the oscillations until they are effectively happening. The aim of this thesis is to improve the operation of the whole system by adding a short-term prediction block to the control, so that it knows in advance when a power fluctuation is coming.

For this purpose, autoregressive (AR) models have been studied, and a consistent part of the thesis is dedicated to the attempt to predict the power generated by a wave energy converter using AR models, especially in the case of real irregular waves. Afterwards, the obtained prediction is integrated in the control of the aforementioned power smoothing system. To evaluate the functioning of the system, simulations with the software Matlab-Simulink have been carried out. In addition, a laboratory test bench has been used to emulate wave power oscillations and to test the proposed PSS. The document includes the experimental results, that are analyzed and compared with the results obtained in the simulations.

Contents

1 - INTRODUCTION

During the last decades, due to the increase in fossil fuel prices and to the environmental problems caused by the use of conventional fuels, a new and strong drive for many forms of renewable energy sources has been experienced. One of the big issues of most of the renewable energies is their high variability together with the lack of predictability. In the particular case of wave energy this variability, represented by the oscillating nature of the waves, leads to the oscillation of the generated power. These power fluctuations may have an important undesired impact on the electrical grid, such as instability problems and frequency and voltage deviations.

The research group of CIEMAT has already developed a system which improves the quality of the power injected to the grid from a single Wave Energy Converter (WEC) or from a whole wave farm. This system uses a supercapacitor-based energy storage to smooth the power generated by the WEC, so that the power injected into the grid presents much smaller oscillations. The system performs correctly, but the aim of the work presented in this document is to improve it. At the moment the control system works with real-time measurements, which means that it doesn't see the oscillations until they are effectively happening. The idea here is to add a prediction block to the control system so that it knows in advance when a power oscillation is coming. The above mentioned prediction is supposed to be a short-term prediction, around 15-20 seconds at least. More specifically, the prediction tool implemented in the work consists mainly of autoregressive (AR) models.

The first part of the document will be an introduction to the wave energy production, with a presentation of the main technologies, their development and the future perspectives of this source of renewable energy. The intent of this first part is to become a little more familiar with the topic of wave energy, which will be the base of the work.

After that, a more detailed explanation of the problem of the oscillation of power will be made, and the already discussed solution proposed by CIEMAT will be presented, consisting in the use of energy storage to smooth the power and a

control system based on a MA (Moving Average) criteria. Then the central part of the work will begin, with all the focus put on AR models. The theoretical and the mathematical concepts behind AR models will be first analyzed, and then applied to a real case of a sea wave in a specific location, with the attempt to make a short-term prediction of its height and of the power generated by the WEC. This prediction work will be carried out with the use of the software Matlab, and the codes written are collected in the appendix B at the end of the paper.

The next step will be the implementation of the AR power prediction tool in a simulation model which contains a single WEC, a power smoothing system and a grid connection. All the simulations will be done with the software Simulink, integrated with Matlab. The simulations will be made both with a Moving Average (MA) control system and with a predictive control system, and the results of the two cases will be compared.

The last part of the work consists in the implementation of the prediction tool in a laboratory test bench already built and specifically assembled for this project. Different tests will be made and presented, both with a MA and an autoregressive prediction criteria, and the results will be analyzed and compared with the results obtained by the simulations carried out with Simulink. After the analysis of the results, some conclusions will be drawn, together with some ideas and possibilities of future development.

2 - WAVE ENERGY

2.1 – Energy in the oceans

Oceans and seas cover approximately the 72 % of the Earth's surface, carrying with themselves a huge amount of energy. This energy can be considered free and inexhaustible, and this is why ocean energy is classified as a renewable source. There are many different ways to use and convert this energy, which can be classified into five main technologies [1].

Wave energy: it's the kinetic energy transported by the wind waves, which is converted into electric power through some devices generally known as Wave Energy Converters (WECs). These devices are usually floating on the ocean surface or moored to the sea bottom, and present a wide variety of techniques to generate electricity, which will be discussed and analyzed later.

Tidal stream: the marine current, which is basically ocean water moving in one direction, carries a certain amount of kinetic energy, which can be converted once again into electricity through submerged turbines. Although not widely used at present, marine current power has an important potential in regions with strong and powerful ocean currents, like the Gulf Stream which is mainly found off the coast of Florida.

Tidal energy: the gravitational force of the moon causes a tidal cycle of approximately 12 hours, in which there's an alternation of low tide and high tide states of the sea. The difference in height between low and high tide is potential energy which, with the same principles as conventional hydropower, can be used to generate electric power. The water can be stored with a barrier during high tide, and then forced through a hydro-turbine during low tide. To capture enough potential power the height of the high tide must be at least five meters more than the low one [2], and there are only twenty locations on our planet which satisfy this condition.

Ocean Thermal Energy Conversion (OTEC): exploits the temperature difference between the warm shallow water and the deep cold ocean water in order to produce electric power. There are two main OTEC technologies being investigated and developed [2], both consisting basically in a Rankine cycle but with some differences:

- Closed cycle: a working fluid is pumped through a heat exchanger where it evaporates, and then runs a turbine. To close the cycle, the steam is refrigerated and condensed again into a fluid form by releasing heat to the cold deep ocean water. The fluid is then ready to pass again in the heat exchanger, restarting the cycle.
- Open cycle: the main difference is that in this case the working fluid is the ocean water itself. The warm water from the surface is pressurized in a vacuum chamber and vaporized to run the turbine. Then again the steam is condensed using cold water from the depths of the ocean.

Salinity gradient power generation: uses the difference in salt concentration between the sea saltwater and freshwater which comes from the rivers to produce electricity through different osmotic processes. This technology could be applied in areas as deltas or fjords, where both salty and fresh water can be found.

All these technologies are still in a research or early commercial stage, but the energetic potential is absolutely significant. According to [3], there is a global potential to reach a value of 80,000 TWh of electric energy generated in one year with the combination of the technologies presented. More specifically, the generation potential of marine energy is shown in the table 2.1.
Ocean energy's first deployment in Europe was in 1966 when a 240 MW tidal range project was built in La Rance, France. For three decades there was little deployment of ocean energy technologies until 1999, when a wave energy device was tested in Portugal. By mid-2015, 11 MW of tidal stream and 8 MW of wave energy had been deployed, bringing cumulative deployed capacity in Europe to 261 MW. [1]

Form	Annual generation potential (TWh/year)
Tidal energy	>300
Tidal stream (current power)	>800
Salinity gradient	2,000
OTEC	10,000
Wave energy	80,000

Table 2.1 – Estimation of annual electric generation potential of ocean energy resources [3]

As can be seen in table 2.1, the most promising form of ocean energy is wave energy, which will be the one investigated in the work presented in this dissertation. Therefore, no more focus will be put on the other possibilities just discussed.

2.2 – Wave Energy

Waves are formed by winds blowing over water, and will occur only in water near the sea surface. The size of the waves generated will depend upon the wind speed, its duration, and the fetch, that is distance of water over which it blows. The resultant movement of water carries kinetic energy which can be harnessed by wave energy devices. The main physical parameters describing waves are height and the period (or the wavelength).

Once created, these waves can travel thousands of kilometers with little energy loss, a property that makes them very interesting from an energetic point of view. Moreover, the power density of waves is in the order of 40 kW/m^2, about 10 times higher than wind energy and 100 times higher than solar radiation [4].

The common measure for wave power levels is the average annual power per meter of wave crest width parallel to the shoreline. The crest length is measured

from one crest to the next. Like most forms of renewable energy sources, wave energy is distributed unevenly around the world, as can be seen in figure 2.1.

Figure 2.1 – Distribution of Wave Energy levels in KW/m of crest length [2]

The best wave resources occur in areas where strong winds have travelled over long distances. Increased wave activity is found between the latitudes of approximately 30° and 60° in both the hemispheres [5], induced by the prevailing western winds blowing in these regions. For these reasons the countries best suited for wave energy conversion are Great Britain, Ireland, Norway, New Zealand, Southern Australia, Chile, followed by Northern Spain, France, Portugal, North and South American coasts and South Africa. The annual average power level is useful to compare the potential of different regions, but can be misleading if not interpreted together with the seasonal variability, which can be very high.

2.3 – History and development of wave energy

The interest in extracting energy from the ocean waves began in the 18th century, when the French Girard received the first recorded patent for wave energy conversion (1799) [6]. Together with his son, Monsieur Girard designed a device consisting of a ship attached to shore with waves driving pumps, saws and other

machineries. Between 1800 and the 1960s only occasional attempts to harness the ocean's energy were made. For example, around 1910 Bochaux-Praceique constructed a wave power based device to light and power his house at Royan, near Bordeaux. This machine is considered the first oscillating water column type of wave energy device.

The oil crises of 1973 led to a new interest in wave energy and in other types of renewable energies as well. A wide variety of wave energy devices were proposed and developed at this time, but the success was in general far below the expectations. In many cases the destructive forces of the ocean waves were largely underestimated, and the first devices did not show satisfactory results. As a consequence, when the oil crises came to an end the interest in wave energy decreased and in the early 1980s many of the trials were already interrupted.

A revival in the interest and research about wave energy started again in 2000, due to the increase in oil prices and to the new drive for renewable energies. Since then, a big amount of devices have been developed and many projects have been carried out all around the world. In the following section the main modern technologies in this field will be presented.

2.4 – Wave Energy Converters

A great variety of different conversion techniques have been developed so far, which can be classified according to their location and to the method used to capture wave power [7].

2.4.1 – Classification by location

According to the characteristics of their deployment sites, WECs can be divided into shoreline (or coastal), near-shore and offshore devices. The physical conditions relevant for wave energy conversion are different according to the water depth and distance from shore.

Offshore devices: They are generally located in deep water, although there are different definitions of what constitutes ‘deep’ water. Typical water depths for offshore technologies are in the range of 50 m [4]. In such deep water waves travel almost without energy losses, which is why offshore devices are expected to have the largest potential for large-scale implementation. On the other side, offshore WECs are more difficult to construct and maintain, and because of the greater wave height and energy content in the waves, need to be designed to survive to more extreme conditions, adding cost to construction.

Near-shore devices: They are located in relatively shallow water. In these conditions, the waves suffer increasingly from bottom friction, making such sites less interesting from an energetic point of view. The advantage of near-shore WECs is that as they are closer to shore, mooring and grid connection costs decrease, and often it is also possible to attach these devices directly to the seabed.

Shoreline devices: They are typically integrated in the shoreline or into an artificial coastal structure. Shoreline WECs have the advantage of being close to the utility network, are easy to maintain and have a reduced likelihood of being damaged. The main disadvantage is that shallow water leads to significantly lower incident power levels. In addition, by nature of their location, there are often site-specific requirements and characteristics that need to be taken into account, including shoreline geometry and geology and preservation of coastal scenery, so that shoreline devices can’t be designed for mass manufacturing [7].

2.4.2 – Classification by type

Despite the large variations in design and concepts, WECs can be classified in 6 main different technologies.

Attenuator: This device consists of multiple floating segments which lie parallel to the predominant wave direction (perpendicular to the wave front). The attenuator effectively rides the waves and captures the energy as the waves move past by selectively constraining the movement along its length.

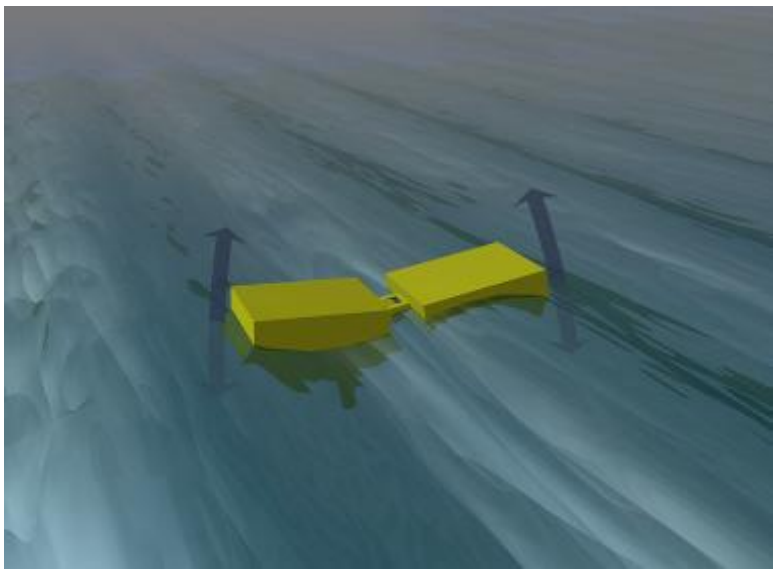

Figure 2.2 – Example of an Attenuator WEC [4]

An example of attenuator is the Pelamis Wave Energy Converter, which so far is one of the most successful WEC technology, represented in figure 2.3.

Figure 2.3 – Pelamis Wave Farm [7]

Point absorber: A point absorber is a device that has small dimensions relative to the incident wavelength. It can be a floating structure that heave up and down on the surface of the water or submerged below the surface relying on pressure

differential. Because of their small size, wave direction is not important for this kind of WECs. Typically, but not necessarily, these devices are axisymmetric.

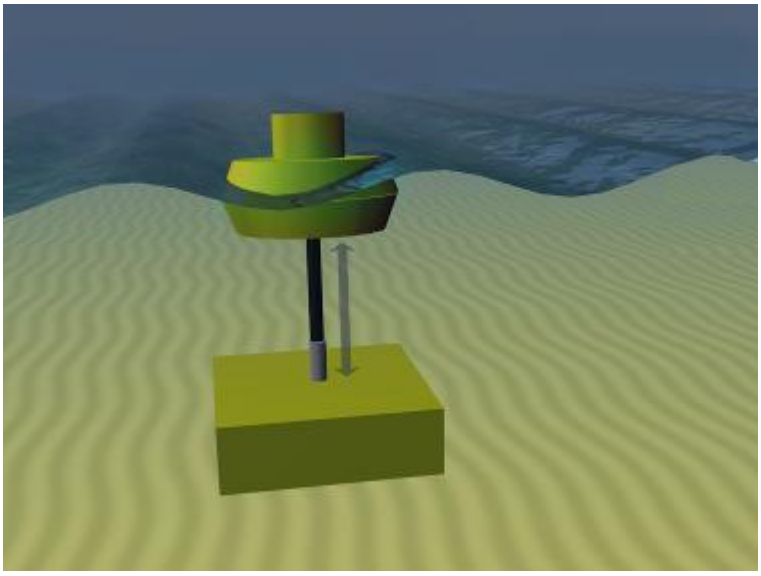

Figure 2.4 – Example of Point Absorber [4]

Oscillating Wave Surge Converter (OWSC): These devices typically have one end fixed to a structure or the seabed while the other end is free to move near the surface. The arm that connects the two parts oscillates as an inverted pendulum due to the movement of the water particles in the waves.

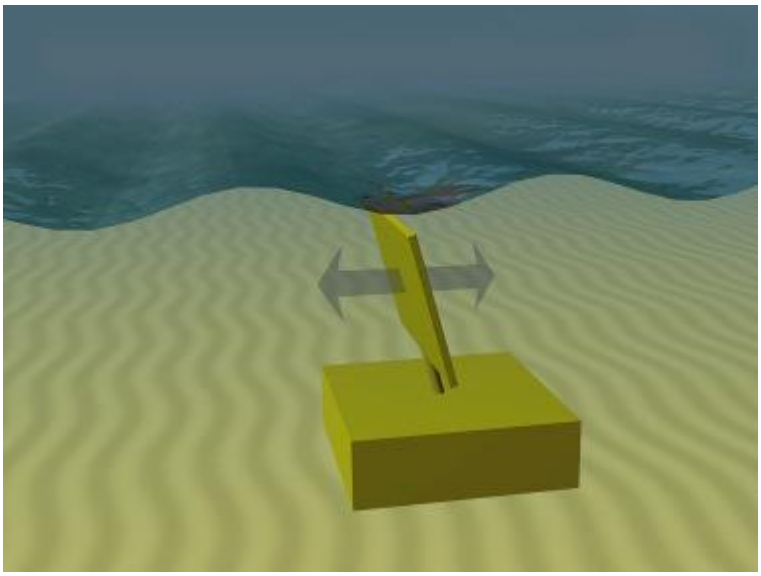

Figure 2.5 – Example of Oscillating Wave Surge Converter [4]

Oscillating Water Column (OWC): These devices can be located on shore or in deeper water offshore. They consist of a partially submerged structure which is

open to the sea below the water surface, so that it contains air trapped in a chamber above a column of water. Waves cause the column to rise and fall, acting like a piston, compressing and decompressing the air, which when compressed is forced through an air turbine to produce electricity.

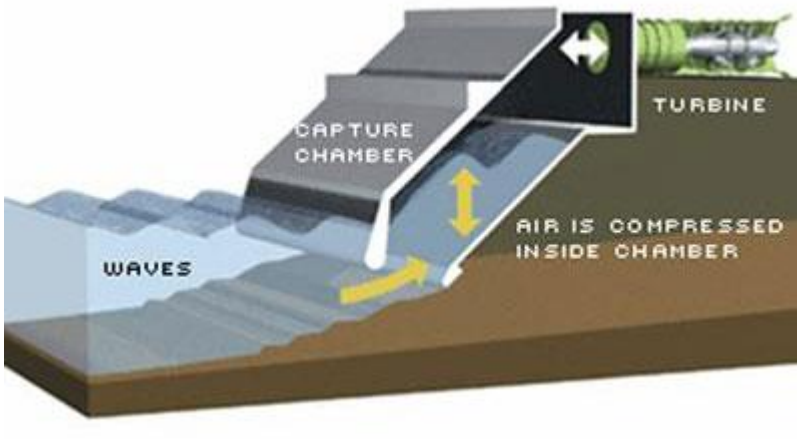

Figure 2.6 – Example and operating principle of an Oscillating Water Column device

Overtopping device: An overtopping device captures sea water of incident waves in a reservoir above the sea level, then releases the water back to sea through turbines. Overtopping devices are typically large structures due to the space requirement for the reservoir, which needs to have a minimum storage capacity. They can be located either on shore or floating offshore.

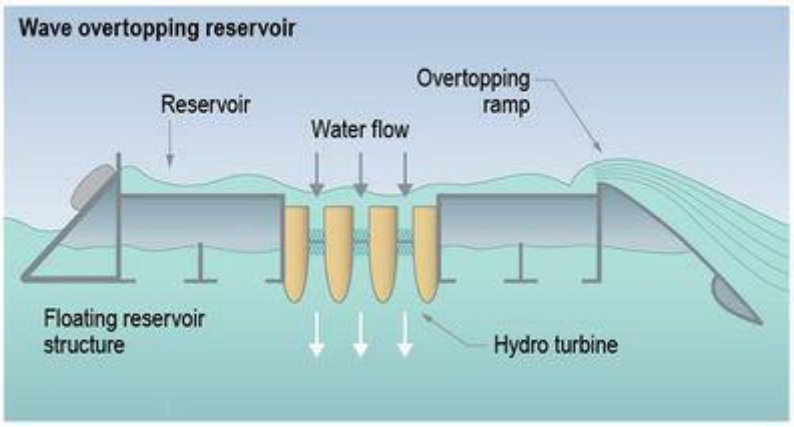

Figure 2.7 – Example of Overtopping Device

Submerged Pressure Differential: This is a submerged device typically located near shore and attached to the seabed. The motion of the waves causes the sea level to rise and fall above the device, inducing a pressure differential which

causes the device to rise and fall with the waves. When properly designed for the sea state, this category also has significant point absorbing characteristics.

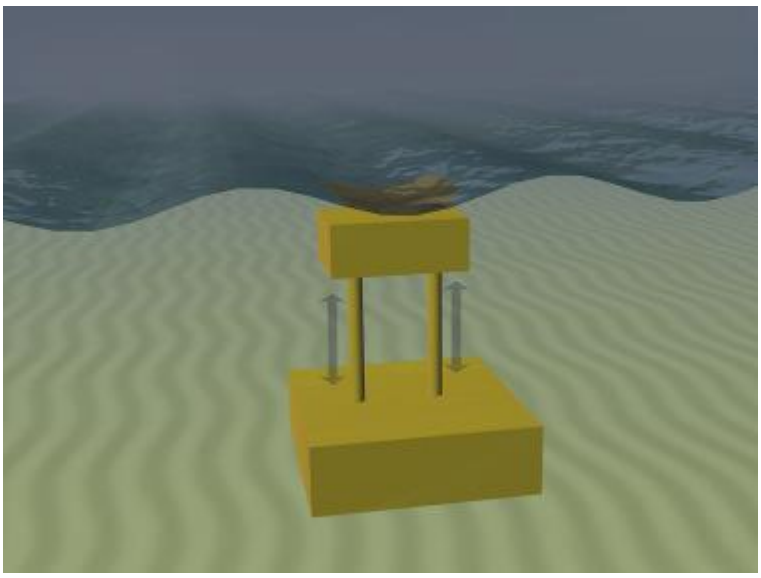

Figure 2.8 – Example of Submerged Pressure Differential device [4]

2.4.3 – Power Take Off Methods

There are a number of different Power Take Off (PTO) systems that can be used to convert wave power into electricity: air or water turbines, hydraulic systems and electrical linear generators. Among the current WECs concepts developed so far, 42% use hydraulic systems, 30% direct-drive systems (mostly linear generators), 11% hydraulic turbines, and 11% air turbines [8].

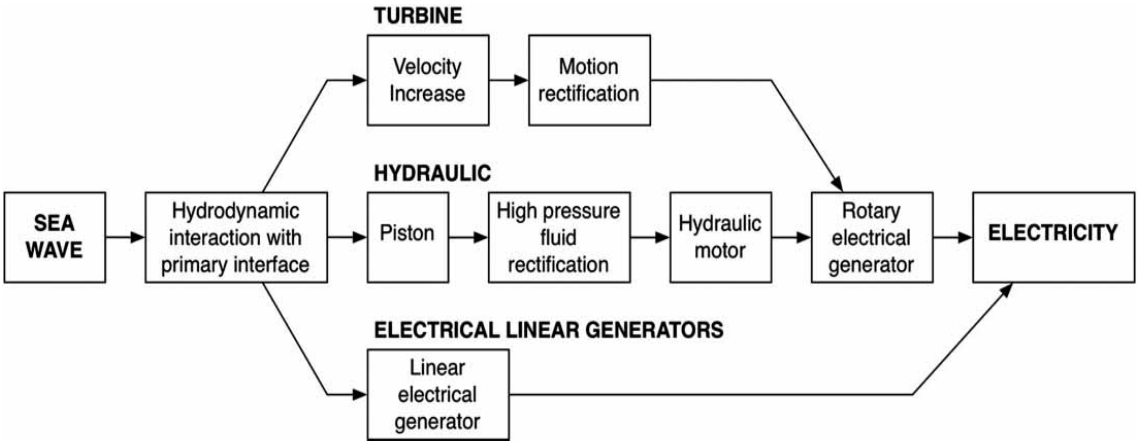

Figure 1.9 – Alternative PTO mechanisms [7]

Air turbine: Using air as the working fluid has the advantage of increasing the slow velocities of waves to high air flow rate. The most popular air turbine design is the Wells turbine, because of its ability to rotate in the same direction, irrespective of airflow direction. Air turbines (also referred as pneumatic systems) are often used in OWC devices. The main disadvantage is the efficiency, which can only reach 50-60% [8].

Water turbine: The significant advantage of using sea water turbines is that leakage of fluid causes no environmental problems. The disadvantage is that sea water is a complex fluid with various unpredictable constituents. The efficiency in this case is higher, values of 70-90% can be reached.

Hydraulic motors/generators: Waves apply large forces at slow speeds and hydraulic systems are well suited to absorb energy in these situations [9]. A simple hydraulic PTO system is shown in figure 2.10. The operating principle is basically that the relative motion of the WEC device caused by waves drives high pressure fluids through the hydraulic motor, mechanically connected to the power generator.

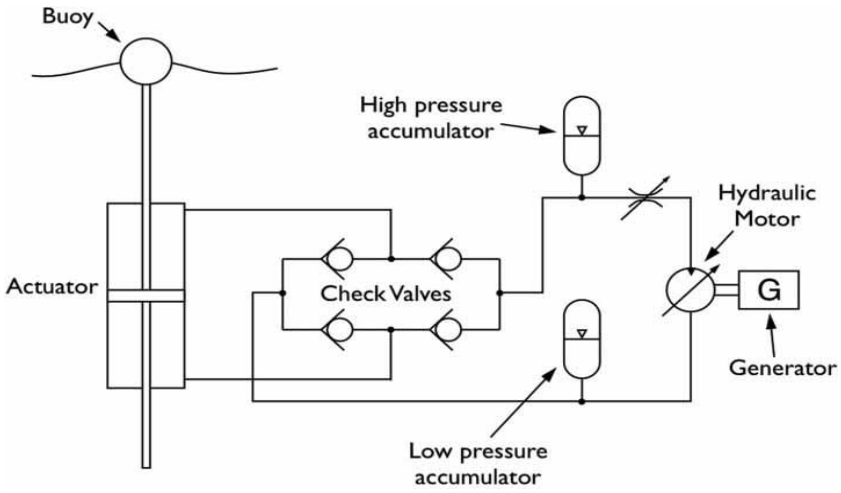

Figure 2.10 – Typical hydraulic circuit for WEC [7]

Electrical linear generator: A linear generator offers the possibility of directly converting mechanical energy into electrical energy, with no intermediate steps. During early wave power research, the possibility of use these generators was investigated but considered too expensive and inefficient. New magnetic materials and the reduced costs of frequency converting electronics mean that this technology may now be feasible.

2.5 – Advantages and disadvantages of using wave energy

When comparing wave energy with other energy sources, in particular with renewable sources as solar and wind energy, there are both advantages and disadvantages to highlight.

Speaking of advantages, the first and probably most relevant one is that ocean waves offer the biggest energy density among renewable energy sources [6]. In addition, waves have a unique feature, that they can travel large distances with little energy losses. Another important characteristic is the natural seasonal variability of wave energy, which follows the electricity demand in temperate climates [6]. It is also reported that wave power devices can generate power up to 90% of the time, which is a lot compared to the approximately 20-40% of wind and solar power devices [10]. Other positive aspects are the small visual impact on the shoreline, the negligible demand on land use [6], and that the environmental impacts, summarized in table 2.2, seem to be limited. The last one is a discussed topic, because even if it is recognized that small-scale wave energy plants are likely to have minimal environmental impacts, on the other side some of the proposed large-scale projects have the potential for harming ocean ecosystems. Therefore, this aspect should not be neglected and it requires a special attention.

Environmental Effects	Shoreline	Nearshore	Offshore
Land use/sterilization	W		
Construction/maintenance sites	W		
Recreation	W	W	
Coastal erosion	W	W–M	W–M
Sedimentary flow patterns		W	W
Navigation hazard		W	W
Fish & marine biota	W	W	W
Acoustic noise	W		
Working fluid losses		W	W
Endangered species	W	W	
Device/mooring damage		W–M	W–M

W: Weak effect; M: Medium effect

Table 2.2 – Summary of environmental impacts of wave energy conversion technologies [11]

Once listed and appreciated all the positive features of wave energy, it's important as well to say something about the disadvantages and difficulties related with wave power development. First of all, the irregularity in wave amplitude, frequency, phase and direction makes it complicated to obtain maximum efficiencies from the WEC devices. Moreover, in case of extreme weather conditions, the structural loading may be up to 100 times higher than the average loading. This is a huge problem, not only technically, but also economically, and it has to be seriously taken into account in the design phase. Another problem is the coupling of the irregular, slow motion (frequency around 0.1 Hz) of a wave to electrical grids, which require typically about 500 times greater frequency (frequency around 50 Hz) [6]. It becomes apparent that the design of a wave energy converter has to be highly sophisticated to be operationally efficient and reliable on the one hand, and economically feasible on the other.

2.6 – Current status and future perspectives of wave energy

As already mentioned in the previous paragraphs, the most energetically promising application for WECs is the offshore. Despite this, almost all the first generation wave energy systems, based on the previously described technologies, have been placed at the shoreline or near shore. The main reason for this is economical, to avoid too high grid connection costs, and also because testing a new technology like this onshore is more safe and reasonable than doing it directly off-shore, at least for the first steps of its development. Although 67% of the current WEC concepts are floating, and only 19% are fixed [8], experience so far has mostly been with:

- OWCs placed on the shoreline, on natural cliffs or breakwaters.
- Near-shore technologies based on bottom fixed solutions, often with terminal absorbers.
- Offshore technologies at specific testing or pilot emplacements.

Since the beginning Europe has been the leading market in the field of wave energy, but also other countries and regions have been making fast progresses

in the last few years. Many research and development programs have been carried out in many countries all around the world, and many others are going to start in the next years. As estimated by some recent reviews [8], in 2013 there were more than a hundred projects at various stages of development. Obviously, the countries that are more active in this field are all located in regions with high wave energy resources, where wave power could cover a significant part of the energy demand in the country and even become a primary source of energy. Countries with moderate, though feasible resources, could utilize wave energy supplementary to other available renewable and/or conventional sources of energy.

The next step for wave energy is to move from full-scale testing of individual technologies to the deployment of array and cost reduction measures. Furthermore, the next generation of WECs are expected to go further offshore, reaching bigger depths and higher waves. At the moment, existing wave test facilities are available for testing up to 5 km offshore, and up to 50 m in depth [8], but test facilities with 100 m water depth and 15 km offshore have already been planned.

In order to reach those targets and to increase the penetration of wave energy technologies in the energy market, there are both technical and economic issues to face. The main technical challenges that need to be overcome and investigated are the following [7]-[8]:

- As wave direction is highly variable, WEC devices have to align themselves accordingly on compliant moorings to be able to capture the energy from the waves.
- There is a need to find new materials to reduce the device's weight and biofouling effects on the marine environment.
- To operate efficiently, the device and corresponding systems have to be rated for the most common wave power levels. Not only does this pose difficult structural engineering challenges, but it also presents one of the economic challenges as the normal output of the device (and hence the revenue) are produced by the most commonly occurring waves, but the capital cost of the device construction is driven by a need to withstand the high power level of the extreme, yet infrequent, waves [12].

- Develop new mooring systems for floating devices adapted to the wave energy needs for increased safety and or better interaction with the converter.
- Design challenge in order to mitigate the highly corrosive environment of devices operating at the water surface [6].
- Underwater power connectors that allow easy underwater operability and quick, easy and low cost maintenance interventions.
- A significant challenge is the conversion of the slow (~0.1 Hz), random, and high-force oscillatory motion into useful motion to drive a generator with output quality acceptable to the utility network. As waves vary in height and period, their respective power levels vary accordingly. This variable input has to be converted into smooth electrical output and hence usually necessitates some type of energy storage system or other means of compensation.

In addition to all these technical challenges, another interesting perspective for offshore wave energy is represented by the new concept of multiplatform or hybrid devices, where wave energy technologies would be integrated or share the same infrastructure as other marine users, wind energy or aquaculture. The biggest advantage of these systems would be the reduced capital and operation costs, since the same structure or part of them would be shared for different technologies.

As seen during this chapter, wave energy technology is still quite immature and there are many technical challenges to overcome in order to make it more attractive for the energy market. Despite the technical problems, the main obstacle to its spread is probably economic, even if in the end the two things are related. The actual estimated operational costs for a wave energy farm of 10 MW are between 330 and 630 €/MWh [8], considerably higher than other forms of renewables, including the expensive offshore wind and tidal current technologies. This is not surprising, as wave technologies are in an earlier stage of development. The latest estimates for European wave energy projects suggest that the PTO system accounts for 22% of the total lifetime project costs, installation 18%, O&M 17%, foundation and mooring 6%, and grid connection 5% [8].

As a matter of fact, a lot of work of Research & Development is still needed to reduce costs and to make the technology safer, more resistant and long-lasting. Given the big potential of wave energy, its costs are expected to significantly fall in the next years. In particular, the costs are expected to be reduced of approximately 70% by 2030, thanks to technologic progress and economies of scale in the sector. This would mean to reach an average cost of around 150-180 €/MWh by 2030.

The current estimated costs for wave energy are illustrated in table 2.3 taken from [8] and showed in the following page, together with the estimated cost projections for the future, up to the year 2050.

	Source	2010-2012	2020	2030	2050
Capital cost of farms [EUR/kW]	IEA	5 650	4 070	3 350	1 750
	UK	5 000-9 000	3 000-5 000		2 500-3 000
	ETI[a]/ UKERC	4 840-9 680	2 723-4 235	2 118-2 723	1 513-2 118
Operation & Maintenance cost [EUR/kW/yr.]	IEA	86 (projected to decrease to 47)			
	ETI/ UKERC	48-97	30-73	18-30	12-24
Availability [%]	UK	75-85		90	90-95
	ETI/ UKERC	70-80	90	90-95	95-98
Array load factor [%]	ETI/ UKERC	25-35	32-40	35-42	37-45
Total electricity production cost [EUR/MWh]	IEA	286	207	172	
	UK	213-500		113-226	88-125
	ETI/ UKERC	242-605	121-242	85-121	61-97
Average levelised cost of energy per MWh	E&Y	505	268	148	108
	SI Ocean	330-630[b]	280-350[c]	150-180[d]	
EU Market share, % of global electricity output	JRC	0	<<1	~1-2	> 10
Emissions (direct operation)	JRC	0			
Emissions indirect (as manufacturing, fabrication, installation, maintenance and commissioning)	JRC	25-50 gram/kWh (wave energy converters of 665 tonnes of steel and production 2.3 gigawatt-hour per year — GWh/yr.)			

Table 2.3 – Current estimated costs and cost projections for wave energy until 2050 [8]

3 – THE PROBLEM OF OSCILLATION OF THE POWER GENERATED BY A WEC

One of the main unsolved issues of wave energy is the oscillation of the generated power (also known as power ripple), which is due to the oscillating nature of the waves [13]. An example of a power profile generated by a wave energy converter (WEC) with a direct drive power take-off (PTO) is shown in figure 3.1 [14], which depicts the instantaneous power generated by a single 1-body point absorber WEC. These fluctuations, whose period usually ranges from 5 to 25 seconds, may have an important undesired impact on the electrical grid, especially in the case of weak grids. In addition, this problem is expected to be more acute once wave energy technologies reach maturity and expand massively. In this chapter the concept of weak grid and the problem of oscillation of power will be analyzed, trying to shed light on the effects on the grid caused by the fluctuations, and a possible solution to the problem will be presented.

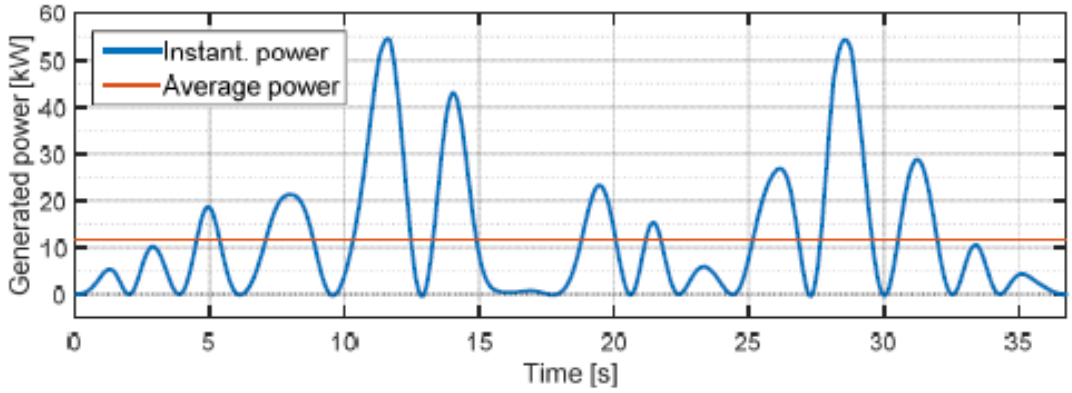

Figure 3.1 - Power generated by a single point absorber WEC under real wave conditions [14]

3.1 – Weak Grids

Weak power grids can be defined as electric grids where the variations in loads or generators produce important variations of the grid parameters such as frequency and voltage. Weak grids can be interconnected to the main grid, but

also isolated power systems with no connection to the main grid are included in the definition.

In general, speaking about renewable energies, the best resources are often located at remote or even isolated regions. This is true also in the particular case of wave energy, as it is quite common to have high wave energy potential in regions with many islands or peninsulas. These kind of locations normally have a weak electric grid in the sense previously defined, and the integration of variable energy sources in such weak grids poses many technical and economical issues. Standard IEEE 1204 [15] defines a weak Alternating Current (AC) electric grid from two aspects, including static and dynamic performance:

- AC system impedance may be high relative to AC power at the point of connection, which means that short-circuit power at the point of connection may be low.
- AC system mechanical inertia may be inadequate relative to the AC power supply.

The first condition is usually full-filled in weak power grids operated at medium voltage levels with long radial feeders and low X/R ratios, where X and R are respectively the reactance and the resistance of the grid. In small isolated power grids, both static and dynamic aspects do often apply. In addition, power is supplied by few generating groups, mostly fed by diesel or heavy oil, with small unit power and low inertia. Overall, generators are large with respect of the system load for economic reasons, thus higher reserve margins than in interconnected systems are necessary.

Another way to evaluate the strength of a grid is through an index called Short-Circuit Ratio (SCR), defined as:

$$SCR = \frac{S_{sc}}{S_n} \quad \textbf{(1)}$$

Where S_n is the installed capacity (in terms of power) of the generation power plant and S_{sc} is the short circuit level at the Point of Common Coupling (PCC), that is defined as the interface between sources and loads on an electrical system. A power grid is considered strong for SCR values above 20 to 25 and

weak for SCR values below 6-10 [16], although other reference values might be found in the literature.

As already said, the injection of oscillating power in weak grids causes many technical problems. In addition, the frequency and duration of unsafe situations is much greater than in high performance strong grids. These technical issues significantly affect the voltage, the frequency and therefore the stability of the system. As a result, strict performance obligations are imposed on to weak grids through the so called grid codes, which consist of minimum performance parameter and technical requirements that all the parties connected to the grid must follow.

In the next paragraphs the effects of the integration of an oscillating power in the grid will be analyzed more in detail.

3.2 – Grid integration of wave power generation

In the development of wave energy converters, grid integration is usually the last stage and therefore the least explored, as a consequence not many devices have been tested grid-connected and most of the literature about wave energy does not consider this stage, at least under realistic conditions. However, the analysis of the grid integration of the device may provide feedbacks that help to improve the design of the WEC, so it should be always done.

An important part of the challenge of connecting the grid to ocean wave power converters or farms is related to the physical connection to the on-shore electrical substation. This issue has important similarities and the same challenges than the offshore wind power farms and it’s not going to be discussed further in this thesis.

The other critic aspect of the grid integration of wave energy is the negative impact produced by the oscillating power generated by WECs. This paper, and this chapter particularly, focuses on this specific issue. The main problems are related with voltage and frequency fluctuations and stability issues, and are going to be discussed one by one.

Frequency oscillations: The first impact here considered is the effect on grid frequency. When the WEC is directly connected to the grid, the power that it injects, having an oscillating profile, directly affects the behavior of the frequency signal of the system [17]. This phenomenon requires special attention as frequency is one of the most relevant index of the stability of power electric systems. The decrease of frequency is directly related to the amount of power injected into the system through the wave converter. Therefore, the more is the amount of oscillating power introduced, the more will be the drop of frequency, and its signal will present bigger oscillations, which means higher instability of the grid.

Voltage fluctuations: The size of the voltage fluctuations produced by the oscillating WEC power in the electric grid depends on the short circuit power of the nodes, but in most of the situations the variation doesn't break the limits imposed by the local grid codes. Only in the case of a very weak or isolated power grid this problem can be consistent, resulting in phenomenon as voltage dip or swell, overvoltage or undervoltage.

Flicker: Voltage flicker is a phenomenon caused by fast voltage fluctuations and can be detected by the variation of the light intensity of various light sources [18]. Although not particularly harmful to the electrical network, flicker represents a visual disturbance to electricity customers. As small voltage variations can be induced by variable power output generators, this issue is of particular interest in wave energy grid integration research. Light intensity variation frequency is the double of voltage variation frequency, therefore components presenting twice the frequency of the voltage amplitude variations appear. In the case of a wave farm, there is also an aggregation effect that needs to be taken into account in the studies. Combining many WECs in a farm, indeed, may not only increase the frequency of light intensity variations but their magnitude as well.

In general, all the problems just presented related to voltage, frequency and stability of a grid, can be troublesome especially in the case of weak grids. With the increasing penetration of renewable energy sources (and wave energy as well) experienced in the last decades, the impact of these issues is becoming

even more intense. In the following paragraph different solutions for this problem will be presented.

3.3 – Solution: Power Smoothing System (PSS)

In order to avoid the direct injection of oscillating power into the grid, different solutions have been explored. First of all, it is important to observe that this problem involves most of the WEC technology types, but not all of them. As a matter of fact, certain types of WECs, such as oscillating water columns and overtopping devices, do not suffer from power oscillations, since they have an intrinsic energy storage capability. However, for technologies like attenuators, point absorbers and oscillating wave surge converters, wave power conditioning is a real issue. In these cases, it is now evident that without a Power Smoothing System (PSS) of some kind the power fluctuations have a negative impact on the grid.

The problem may be approached from different perspectives. In the case of a wave farm, the first option is to distribute the WECs along the farm considering the most predominant wave period and the main direction of propagation. With an optimal disposal, the power fluctuations of each single WEC could be naturally and partially compensated by the rest under most situations [19]. Another possibility is to control the system with a hybrid strategy that includes a DC-link voltage control and direct power control. A flywheel could also be added to the electric generator in those cases in which the type of WEC allows it (rotatory devices), so that the higher inertia reduces power ripple [14].

Another option for conditioning the instantaneous power delivered to the grid, more promising than the previous ones, consists on the addition of an electrical Energy Storage System (ESS). This solution was first proposed for other renewable energy sources as photovoltaic systems or wind turbines, and only later for wave energy. Different storage technologies can be considered for this application: batteries, supercapacitors and flywheels. To choose among these options many specifications have to be considered, such as power level, energy

level, response speed, charge-discharge frequency, number of operation cycles, maintenance, environmental issues, costs, and so on.

For the wave energy application several statements can be established [19]:

- The amount of energy is low compared to power, so a high power and low energy system will be required.
- The number of operation cycles is very high as well as the frequency since the energy storage system would be operating continuously.
- The response time has to be very high.
- Volume is more critical than mass, so a high power density is more convenient than energy density.
- Maintenance has to be reduced due to the low accessibility of this application.

According to these specifications, the more appropriate technologies are flywheels or supercapacitors, because of their high power density and electrical response, low maintenance required and their extremely high frequency and number of cycles. Some advantages can be found in each one of these two options, so the final choice will depend on the particular scenario considered.

Independently of the ESS technology chosen, the principle of work consists of absorbing the exceeding energy when the instantaneous power produced by the WECs is above a certain value of average power, and returning this energy when the instantaneous power is below the average. Proceeding in this way, a very smooth output power can be delivered to the grid.

A crucial aspect of the control system for the ESS is the concept of average power. In the case of regular waves this reference value can be easily calculated. Considering waves of fundamental period T_F and assuming steady state, the average power is given by the algebraic mean of the instantaneous power generated by the WEC or the Wave Farm (WF) along a time interval equal to T_F [14]:

$$P_{AVG} = \frac{1}{T_F} \cdot \int_0^{T_F} P_{WEC} \cdot dt \qquad \textbf{(2)}$$

Real waves, however, are not regular and consequently don't have a fundamental period. For irregular waves, therefore, the determination of the average reference power is more problematic. An option is to use a recent-history based method called Moving Average (MA). It consists of a moving window of width T_W that contains a time register of the instantaneous power with sampling time T_S. The average power can be then estimate as the algebraic mean of the instantaneous power samples contained in that moving window [14]:

$$P_{AVG} \approx P_{WINDOW} = \frac{1}{T_W} \cdot \sum_{n=1}^{N} P(n) \quad \textbf{(3)}$$

In equation (3) *n=1* and *n=N* refer respectively to the oldest and to the newest sample contained in the window. *N* is the total number of samples in the window:

$$N = \frac{T_W}{T_S} \quad \textbf{(4)}$$

Another possibility for the estimation of the average power is to use a predictive method, such as Auto-Regressive (AR) models. AR models are going to be deeply explained and analyzed in the following chapters of this thesis.

3.4 – Supercapacitor-based Power Smoothing System

The solution proposed to smooth the WECs output power, that is going to be used in the simulations and in the laboratory tests presented in this paper, consists in the integration of a supercapacitor-based ESS in the system containing the wave farm and the connections to the electric grid. A schematic representation of the proposed PSS is showed in figure 3.2.

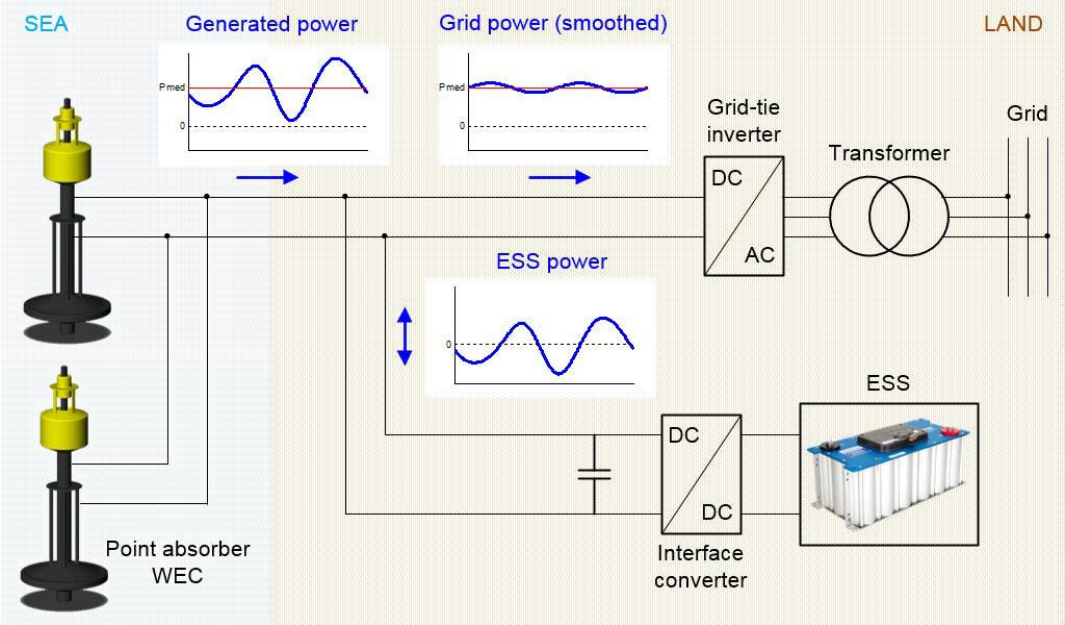

Figure 3.2 – Wave Farm with supercapacitor-based energy storage system for power smoothing

The emulated wave farm is made of a group of Point Absorber WECs and is represented on the left side of the figure. In the scheme are included also some graphs, representing the oscillating power produced by the WECs, the power stored and released by the supercapacitors, and the consequently smoothed profile of grid power. Without the Power Smoothing System the same oscillating power profile would be injected into the grid, worsening its quality and potentially causing instability issues, as previously seen.

The control system for the ESS in the proposed solution will initially use a Moving Average criteria to estimate the reference average power. The intent of this thesis is to investigate on the possibility of substituting this control system with another one based on Auto-Regressive models, in the attempt to improve the effectiveness of the smoothing system.

4 – PREDICTION OF WAVE HEIGHT AND POWER USING AUTOREGRESSIVE MODELS

The final aim of this chapter of the thesis is to have a good enough short-term prediction of the power produced by a group of WECs. The starting point for this work has been the study of various documents of the Italian researcher F. Fusco [20], [21], [22], [23], in which different techniques to predict the incident wave elevation are investigated, focusing on Auto Regressive (AR) processes. The attempt to use Fusco's method and implement it into the software Matlab in order to predict a real wave profile has been one of the biggest challenge of this thesis, whose various steps will be shown and discussed during this chapter. The final part of the chapter investigates on the possibility to use the same method to predict the wave power instead of the wave height, as required by the control system for the Power Smoothing System introduced in the previous chapter.

4.1 – Autoregressive Models

In order to predict wave height or any other wave parameter, a forecasting model has to be used. Forecasting methods are procedures for computing future parameter trends from present and past values, and they can be classified into three main types [24]:

- **Judgemental forecasts**, based on subjective judgement, intuition, inside commercial knowledge, and any other relevant information.
- **Univariate methods,** where forecasts depend only on present and past values of the single series being forecasted.
- **Multivariate methods**, where forecasts of a given variable depend, at least partly, on values of one or more additional time series variables, called predictor or explanatory variables.

Autoregressive models are included in the second category, univariate methods, and they will be used here to predict the height of an incident wave, as proposed by Fusco [23]. The approach commonly followed in the literature consists of a spatial prediction of the wave elevation, meaning that the wave field at a certain location is reconstructed from one or more observations at nearby locations. This means a big complexity of the model, which requires an array of spatial measurements and has to consider the possible multidirectionality of waves, the presence of radiated and refracted waves, and eventual non-linearities in the waves propagation.

The solution used in this thesis is the prediction of the wave height based on its past history, but only at the same point of the sea surface. This alternative approach allows considering the short-term wave forecasting as a univariate time series problem, based on the collection of observations of the wave elevation made sequentially through time, but always at the same location. Moreover, this approach presents many advantages in terms of complexity of the model, since multi-directionality and all the associated issues do not need to be taken into account. It is also a cheaper solution because no additional instrumentation around the device is required. In addition, all the well established theory about univariate time series forecasting may be exploited, including the theory about AR models.

The two just discussed different approaches are well illustrated in figure 4.1, taken from [20].

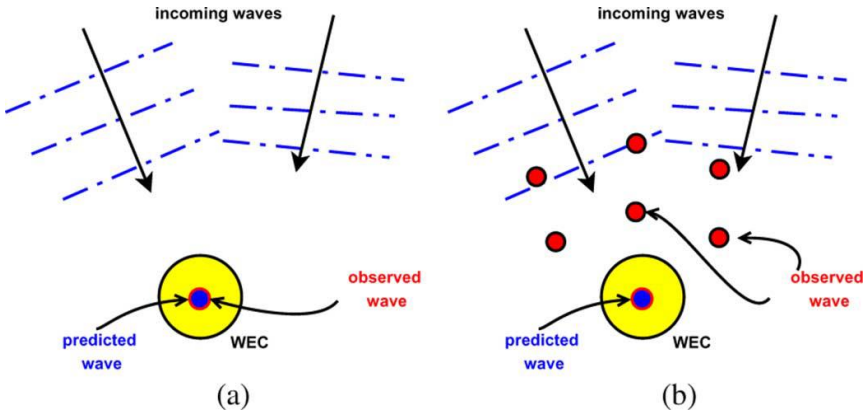

Figure 4.1 - Two main approaches to wave forecasting.
(a) Prediction based only on local single-point measurements.
(b) Prediction based on reconstruction of wave field from array of distant measurements [20]

The AR model used for the wave prediction is expressed by equation **(5)**. The wave elevation $H(k)$ at instant k is assumed to be linearly dependent on a number *n* of its past values, through the parameters a_i [23]:

$$H(k) = \sum_{i=1}^{n} a_i \, H(k-i) + \zeta(k) \qquad (\mathbf{5})$$

where a disturbance term $\zeta(k)$ has been also included, representing a noise. The number *n* of past values corresponds to the order of the model.

If the parameters a_i are estimated and the noise is supposed to be white and Gaussian (normal distribution with zero mean value), the sum of the disturbance terms can be considered equal to zero, and the corresponding best *l*-step ahead prediction of the future wave elevation at instant k, $H_{pred}(k+l|k)$, is given by:

$$H_{pred}(k+l|k) = \sum_{i=1}^{n} a_i(k) \, H_{pred}(k+l-i|k) \qquad (\mathbf{6})$$

For expressions in the form $H_{pred}(a/b)$, which appear in equation (6) and in many following equations, the meaning of the terms contained in brackets need to be explained. The generic left term a corresponds to the instant of time to which the predicted value refers, while b is the moment in which the prediction is done. In other words, the expression means that in the instant b we are predicting the value that the variable H will have at instant a.

To do a *l*-step ahead prediction of the height (or any other parameter) means to estimate what will be the value of this variable a number l of steps in the future, with respect to the present instant here indicated with k. The length of a single step (in terms of time) depends on the sampling period T_s, which is the time difference (in seconds) between one sample value and the following one. The sampling period in turn depends on the sampling frequency f_s, which is defined as the number of samples obtained in one second, thus:

$$f_s = \frac{1}{T_s} \qquad (\mathbf{7})$$

Clearly, the sampling period has to be kept constant for the model to be considered valid.

It is now clear how a l-step ahead prediction of a parameter corresponds to the estimation of its value a number of seconds $l \cdot T_s$ in the future.

Equation **(6)** states that the l-step ahead prediction is calculated using not only past values (up to the instant k in which the prediction is done) but also the predicted values up to the instant $k+l-1$. Thus, if $k+l-i \leq k$, then $H_{pred}(k+l-i|k) \equiv H(k)$, which means that since the information for that instant is already acquired there is no need of prediction and the already known past value of *H* will be used. Therefore, for a 1-step ahead prediction all the needed values of height are already known, and the predicted value can be easily calculated as a combination of only past values, as shown by equation **(8)**.

$$H_{pred}(k+1|k) = \sum_{i=1}^{n} a_i(k)\, H(k+1-i|k) \qquad (8)$$

For a longer term prediction, we have to consider that a bad prediction implies someway a bad feedback to itself, in the sense that if the prediction of the first steps is not very accurate, the prediction of the further steps will be even worse, as it will use the bad predictive values of the first steps. Clearly, as we increase the horizon every AR prediction tends to deteriorate, but how fast this deterioration is realized depends on the accuracy of the prediction, and this is a crucial aspect for AR models.

4.1.1 – Estimation of the AR coefficients

AR models present a very simple mathematic expression, consisting in a linear combination of *n* values of wave elevation weighted through some coefficients a_i. The estimation of these coefficients is not simple, and it is the main issue to solve for the implementation of AR processes. Many different approaches have been proposed in the literature and there is not a unique best option, as it strongly depends on the features of the specific case. Under the assumption of Gaussian error, a quite easy standard approach is to minimize the sum of squares of the

one-step ahead prediction error through regular Least Squares (LS), a classic method for regression analysis. Given a number *N* of batch wave elevation observations, the objective function to minimize with a standard LS approach would be the following:

$$J_{LS} = \sum_{k=1}^{N} \left[H(k) - H_{pred}(k|k-1) \right]^2 \qquad (\mathbf{9})$$

$H_{pred}(k|k\text{-}1)$ is expressed as in equation **(8)**, containing the unknown coefficients a_i.

Since the model will be utilized for multi-steps ahead forecasting, however, regular least squares is not an optimal solution. The reason is that there could be many models which are almost equivalent in terms of one-step ahead prediction, but show a quite different behavior in longer-term predictions [25].

The approach that seems to be more suitable for a short-term prediction of the wave height is the one firstly introduced by Shook-Mohtadi-Shah [26] and proposed by Fusco for the same application [23]. This method is called Long-Range Predictive Identification (LRPI) and consists in the minimization of a multi-steps ahead cost function, J_{LRPI}:

$$J_{LRPI} = \sum_{k=1}^{N} \sum_{j=N1}^{N2} \left[H(k) - H_{pred}(k|k-j) \right]^2 \qquad (\mathbf{10})$$

where *N1* and *N2* are respectively the minimum and the maximum prediction horizon. The value of *N1* is usually set equal to 1, while the value of *N2* depends on the specific application and on the sampling period. The term $H_{pred}(k|k\text{-}j)$ is expressed as in equation (6), as a linear combination of wave elevation values weighted through the coefficients a_i.

The minimization of J_{LRPI} is quite problematic as it is a nonlinear function usually containing a huge number of terms. This issue will be treated later, showing how to implement equation **(10)** in Matlab.

It is important to observe that the estimation of the parameters a_i is done in a specific instant of time, with a certain sea state and a wave profile of specific

conditions. These conditions are likely to change with time, thus also the optimal values of a_i should change and be recalculated, instant by instant, adapting the model to the momentary conditions. However, as shown in [23], a static AR model keeps its validity for a quite long time after being estimated, even more than two hours, in spite of wave spectral variations. Consequently, very complex adaptive models are not necessary in this case, it is enough to repeat the offline estimation of the coefficients every one or two hours to have good results.

4.2 – Data Analysis

The wave forecasting AR models are tested with a data set containing real wave observations at a specific sea location. The location where the data were collected is the Biscay Marine Energy Platform (BIMEP), an offshore infrastructure for the demonstration and proving of wave energy generation devices over a sustained period of time.

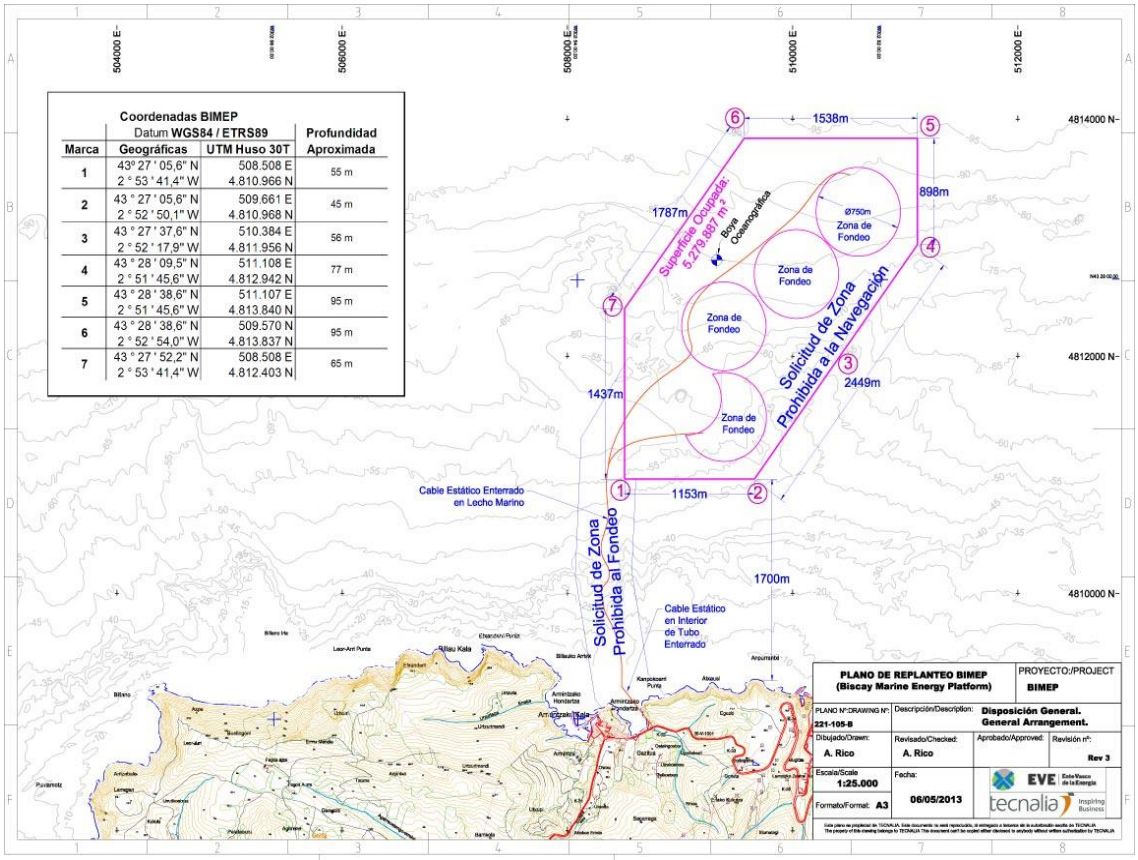

Figure 4.2 – General layout and geographical coordinates of the BIMEP platform [29]

The site is located in the Cantabrian Sea, about 1,7 km from the coast of Armintza, a small village of the Basque Country in the Northern Spain, at a water depth between 45 m and 95 m approximately. The BIMEP covers a total sea surface of about 5,3 km^2, delimited by six different vertices. The map of figure 4.2, taken from the BIMEP website [29], shows the general layout of the platform and the geographical coordinates of the six vertices. The installed power capacity of the platform is 20 MW, with four connection point for WECs, connected to the onshore substation through four static submarine cables and to the WECs through dynamic submarine cables.

In the test area there is also an oceanographic buoy, equipped with several different sensors to monitor atmospheric and wave conditions and provide information on the marine climate. This buoy is the one were the data used in this work were collected, and it is registered on the website of the Spanish Ministry of Public Works and Transport [30] as the buoy n° 3159035.

The data refers to a specific sea state, characterized by:

- Significant wave height H_s = 2 m;
- Peak wave period T_p = 12 s.

The sea state is the general condition of a free sea surface, and H_s and T_p are the main parameters characterizing a certain sea state. The significant wave height H_s is approximately equal to the mean wave height (from trough to crest) of the one third highest waves, and it is considered the most representative parameter of a sea state. The peak wave period T_p is the time period of the wave with the highest energy. Other significant parameters are the mean wave period T_m, defined as the mean of all the wave periods in a time series representing a certain sea state, and the mean wave direction θ_m, which is the mean of all the individual wave directions.

From here on out, the wave profile extrapolated from the observations collected by the BIMEP will be called Wave1, and all the information about wave height and other parameters defining these profiles is available in the form of a Matlab file, *Wave1.mat*. This file will be used to carry out the Matlab and Simulink simulations for the prediction of wave elevation and power.

4.2.1 – Choice of cut-off frequency

One characteristic that emerges from many wave predictability analysis [21]-[22] is that the low frequency components of the wave spectra are the most interesting from an energetic point of view, as a very significant portion of the wave energy is usually concentrated at low frequencies. In addition, with respect to high frequency components, low frequency waves are more regular and less affected by nonlinearities, so they can be predicted more accurately and further into the future. For these two reasons it is reasonable to low-pass filter the wave elevation and focus the prediction only on the low frequencies, in order to get an improvement in the accuracy and in the length of the forecast. On the other side, with a low-pass filter all the high frequency components of the waves are totally neglected, and this means a loss of information and a small loss of energy as well.

Another thing that needs to be considered is that the use of a real time filter introduces an error, in terms of signal amplitude and time delay. The effects on the forecast of these errors could be significant, so it is important to select an appropriate filter among the several possibilities, with performance good enough to limit the errors.

From what explained above, it is evident that the choice of the cut-off frequency f_c represents a compromise between an improvement in the forecasts and the loss of energy of the neglected waves. Thus, the choice of f_c should be made carefully, accordingly to the spectral distribution of the specific sea state.

As described later, this low-pass filtering functionality has also been introduced in the Matlab simulations, using different values of cut-off frequencies to check the system response.

4.2.2 – Choice of the sampling frequency

If a wave elevation time series is low-pass filtered before the prediction, this means that it can be sampled without any loss of information [20] if:

$$f_s \geq f_c/2 \qquad (\mathbf{11})$$

where f_s is the sampling frequency and f_c is the cut-off frequency of the filter. Lower sampling frequencies would give raise to the aliasing phenomenon, causing the sampled time series not to be uniquely representative of the original signal.

In theory, once **(11)** is respected and aliasing is avoided, the information that the past of a signal has about its future will not be affected by the sampling frequency. Therefore, a proper forecasting model that manages to extract all the information to produce the prediction, should not perform differently by changing the sampling frequency. In [20] this fact is also demonstrated in practice.

As a consequence, the choice of the sampling frequency will not represent a problem during the simulations once the above mentioned condition is respected.

4.3 – Prediction of wave height

The task carried out in this section of the chapter is the prediction of the height of the wave using autoregressive models, through simulations with the software Matlab, version R2015b. The work has been done in different steps, starting from a very simple example of a regular wave with only 3 harmonic components, and finishing with a more complex case of a real wave profile, using the data introduced in the previous section.

To check the accuracy of the predictions, in addition to a graphic evaluation, the following index of fitness (*FIT*) [23] will be used:

$$FIT(l) = \left(1 - \frac{\sqrt{\sum_k \left[H(k+l) - H_{pred}(k+l|k)\right]^2}}{\sqrt{\sum_k H(k)^2}}\right) \cdot 100\% \qquad (\mathbf{12})$$

Here $H(k+l)$ is the wave elevation at the instant $k+l$, and $H_{pred}(k+l|k)$ is its prediction based on the information up to instant k. The value of the index is a percentage, and represents a measure of the accuracy of the forecast. A 100% value for $FIT(l)$ means that the wave height is perfectly predicted l steps into the

future. Therefore, the smaller is the percentage, the worse is the prediction precision.

In this section, the concepts behind every Matlab simulation and its results will be discussed, while all the scripts are collected in the appendix B at the end of the thesis.

4.3.1 – Example 1: simple wave with 3 harmonic components

In this first example a simple ideal wave with only 3 harmonic components has been assessed. The script of the Matlab code is saved as *AR_example.m*, and it can be found in the appendix B, section B.1.

The main difficulty in the implementation of the autoregressive method is the estimation of the coefficients a_i. The other troublesome part, once the coefficients are estimated, is to predict the future wave using those coefficients.

In order to solve these issues, the idea has been to start from this simple example and then to proceed increasing step by step the complexity of the model.

For this reason a basic wave, not representative of a real one, has been initially used. The amplitudes A_i and the frequencies f_i of the three components have been chosen arbitrarily, and the resulting wave height profile consists in the combination of the three harmonics:

$$H = A_1 * \sin(2\pi f_1 t) + A_2 * \sin(2\pi f_2 t) + A_3 * \sin(2\pi f_3 t) \qquad (\mathbf{13})$$

For this simulation a time span of 100 s has been assessed, with a sampling frequency f_s of 1 Hz. This means that we have a sample every second, and that the length of the single steps of the prediction is also 1 s. Thus, the total number of samples is *N*=101, and they have to be used for the estimation of the coefficients.

The chosen values of amplitude are in order: A_1 = 1 m, A_2 = 0,5 m, A_3 = 0,3 m. The frequencies for the three harmonics are: f_1 = 0,03 Hz, f_2 = 0,12 Hz, f_3 = 0,015 Hz. The resulting wave profile is depicted in figure 4.3.

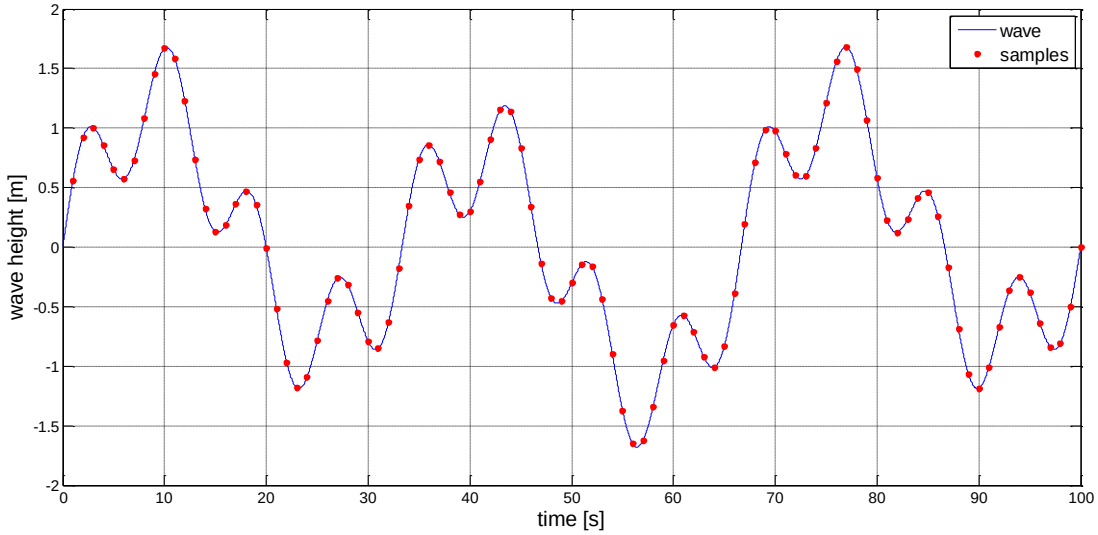

Figure 4.3 – Wave elevation profile and samples

To do the prediction we have to implement the formula of equation **(6)**, already explained in section 4.1 and repeated here for convenience:

$$H_{pred}(k+l|k) = \sum_{i=1}^{n} a_i(k)\, H_{pred}(k+l-i|k)$$

Therefore, an estimation of the coefficients a_i is required, through the minimization of the Long Range Predictive Identification objective function of equation **(10)**:

$$J_{LRPI} = \sum_{k=1}^{N} \sum_{j=N1}^{N2} \left[H(k) - H_{pred}(k|k-j)\right]^2$$

As the implementation of this formula in Matlab is quite complicated, for this first case to simplify the procedure the maximum prediction horizon *N2* has been set equal to 1. In this way, the LRPI approach corresponds exactly to a standard least squares minimization, as equation **(10)** with *N2*=1 turns out to be identical to equation **(9)**:

$$J_{LRPI} = J_{LS} = \sum_{k=1}^{N} \left[H(k) - H_{pred}(k|k-1)\right]^2$$

This formula has been implemented through the function *onepred.m*, which can be found in section B.2 of the appendix B.

The objective function J_{LRPI} has been minimized through the solver *fminunc*, already implemented in the software Matlab, which is normally used to find the minimum of unconstrained multivariable function. Given a fixed starting point, this solver proceeds iteratively until it finds the solution. The choice of the starting point could be problematic, since a bad starting point could lead to a non-converging solution or to find a local minimum and not a global one. If the starting point is changed, indeed, the solution may change. In the attempt to solve this problem also the Matlab tool *MultiStart* has been used, which using information from the minimization problem, creates a chosen and fixed number of random different starting points. In this case we chose 50 starting points: the program will then run the solver *fminunc* from each of the 50 points, giving as final solution the minimum among all the 50 solutions calculated. In this way, the likelihood of finding a global minimum increases.

Regarding the order of the model, since the wave only has three harmonic components, a high order is not necessary. Thus, simulations have been made twice, once with order n=5 and once with order n=10. The order of the model corresponds also to the dimension of the vectors of parameters, for the starting points and for the final solutions as well. In both cases, repeating the optimization process many times shows that results (parameters values) are not always the same (they depend on the starting points, which are chosen randomly). But while in the first case (order 5) the solutions are always similar, with order 10 the values of the parameters are sometimes very different. Figures 4.4 and 4.5 illustrate this fact. They show the distribution in space of the values of starting points (blue circles) and the solution (red crosses), considering only the first two components a_1 and a_2 of the vectors $\bar{a} = (a_1, a_2, \dots a_n)$.

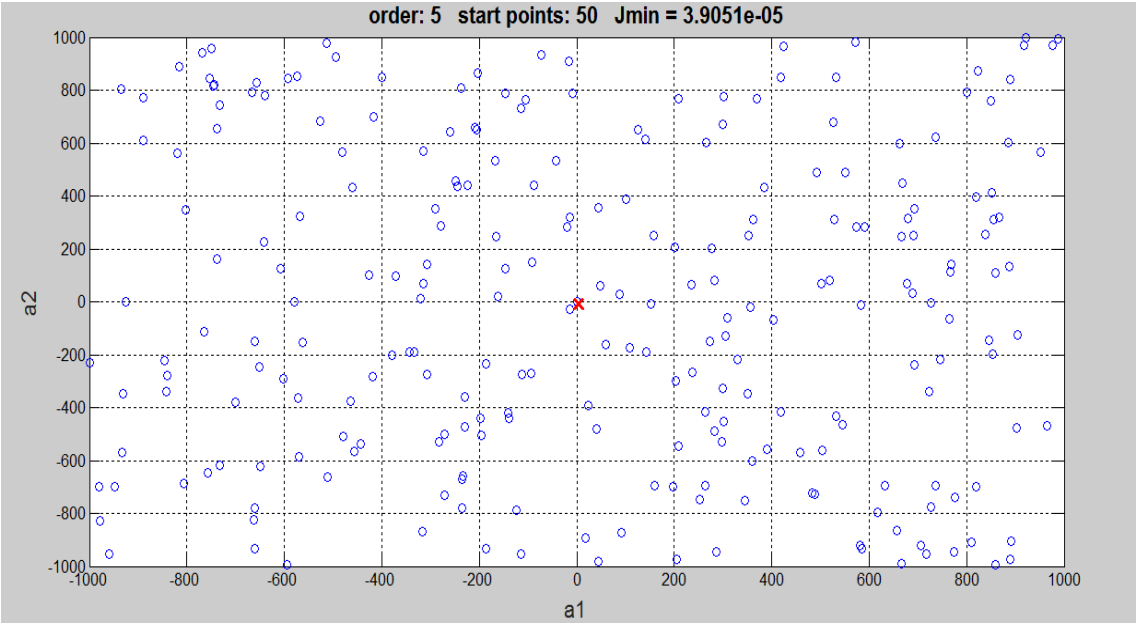

Figure 4.4 – Space distribution of the first two coefficients of the starting points and the solution vectors, n= 5

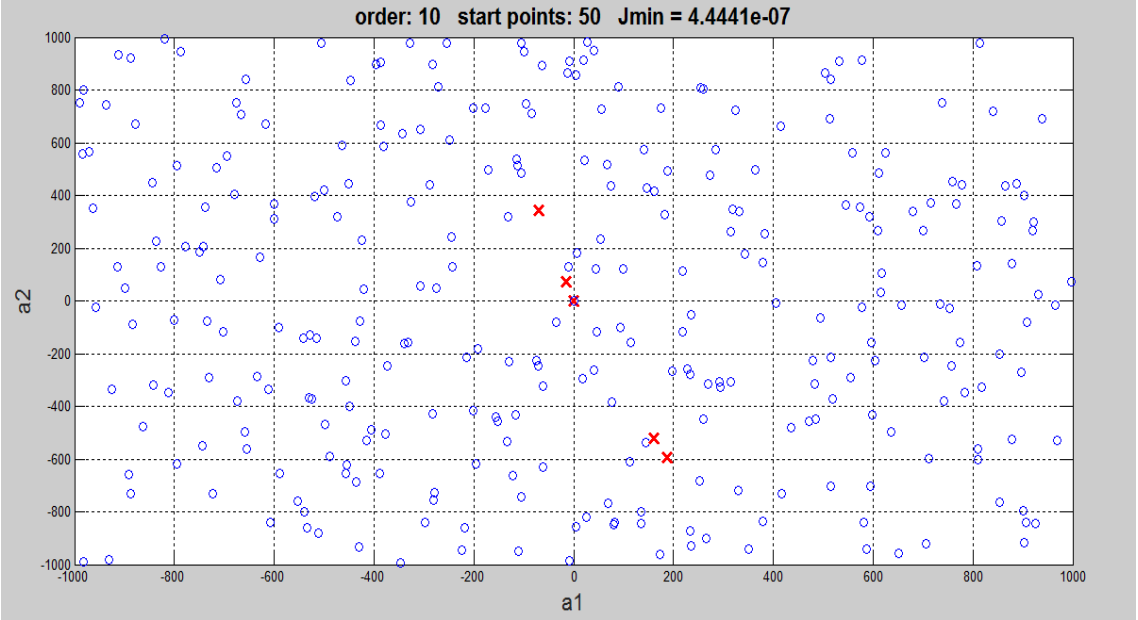

Figure 4.5 – Space distribution of the first two coefficients of the starting points and the solutions, n=10

These graphs have been made for two reasons mainly: to check how the Multistart algorithm works when it generates the starting points, and to see if the solution remains the same when the calculations are repeated. Regarding the first issue, we can see that the blue circles are randomly distributed and all the space is investigated.

About the second problem, with order 5 (figure 4.4) there is only one red cross and this means that the solution is always approximately the same and it probably represents a global minimum. With order 10, on the other hand, the solution changes substantially every time, the red crosses of figure 4.5 are quite far one from each other and they represent local minimums. This can be explained by the fact that when the order is too high, too many coefficients are used, and the system of equations becomes more and more dependent. As a consequence, more solutions appear. This, however, should not affect the accuracy of the model.

Both with order 5 and 10, the estimated coefficients have then been used to do the prediction as in equation **(6)**. As we are considering a simplified model with a regular least squares estimation that is not optimal for a multi-steps prediction, only a 1 step forecast has been made here. Since the sampling period is 1 s, this means we are predicting the wave height only one second in advance.

A graphic evaluation of how good is the prediction is possible through figure 4.6, that shows in blue the real wave and in red the 1-step prediction of the same wave with order 10.

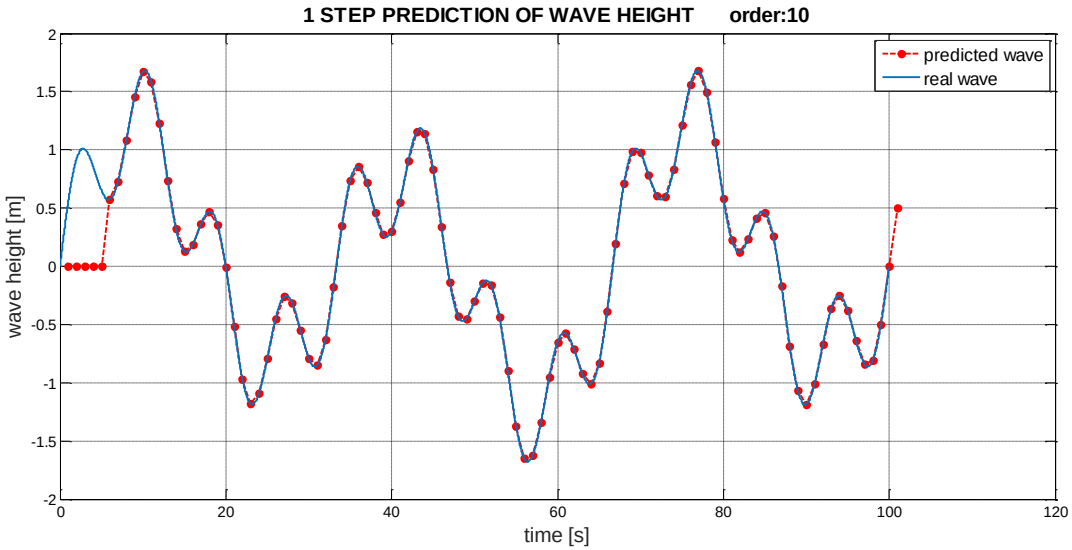

Figure 4.6 – Comparison between the real wave and the 1-step prediction with order 10

Every point of the red profile of figure 4.6 is predicted one step (i.e. one second) ahead, and the curve is built connecting these points. As expected, for such a short-term forecast the precision seems to be quite good. No big differences can

be noticed between the graph for order 5 and the one for order 10, that is why only one of them has been reported here.

In order to try to solve the problem of the different local minimums, some bounds have been applied to the multistart algorithm, restricting the searching space for the generated started points. The reason is that the values of wave height are in the order of a couple of meters (positive or negative) and not more, so it is reasonable to expect coefficients values of the same order of magnitude. Therefore, it seems not worth to search the solution outside of a certain range of values. Without any fixed bounds, the limits are automatically set to [-1000,1000] for both axis, as can be seen in figures 4.4 and 4.5. In the script *AR_example-bound.m* [appendix B.3], these bounds have been reduced to -100 for the minimum value and 100 for the maximum.

Now the minimization problem is constrained and the algorithm *fminunc* is not valid anymore. Thus, in this program it has been replaced by the solver *fmincon*, which is used to find the minimum of constrained nonlinear functions. Apart from this substitution, the syntax of the Matlab code remains the same of the previous unconstrained one. Introducing these bounds, the searching space for the starting points is reduced, and the result in the order 10 case is that the solutions are closer than they were with the unconstrained method, as depicted by figure 4.7.

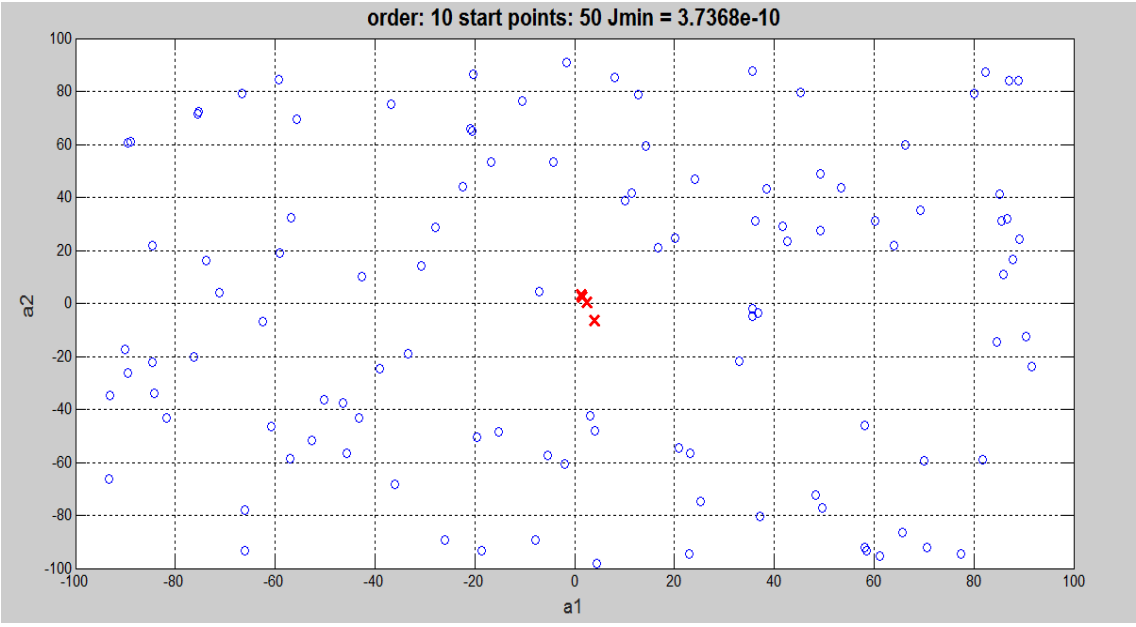

Figure 4.7 – Space distribution of starting points and solutions with order 10 and bounds [-100,100]

The positive contribution of introducing some constraints is apparent in figure 4.7, as running the program multiple times the solutions are always similar, so we are closer to find a global minimum. On the other side, the calculation time in this case is significantly longer, as the optimization process now is more complex. Instead of introducing some constraints, provided that all the solutions are similar in terms of accuracy, we can choose among the solutions with smaller coefficients, not considering solutions with larger coefficients values that cancel each other. Moreover, the choice of a proper order for the AR model should make this issue less relevant, eliminating the need of introducing some bounds in the minimization problem. For all these reasons, this approach seems not to be totally worth it, and it will not be used further in the following simulations.

4.3.2 – Example 2: wave with 9 harmonic components

In this second example the number of harmonic components of the regular wave has been increased from three to nine, with the intent to add a level of complexity to the model and make it a little bit more similar to a real case. The wave has been created like in the previous case, fixing the values of amplitude and frequency of the harmonics and combining them as showed by equation **(13)**. The code written for this simulation can be found in the appendix B.4, entitled *AR_example2.m*.

The number of samples is again *N*=101, sampled every one second (sampling frequency of 1 Hz). The generated wave profile is represented in figure 4.8.

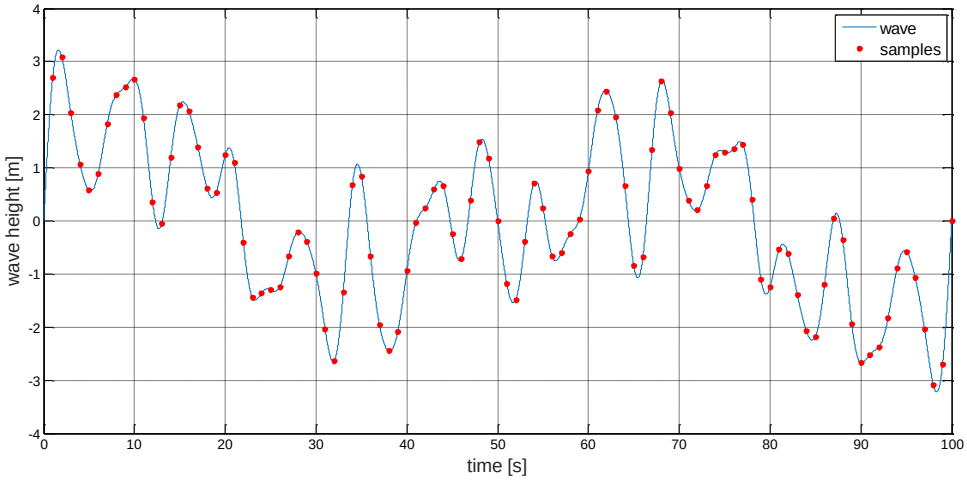

Figure 4.8 – Example 2: wave height profile and samples

From a first look, this profile looks more irregular than the one of the first example. With the samples taken from this new profile, exactly the same procedure of the previous simulation has been repeated, using the *multistart* approach to generate the starting points for the minimization process, realized with the solver *fminunc*. The simulation has been done both with order *n*=5 for the autoregressive model, and with order *n*=10. Every time we run the program the *multistart* algorithm generates 50 different starting points for the iterative minimization process. Again, to have an idea of how these points are distributed in the multidimensional space, we can take a look at figure 4.9 and 4.10, for order 5 and 10 respectively.

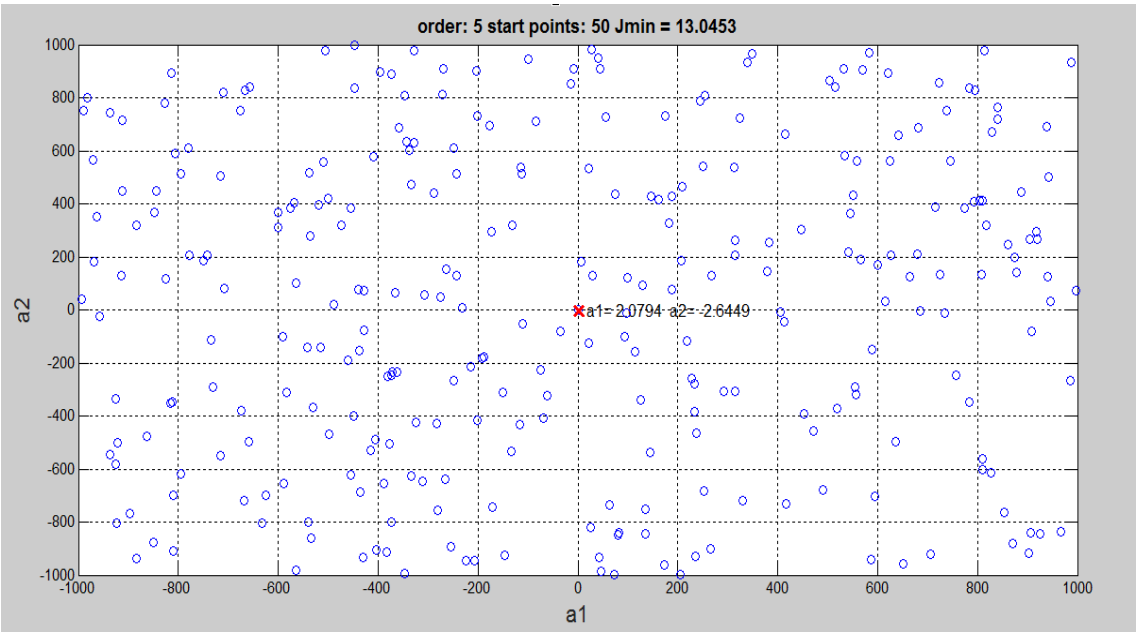

Figure 4.9 – Space distribution of the first two coefficients of the starting points and the solution vectors, n= 5

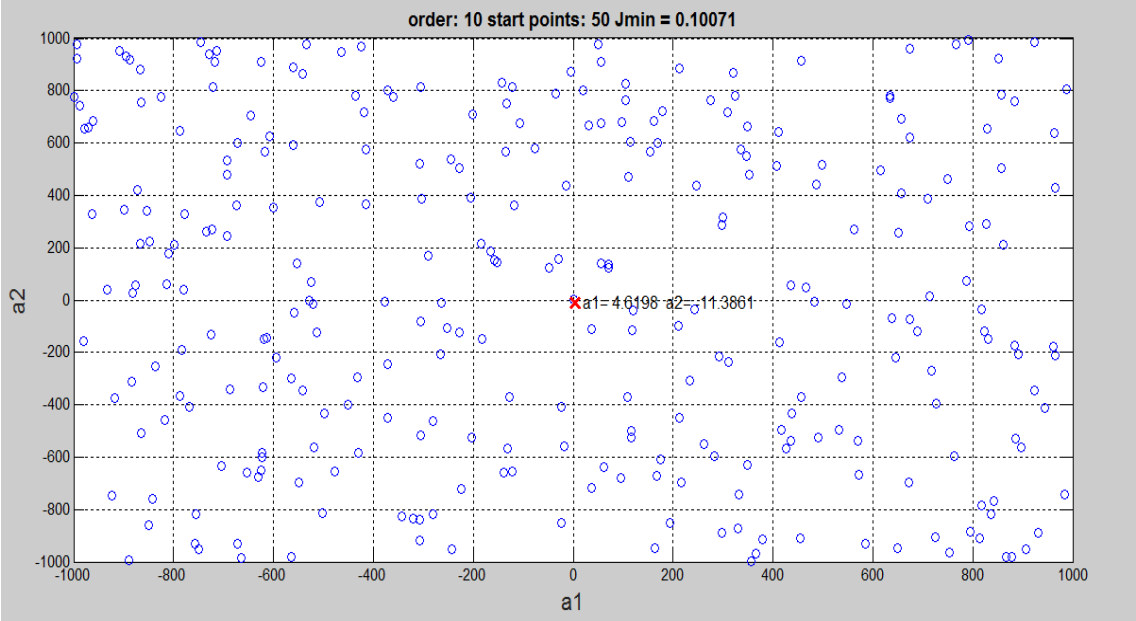

Figure 4.10 – Space distribution of the first two coefficients of the starting points and the solutions, n=10

In figure 4.9 and 4.10 only the first two values of the vector of parameters are considered, and this approximation is done only to have a visual two-dimensional idea of their distribution in the space. The blue circles represent the starting points, while the red crosses represent the solution, which is the vector of parameters that will be used for the prediction. Each time the program is run, 50 more blue circles and one red cross appear on the graph. In this case we can see that in both cases there is only one red cross, which means that the solution is always the same and it is very likely to be a global minimum.

Once estimated the coefficients a_i, they have been used for a single step prediction of the wave height. Also in this example the only method used to evaluate if the prediction is good is to compare graphically the predicted wave and the real one. The comparison between the real wave and its 1-step prediction made with order 5 is showed in figure 4.11, while figure 4.12 in the next page is the same but for the prediction made with the AR model of order 10.

As the wave is more complex than in the previous example, it is also expected to be harder to predict. With *n*=5, indeed, even a single step prediction is not perfectly accurate, as can be seen from figure 4.11. This means that the order is too low, a higher order is required for this wave and the results should be better. Doubling the order, in figure 4.12 we can clearly see that the prediction is

significantly better, as the two wave profiles (the real wave in blue and the predicted in red) are almost coinciding. In the next paragraph this procedure will be repeated using the data of real ocean waves.

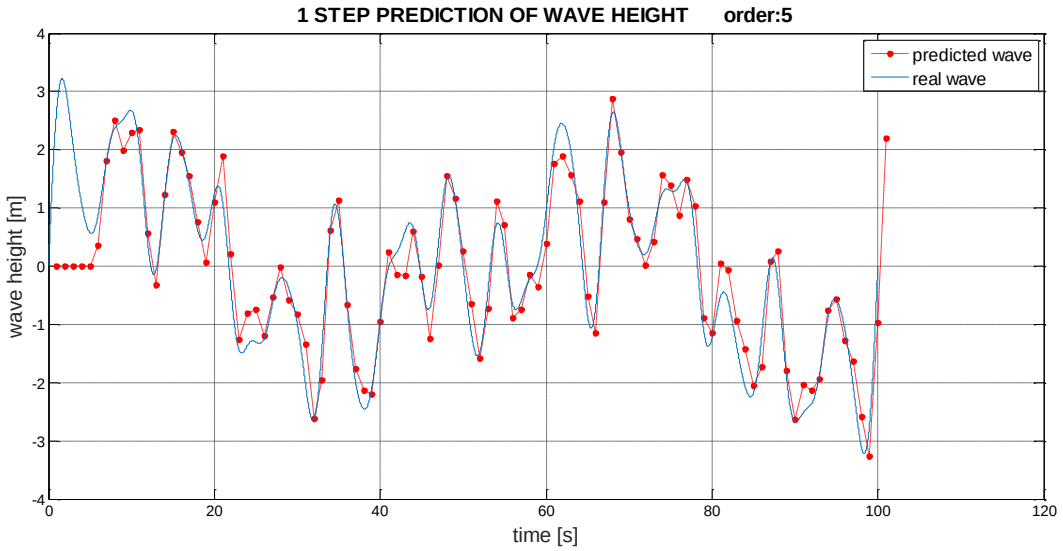

Figure 4.11 – Comparison between the real wave and the 1-step prediction with order 5

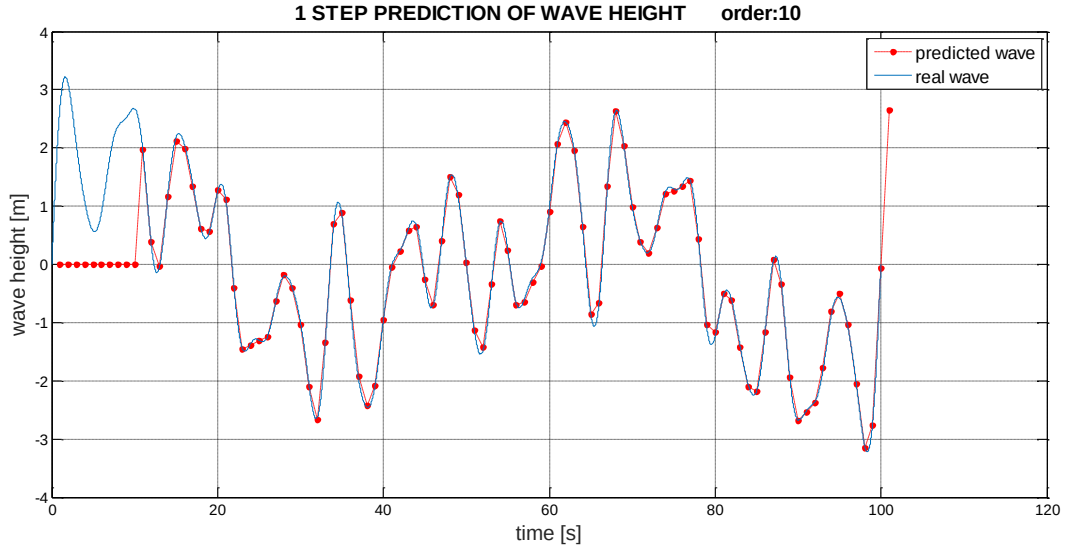

Figure 4.12 – Comparison between the real wave and the 1-step prediction with order 10

4.3.3 – One-step prediction of a real wave profile

In this simulation the same procedure successfully implemented for a single-step prediction of two different basic regular waves will be used for a real case of irregular ocean waves, using the data collected in the BIMEP as seen in

paragraph 4.2. These data have been loaded in the Matlab file *Wave1.mat* and used to run the Simulink model of figure 4.13.

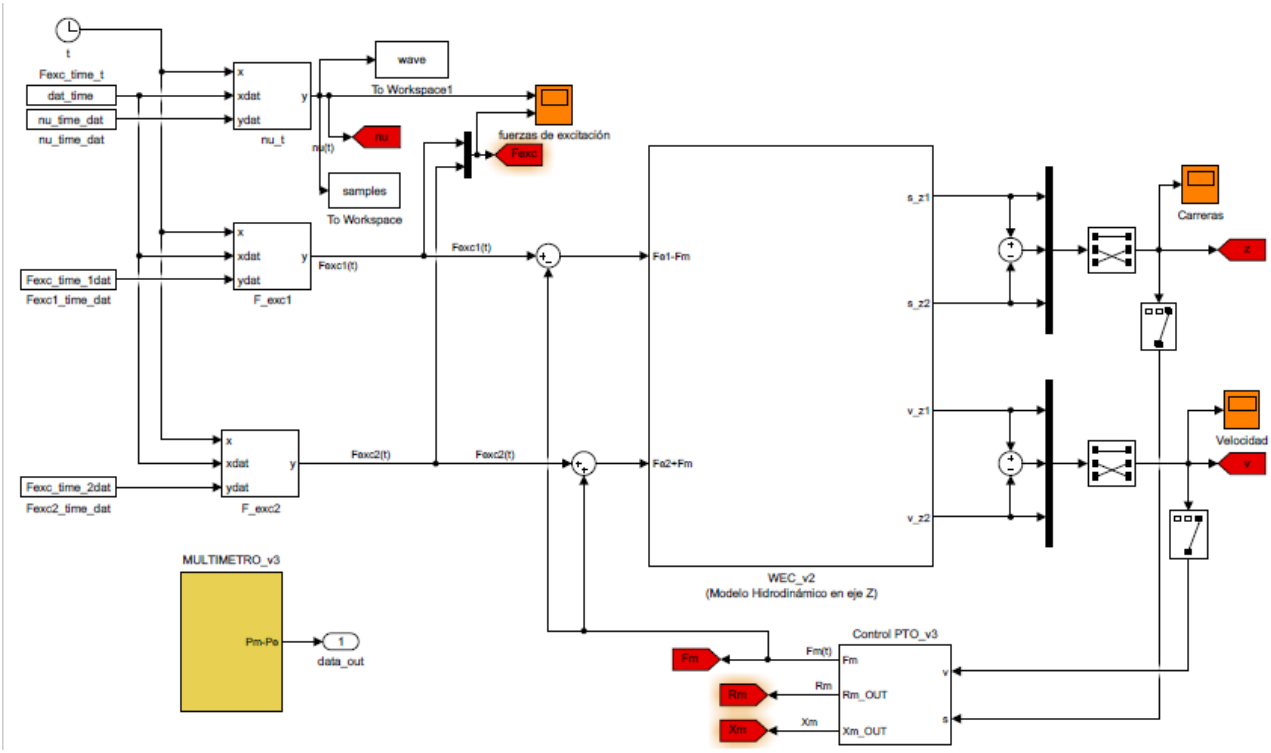

Figure 4.13 – Hydrodynamic Simulink model of a point absorber WEC

This Simulink model represents the hydrodynamic model of a point absorber type of wave energy converter. Given a set of wave profile data, the model calculates all the hydrodynamic parameters and the power generated by the WEC in those conditions. In this simulation the model will be used only to extrapolate the values of wave height needed for the estimation of the autoregressive coefficients in the predictive Matlab code. Therefore, its functioning will not be analyzed in detail.
The total simulation time for this application is 20 minutes, which is representative enough as the wave profile presents many peaks and troughs during this time. The data extracted from the model are used in the Matlab code *AR3.m* (appendix B.5) to build an offline autoregressive process for the one-step prediction of the profile. Apart from using a real wave profile instead of an ideal one, the code works exactly as in the previous examples. Figure 4.14 shows a portion (comprised between 600 s and 800 s from the begin of the simulation) of the complete 20 minutes wave profile extracted from Simulink.

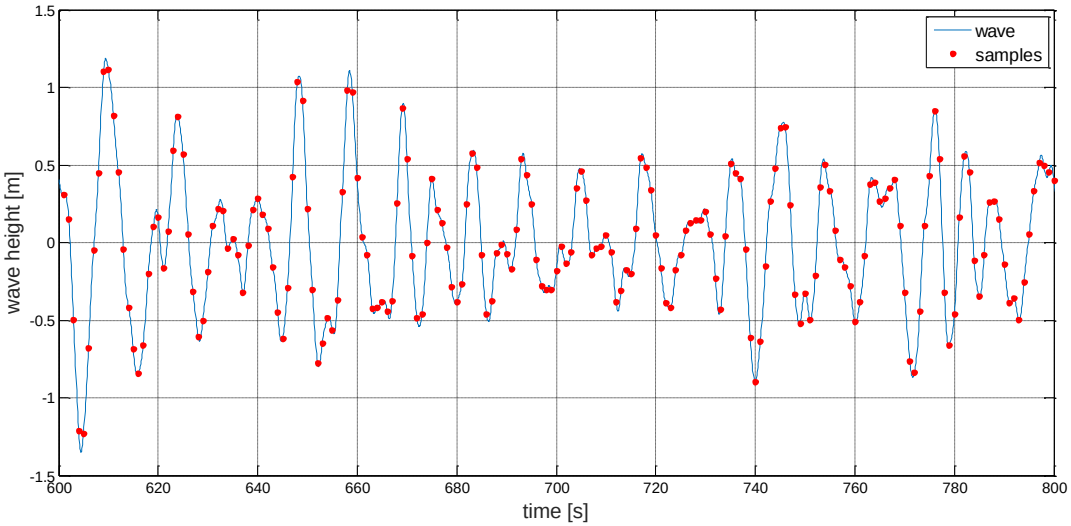

Figure 4.14 – Real wave height profile and samples

The simulations have been repeated using different values for the order of the AR process: 10, 20, 25, and 30. In all of the four cases the estimation of the AR coefficients has given a unique result, in contrast with what happened in the first example of wave made by three harmonics. Regarding the prediction part, again the accuracy is only evaluated through the value of the minimized function J_{MIN} and through a graphic comparison between the predicted profile and the real one. Generally, it looks apparent that increasing the order the two profiles are more similar, so the forecast is better. To illustrate this, figure 4.15 a) and b) compares the original wave with the 1-step prediction resulting from a 10 order model and a 30 order model, respectively.

For the case of order *n*=10, fig.4.15 a), it is possible to notice that in some points the predicted curve deviates from the real wave, while with order *n*=30, fig.4.15 b), the two profiles are almost overlaid.

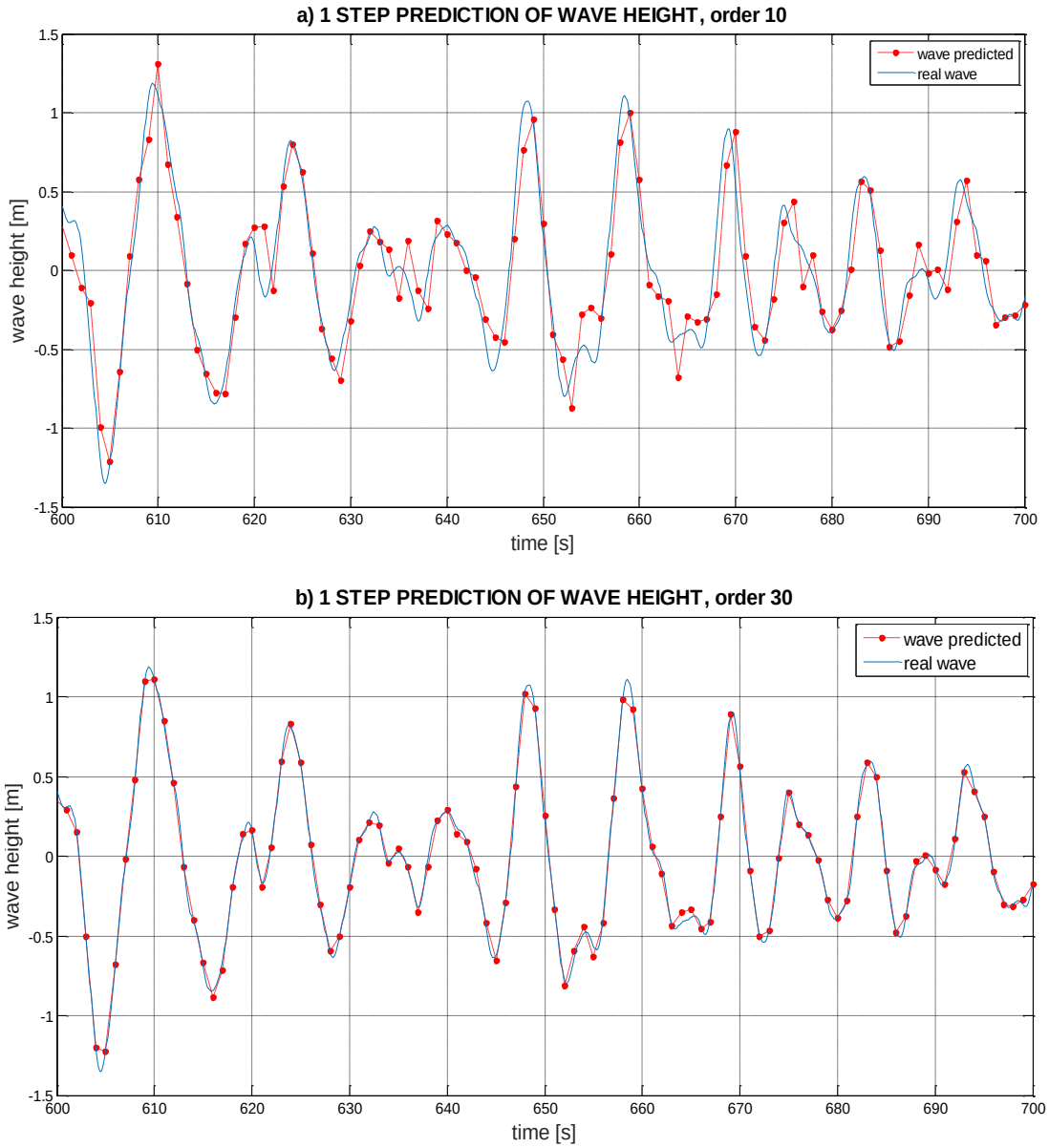

Figure 4.15 – Comparison between a portion of the real wave and its prediction for order 10 (a) and 30 (b)

4.3.4 – Multi-step ahead prediction of a real wave profile

In this code (*AR7.m*, appendix B.6) the information about the wave profile is taken from the same Simulink model of figure 4.13, again for a total time of 20 minutes and with sampling period T_S = 1 s. Therefore, the resulting wave height profile and the number of samples are exactly the same that we used in the one-step prediction code, shown in figure 4.14.

With respect to the previous simulation, in this code two things have been added:

- The estimation of the autoregressive parameters through the minimization of the Long Range Predictive Identification (LRPI) J_{LRPI} function of equation **(10)**, which is more appropriate for a multi-step prediction than the regular least squares approach used so far. The objective function J_{LRPI} has been implemented as a Matlab function, *longpred5.m* (appendix B.7), and the maximum prediction horizon *N2* has been set equal to 20 steps, which means 20 seconds, as the length of a single step is 1 second. The value of *N2* has been chosen because the prediction will not be made for more than 20 seconds ahead (the maximum will be 15 steps, as we will see later), and also because a higher value implies a longer calculation time. Regarding the minimization process, again the solver *fminunc* will be used, initialized with the results of the standard Least Squares estimation.
- The calculation of the index of fitness (equation **(12)**) that gives a numerical measure of the accuracy of the prediction. The index has been implemented in the code through the Matlab function *fitness.m* (appendix B.8).

The simulation for the l -step ahead prediction of the wave height profile has been repeated many times, changing the order n of the AR model and the lead time l. For the order the values of 10-15-20-25-30 have been tested, while for l the values 1-5-10-15 have been used.

The results of all the simulations, in terms of index of fitness, are showed in table 4.1.

Index of fitness for the *l*-steps ahead prediction, N2=20					
n / ***l***	**10**	**15**	**20**	**25**	**30**
1	65,55%	67,00%	83,48%	89,42%	91,83%
5	32,45%	33,04%	38,90%	44,62%	57,65%
10	11,94%	13,36%	17,49%	20,63%	25,32%
15	2,98%	4,66%	8,45%	10,54%	12,38%

Table 4.1 – Index of fitness of the predictions, AR parameters estimated with LRPI approach

Looking at the results, it is evident how the accuracy of the prediction increases with the order of the autoregressive model, with the maximum values achieved for *n*=30, with an index of fitness *FIT* = 91,83% for a 1 second-ahead prediction, and a *FIT* of 12,38% for a 15 seconds-ahead prediction. An order higher than 30 has not been tested because it would require a too long calculation time. The index of fitness also shows clearly that, increasing the lead time *l*, the forecast gets worse. This is totally logical and expected, the further in the future we try to predict, the less accurate will be the prediction, as it will be based on the use of less measured past values and more estimated values. The maximum forecast horizon tested in this work is 15 seconds, and as the values of *FIT* are already very small it does not seem reasonable to predict further.

The estimation of the parameters has been done also with the simpler least squares (LS) approach used in the previous examples for the one-step forecast. These parameters have been used also for a longer-term prediction, to compare with the LRPI method which is supposed to be more appropriate, and the results of the simulations are showed in table 4.2.

Index of fitness for the *l*-steps ahead prediction, N2=1					
n / ***l***	**10**	**15**	**20**	**25**	**30**
1	67,79%	71,38%	86,31%	94,49%	96,85%
5	30,75%	31,42%	35,89%	46,50%	51,48%
10	8,17%	8,77%	11,18%	16,83%	21,16%
15	-1,07%	-0,36%	0,92%	4,92%	7,98%

Table 4.2 – Index of fitness of the predictions, AR parameters estimated with LS approach

Comparing the results of table 4.2 with those of table 4.1, we can notice that for a 1-step ahead prediction the regular least squares method works better, while for longer-term forecasts the estimation done with the Long Range Predictive Identification function gives better results. This is consistent with what presented in the paragraph 4.1.1, as the LS approach is optimized only for a 1-step prediction.

The values of *FIT* are an index of the goodness of the forecast, but they are not exhaustive, also a graphic evaluation is important. Just to have an example, figure 4.16 shows the difference between a portion of the real wave height profile and its 10-steps ahead prediction of order 25, that has an index of fitness of approximately 20%..

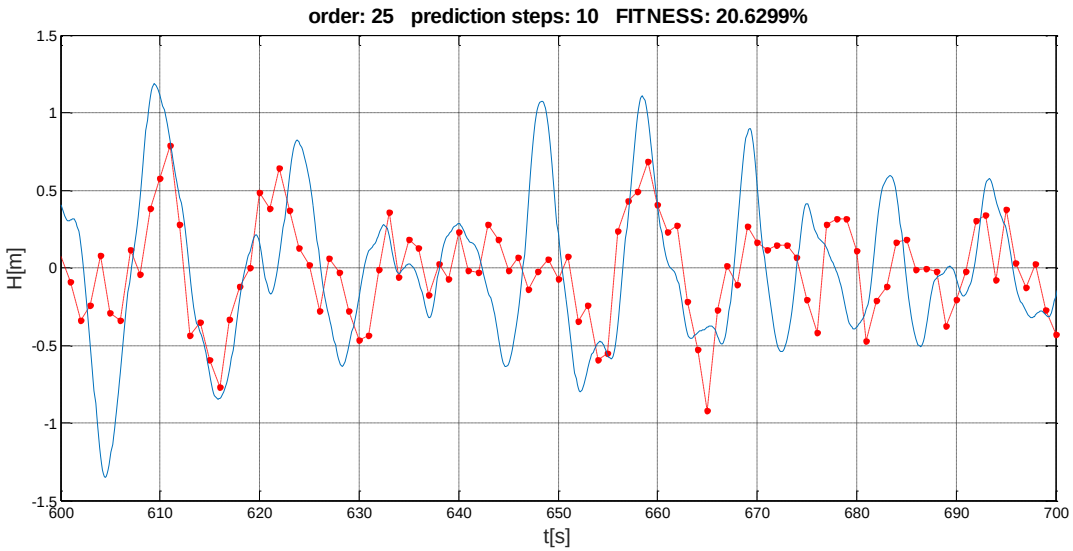

Figure 4.16 – Comparison between the real wave and the 10-steps ahead prediction with order 25

4.3.5 – Multi-step ahead prediction of a low-pass filtered real wave

As discussed in paragraph 4.2.1, the low frequency components of a wave spectra are more energetic and regular than the high frequency's ones. As a consequence, they are also more predictable, and this is the reason why low-pass filter the wave profile could lead to an improvement in the accuracy of the prediction without losing too many information on the signal. To verify the validity of this concept in the practice, a low-pass filter was added to the Simulink model of the point absorber (figure 4.13). This was done through an "Analog Filter Design" block, available in the Simulink's library. With this type of blocks we can decide the filter typology and set the filter order and the cut-off frequency. For this simple application, a standard Butterworth low-pass filter of order 1 has been

chosen. Regarding the cut-off frequency ω_c, two different simulations have been done, one with a cut-off frequency of 1,5 rad/s and the other with $\omega_c = 1$ rad/s. The Simulink Model with the addition of the filter is shown in figure 4.17. Each simulation lasts 20 minutes, and the values of wave height (both filtered and unfiltered) are saved in the Matlab workspace through some "To Workspace" blocks. These values are then used in the Matlab code *ARfilt.m* (appendix B.9) to estimate the autoregressive parameters and predict the wave height. The code is equivalent to the previous one, apart from the fact that it uses the information of filtered wave height for the estimation of the coefficients a_i.

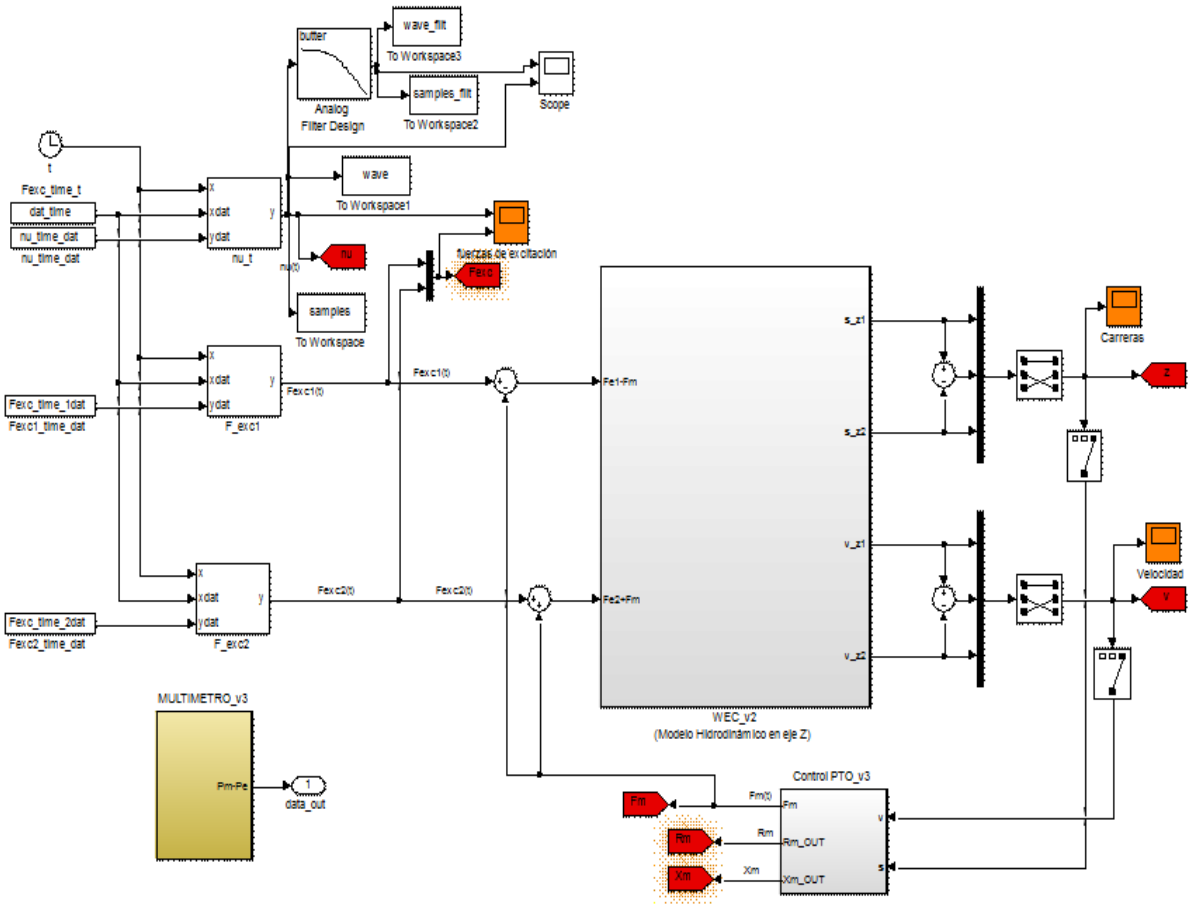

Figure 4.17 – Simulink model of a point absorber WEC with the addition of a low-pass filter to the wave height

For the first simulation, with cut-off frequency ω_c = 1,5 rad/s, the difference between a part of the filtered profile and the unfiltered one is illustrated in figure 4.18.

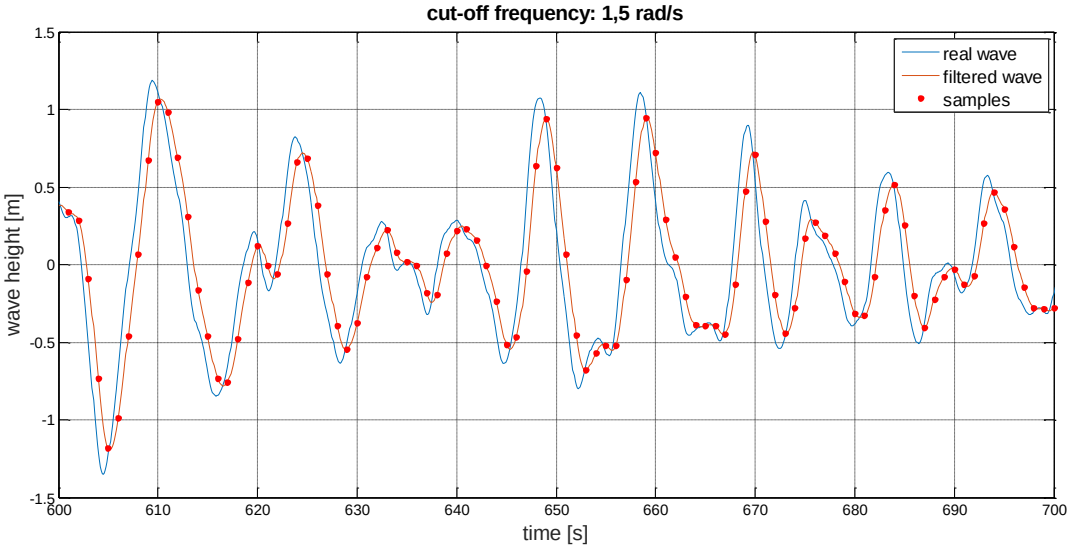

Figure 4.18 – Unfiltered wave height profile (blue) and filtered with ω_c of 1,5 rad/s (red)

From the picture we can see that the filtered signal presents a loss of amplitude and a time delay when compared to the unfiltered one, but their magnitude is not very significant for the purposes of this study. As done in the simulation of the previous paragraph, the prediction code is run many times changing the order *n* of the AR model and the lead time *l*. The results, in terms of index of fitness, are shown in table 4.3:

Index of fitness for the *l*-steps ahead prediction, N2=20					
n / ***l***	**10**	**15**	**20**	**25**	**30**
1	74,17%	74,40%	86,03%	91,31%	88,24%
5	39,70%	40,73%	46,01%	52,79%	53,86%
10	14,47%	16,98%	21,19%	24,88%	25,35%
15	3,57%	5,60%	10,03%	12,57%	12,77%

Table 4.3 – Index of fitness of the predictions, ω_c = 1,5 rad/s

Comparing these results with those of table 4.1, obtained without any filter, we can see that the values of the index are higher of a few percentage units, around a 4-5% on average. This is not true for order 30, that presents almost the same

values that it had without filtering the signal. Obviously, in this case filtering the wave height signal is not worth it.

Figure 4.19 shows a portion of the predicted wave profile for a 10-steps ahead forecast of order 25.

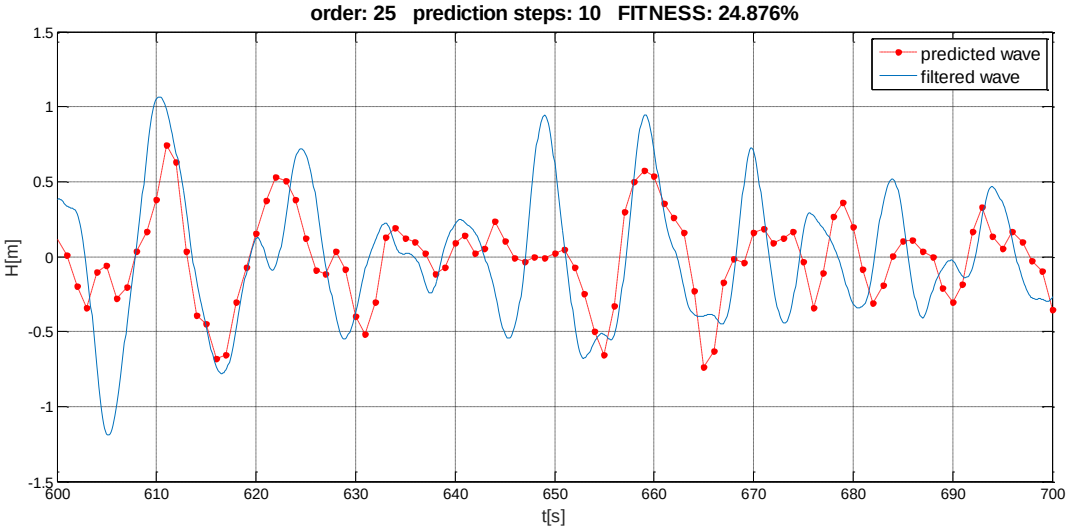

Figure 4.19 – Comparison between the filtered wave and the 10-steps prediction with n = 25, ω_c = 1,5 rad/s

The prediction of fig.4.19 has an index of fitness of 24,88%, while the prediction of fig.4.16 (same order and lead time but without filter) had a value of 20,63%. Thus, the improvement is clear, but not very large.

With a lower value of cut-off frequency, the improvement is expected to be higher. If we set the value of ω_c equal to 1 rad/s, the resulting profile is the following:

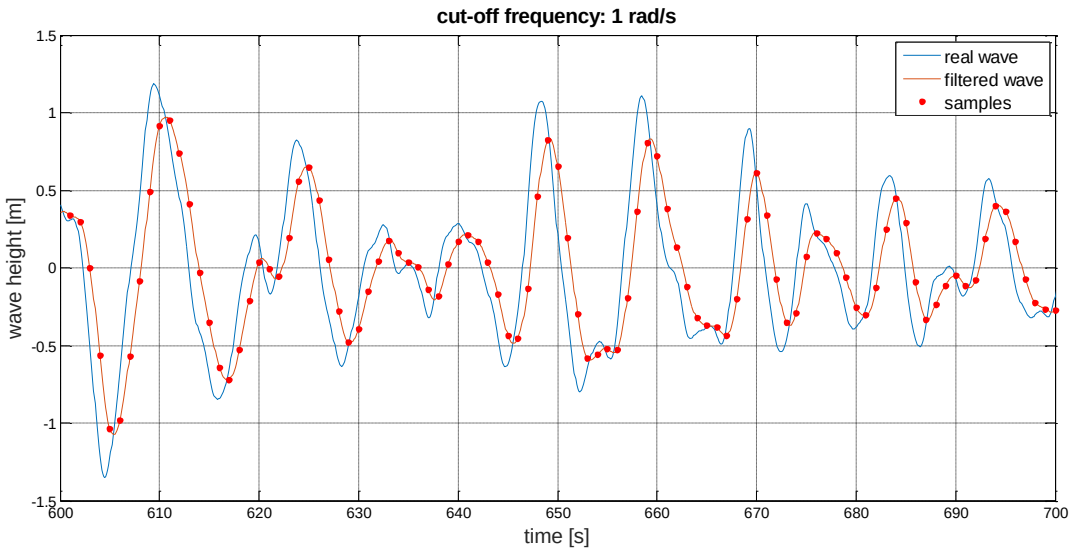

Figure 4.20 – Unfiltered wave height profile (blue) and filtered with ω_c of 1 rad/s (red)

As the value of ω_c is lower than in the previous case, more frequency components of the wave are filtered, and this is why the loss of amplitude from the original signal is larger, and the delay is becoming more significant.

If we run the Matlab code with this cut-off frequency many times, changing the order and the prediction horizon, the results are illustrated in table 4.4.

Index of fitness for the *l*-steps ahead prediction, N2=20					
n \ ***l***	**10**	**15**	**20**	**25**	**30**
1	77,09%	77,01%	87,23%	92,01%	88,79%
5	43,67%	45,15%	50,44%	57,38%	57,87%
10	16,09%	19,40%	24,09%	28,00%	28,35%
15	3,96%	6,32%	11,39%	13,99%	14,49%

Table 4.4 – Index of fitness of the predictions, ω_c = 1 rad/s

As expected, with a lower cut-off frequency the values of the index are higher. For the particular case of 10 steps of prediction with order 25, the value of *FIT* is 28%, compared to the 24,88% with a ω_c of 1,5 rad/s and with the 20,63% with no filter. The accuracy improves, but not in a very significant way. The predicted profile for the case under consideration is depicted in fig.4.21.

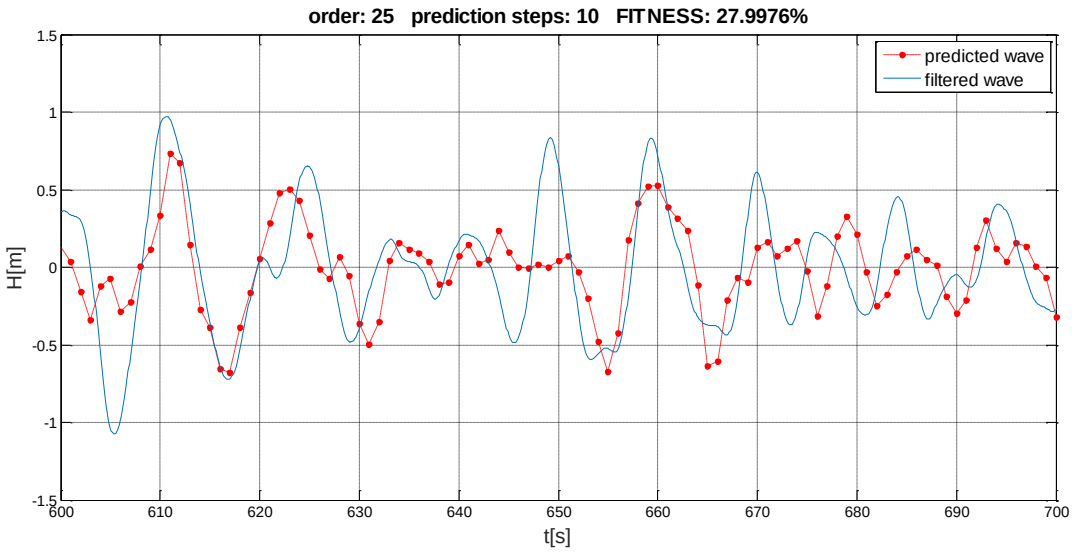

Figure 4.21 – Comparison between the filtered wave and the 10-steps prediction with n = 25, ω_c = 1 rad/s

4.4 – Prediction of wave power

In paragraph 4.3 we have seen the development of a predictive method based on AR models and applied to the prediction of the wave height of a real sea wave profile. However, it is necessary to remind that the final aim of the work is to smooth the oscillating power produced by the wave energy converter through a storage system, and that the control of the smoothing system that we want to develop requires the prediction of the produced power, and not of the wave height. For this reason, the autoregressive predictive method will be used in this section to try to predict the power generated by the WEC. If for a wave height profile the validity of the AR method has been demonstrated, for a power profile it is not obvious and it has to be tested.
Two different approaches were tried:

- Direct prediction of the power through an autoregressive model, replying exactly what previously done with the height of the waves.
- Indirect prediction of the power: the AR method is applied to predict the oscillation velocity of the point absorber WEC and the force induced by the PTO (Power Take-Off) equipment, and the power is calculated as the product of these two variables.

4.4.1 – Direct prediction of the power

As already seen in the previous paragraphs for the height, the l -step ahead prediction of the power with an AR model of order *n* is calculated as:

$$P_{pred}(k+l|k) = \sum_{i=1}^{n} a_i(k)\, P_{pred}(k+l-i|k) \qquad (\mathbf{14})$$

The coefficients a_i need to be estimated through the minimization of the following objective function:

$$J_{LRPI} = \sum_{k=1}^{N} \sum_{j=N1}^{N2} \left[P(k) - P_{pred}(k|k-j)\right]^2 \qquad (\mathbf{15})$$

Equations **(14)** and **(15)** are equivalent to equations **(6)** and **(10)** respectively, with the only difference that the values of wave height have been replaced by the values of power.

The data of power are extracted from the Simulink model of figure 4.13, representing a point absorber WEC. The model is run for 20 minutes always with the same sea state used previously, and the values of power are sent directly to the workspace of Matlab, to be used in the code *ARpower.m* of appendix B.10.

The resulting WEC power profile is illustrated in fig. 4.22. The values of power are sampled again every one second (sampling frequency of 1 Hz), and they are used for the estimation of the coefficients of the AR model.

In this case the power signal has not been low-filtered, also because the use of a filter for the wave height prediction didn't lead to a very significant improvement in the accuracy of the prediction. In addition, the smaller improvements induced by the filter with respect to a prediction without filter were obtained in the case of order 30 of the AR model, which is the same order that will be used here for power.

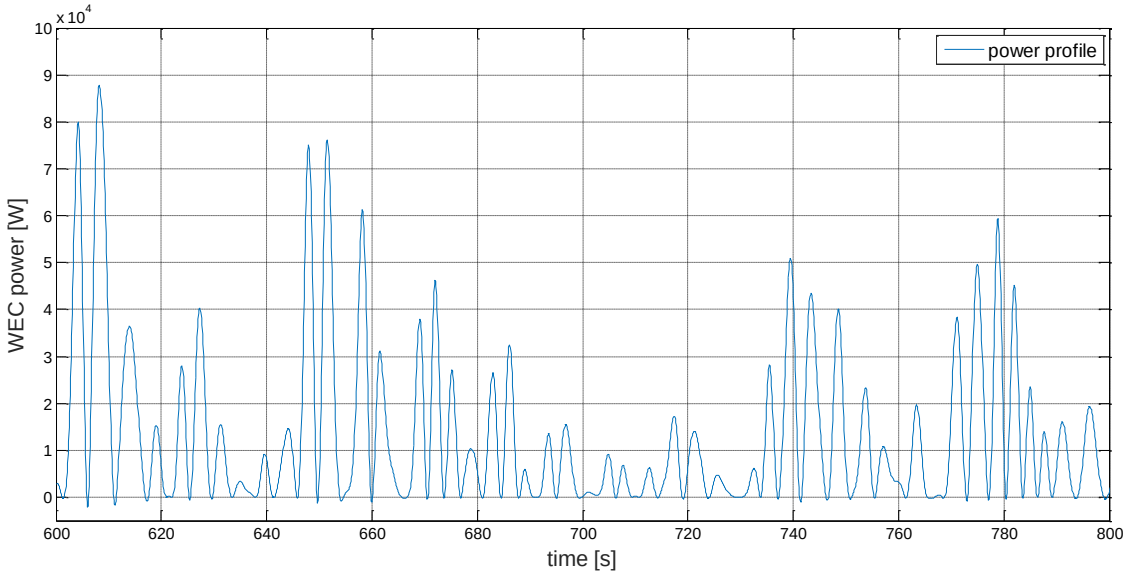

Figure 4.22 – Profile of the power absorbed by a point absorber WEC

Running the code with order 30, the prediction by the use of an autoregressive model has given, in terms of index of fitness, the results shown in table 4.5.

prediction steps	1	5	10
lead time	1 s	5 s	10 s
index of fitness	55,84%	26,11%	15,67%

Table 4.5 – Index of fitness of the direct power prediction

The results are considerably worst compared with those of the unfiltered prediction of wave height made with the same order (table 4.1). For example, for the 1-second ahead prediction we have a fitness index of 55,84%, very low compared to the approximately 90% that we had for the wave elevation in the same condition. This is not unexpected, since the shape of the power profile is very different from the height's one. In the wave height case, indeed, the profile presents many oscillations of small amplitude around a near to zero mean value, while in this case the power curve is almost completely above zero and it shows much bigger oscillations in terms of relative amplitude. As a matter of fact, height is a combination of sinusoidal waveforms, but power is more similar to a combination of squared sinusoidal waveforms. Therefore, AR models seem to be not very appropriate for the direct prediction of power.

4.4.2 – Indirect prediction of the power

Because of the not very good results achieved with the direct prediction, another approach has been tested. It consists in an indirect prediction of power, in the sense that power is calculated from a combination of other predicted variables. More specifically, the instantaneous mechanical power absorbed by the WEC can be calculated as the product of the oscillation velocity v of the point absorber and the PTO force F_{PTO} [31]:

$$P = F_{PTO} \cdot v \qquad (16)$$

This mechanical power differs from the electric power generated by the WEC only because of the power losses in the generator.

Both force and velocity have an oscillating profile more similar to the behavior of the wave height profile with respect to the power, that has a quadratic behavior compared to them. Thus, it is reasonable to think that autoregressive models are more suitable for the prediction of these two variables than in the case of the direct prediction of power. For this reason, the prediction of power in this section is done indirectly, as the variables predicted with AR models are force and velocity, and power is calculated only in the second place.

The values of force and velocity are taken, coherently with the previous simulations, from a 20 minutes run of the point absorber Simulink model of fig.13, and imported in the Matlab workspace. Thereafter, they are used in a Matlab code identical to the one used already for the prediction of height and power.

The curves representing the profile of the PTO force and the oscillation velocity are illustrated respectively in figures 4.23 and 4.24. As we can see from the figures, their shape is more similar to the wave height profile with respect to power, so they look more suitable for the use of AR models.

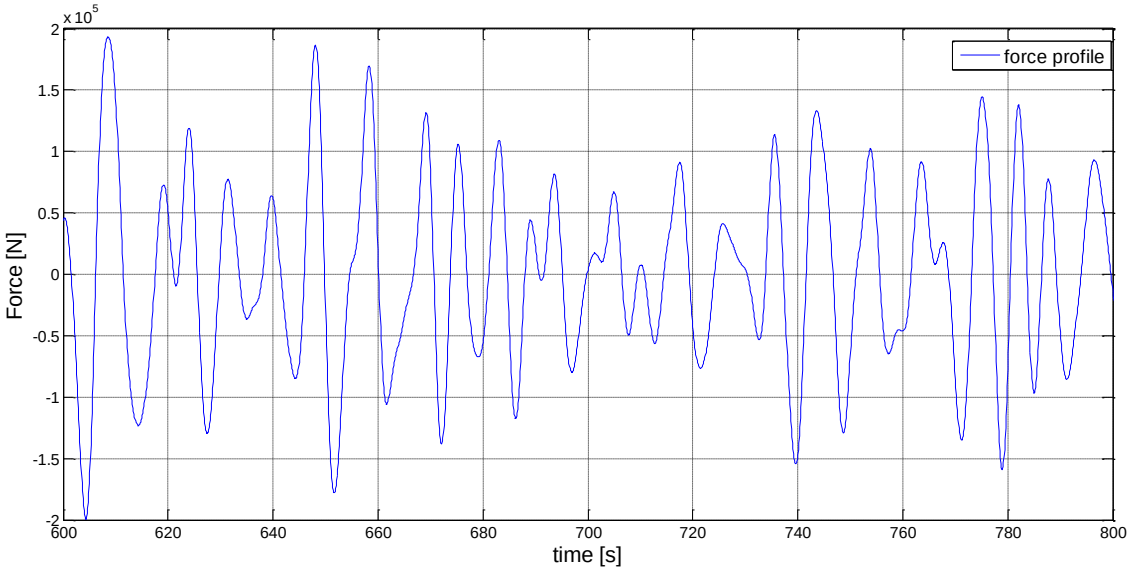

Figure 4.23 – Shape of the PTO force profile

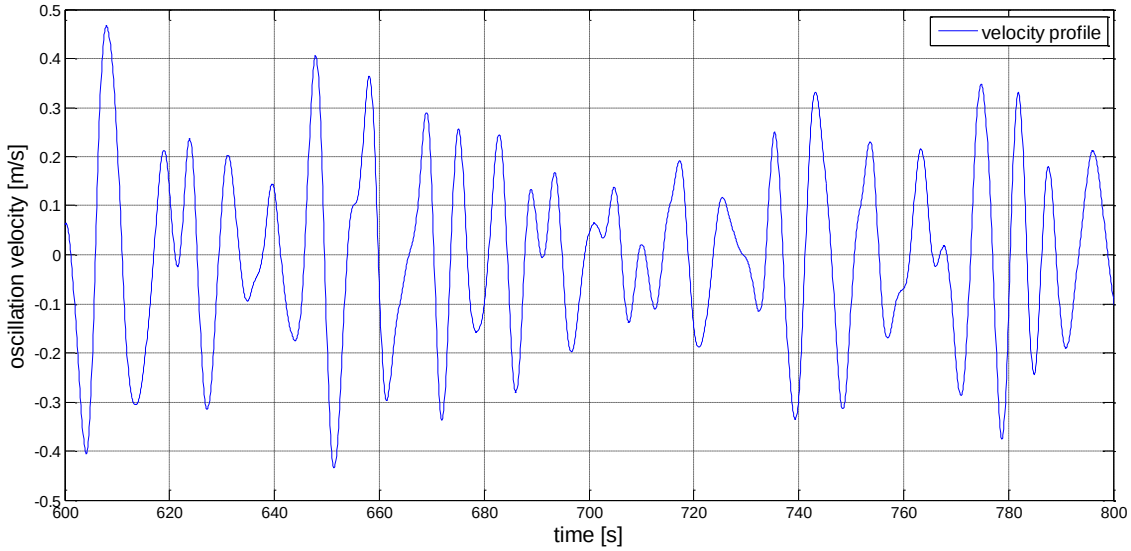

Figure 4.24 – Shape of the WEC oscillation velocity profile

Again with a sampling period of one second and order 30 of the AR model, the prediction of force and power has given the values of index of fitness shown in table 4.6.

Prediction steps *l*	1	5	10
PTO force	80,79%	37,66%	11,64%
velocity	83,57%	38,44%	11,98%

Table 4.6 – Index of fitness of the prediction of force and velocity

We can see that the values of the index are very similar in the two cases, and better than the values obtained for power, although the decrease with time is relatively fast. As previously said the predicted force and velocity are then multiplied to find the indirect forecast of the power absorbed by the WEC. Calculating the index of fitness of the indirect power prediction with respect to the real power profile, we achieve the results of table 4.7.

Prediction steps *l*	1	5	10
Power: $P = F_{PTO} \cdot v$	76,66%	30,92%	8,07%

Table 4.7 – Index of fitness of the indirect prediction of power

Comparing the results of the direct and the indirect power prediction, we can notice that in the short horizon the indirect method is significantly more accurate,

while the *FIT* value for a 10 seconds-ahead prediction is better in the case of direct forecast. The fact that the indirect method loses precision faster makes sense. The multiplication of two estimated variables, indeed, means that also their relative errors are multiplied, and therefore the resulting error for power will be larger than the single errors of force and velocity. When the prediction steps are increased, the errors in the forecast get larger, and this is why the quality of the indirect prediction decreases rapidly.

The results obtained in terms of length and accuracy of the prediction clearly show how none of the two analyzed methods are optimal for the forecast of the power of a wave energy converter. However, the aim of this work is not the power prediction in itself, but to use someway this prediction to mitigate the fluctuations of the power sent to the grid by the WEC. Therefore, the achieved results could be good enough for this application. This will be analyzed in the next chapter, where the AR predictive method will be integrated in a supercapacitor-based Power Smoothing System (PSS).

5 – INTEGRATION OF AR PREDICTION IN THE SIMULINK MODEL OF A POWER SMOOTHING SYSTEM

In this part of the work, the predictive code developed in the previous chapter will be integrated in the control of a Simulink model of a supercapacitor-based PSS (Power Smoothing System). The model, that was already built by the CIEMAT research group, is known as “APOGEO model”. The name APOGEO comes from a project based on an energy storage device to compensate the power oscillations in an electric generation system from the wave energy. This model will be presented in the first section of the chapter. Afterwards, different simulations will be done with it, using at first a control system based on a Moving Average (MA) criteria, and then trying to replace it with the AR approach.

5.1 – The APOGEO model

The APOGEO Simulink model represents basically a wave farm producing power and supplying it to the electric grid, with an energy storage based on Electric Double-Layer Capacitors (EDLC), commonly called supercapacitors, used to smooth the output power. The model includes also the control system and all the power electronic components. The main view of the model is depicted in fig 5.1.

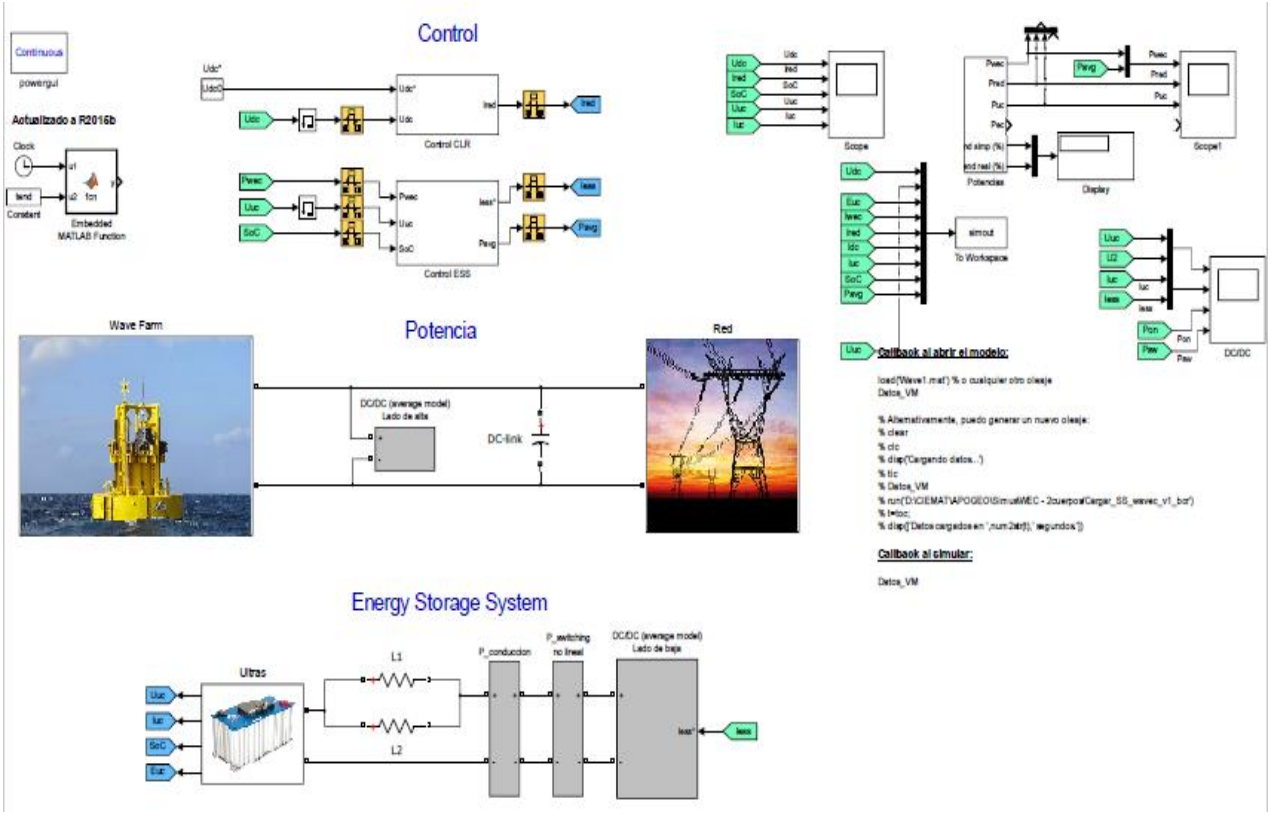

Figure 5.1 – Main view of the APOGEO Simulink model

Three main sections can be identified in the model, each of which includes in turn different subsystems:

- Power system (fig. 5.2), composed by the wave farm and the grid, with a DC-Link capacitor between them. The wave farm block comprises the point absorber hydrodynamic model used in the previous chapter, to get the power produced by the WECs starting from a certain set of data of regular or irregular sea waves, and also the control for the power take-off.

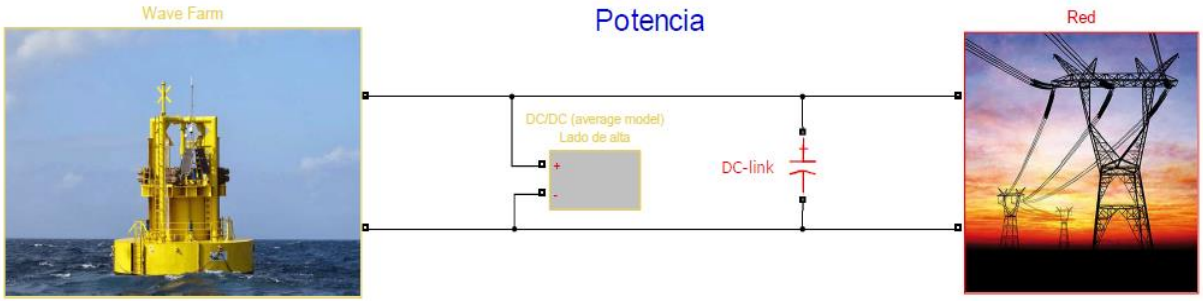

Figure 5.2 – APOGEO model: power system

- Energy Storage System, fig 5.3, including the supercapacitors and their connections. The model contains also the calculation of the power losses for conduction and the switching.

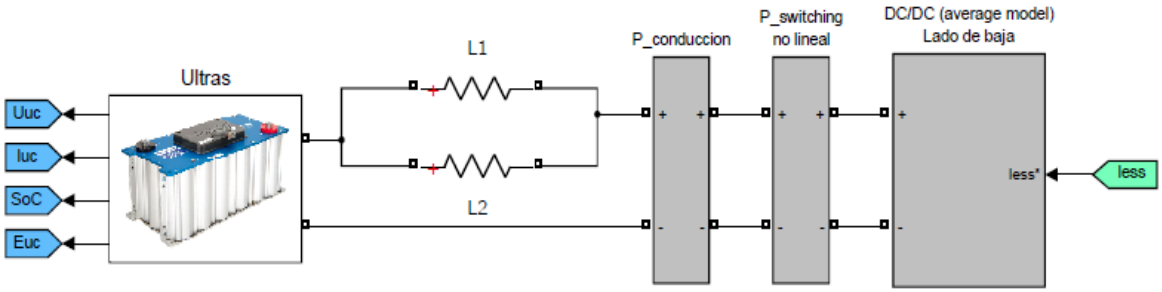

Figure 5.3 – APOGEO model: Energy Storage System

- Control subsystems, fig. 5.4, including two controls: the control for the power converter (which is supposed to keep constant the voltage on the DC-Link) and, more importantly, the control for the ESS, which is the subsystem where the focus is put and that will be modified for our simulations in order to implement the autoregressive prediction.

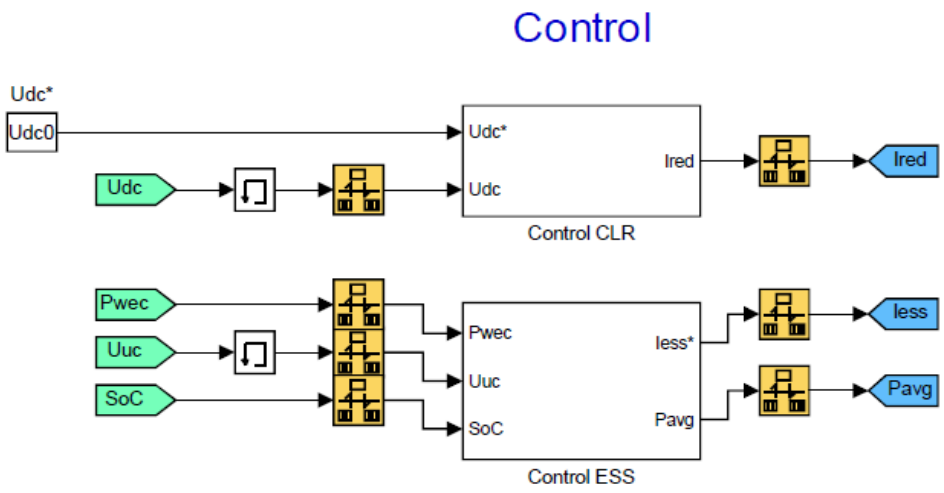

Figure 5.4 – APOGEO model: control subsystems

The controls included in the two boxes of fig. 5.4 are shown in fig. 5.5 a) and b).The first one is the control for the converter, while the second one is the control system for the supercapacitors implemented by CIEMAT group, which works with a Moving Average (MA) criteria.

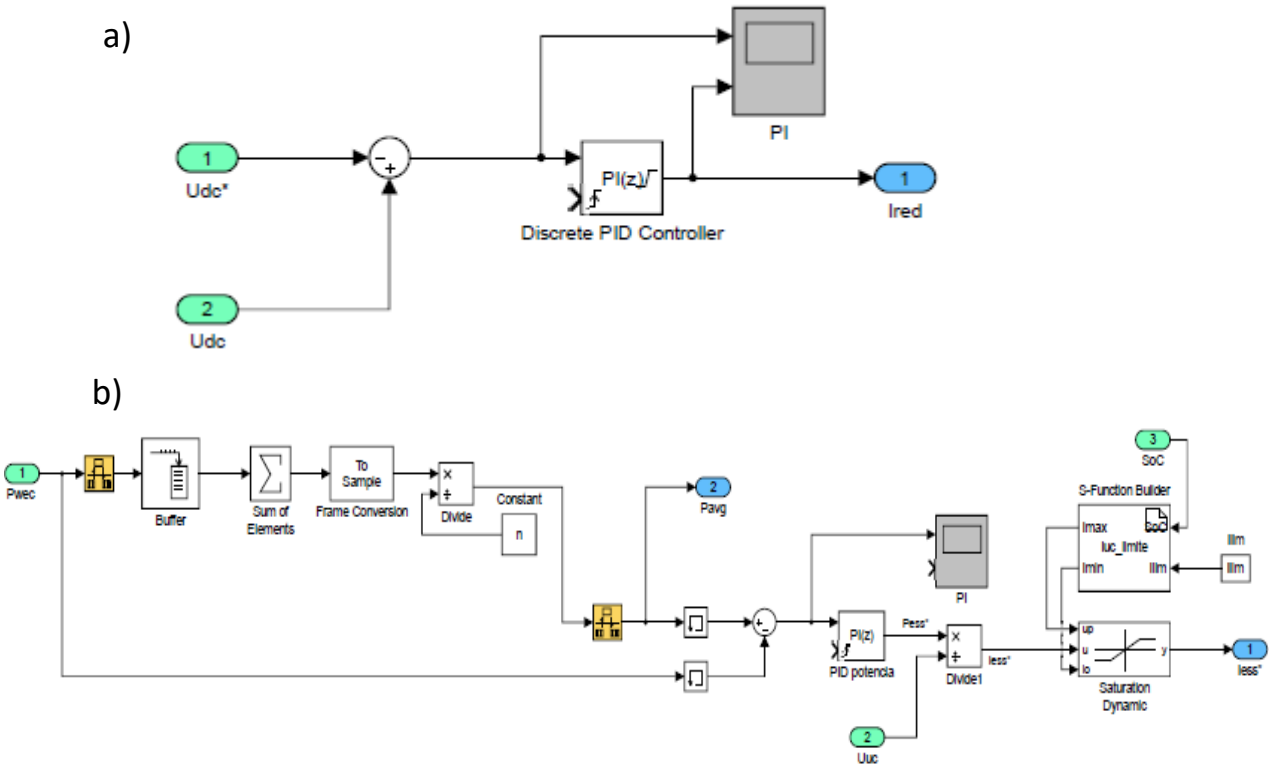

Figure 5.5 – APOGEO control systems: a) control of the power converter, b) control of the ESS

The input for the ESS control is the power P_{wec} produced by the wave energy converters, taken from the wave farm subsystem. With the MA approach, in a certain moment a buffer extracts a fixed number n of past values of P_{wec}. The arithmetic mean P_{avg} of those n values is then calculated, using a block "Sum of Elements" and a block "Divide":

$$P_{avg} = \frac{\sum_{i=1}^{n} P_{wec,i}}{n} \qquad (17)$$

This procedure is repeated and updated in every step of the simulation, and the buffer extracts always the n most recent values of P_{wec}. Thus, the constant n can be considered as the width of a moving window, which instant by instant moves forward, calculating the average P_{avg} of the last n values of P_{wec}. The value of P_{avg} is used as a reference value of power for the storage system, because in every instant it is compared with the instantaneous power P_{wec} produced in that moment through a simple calculation of the difference between them, P_{ess}*.

$$P_{ess}^{*} = P_{avg} - P_{wec} \qquad (18)$$

When the instantaneous power produced by the WECs is bigger than the average reference value ($P_{wec} > P_{avg}$), the value of P_{ess}* is negative. In this case the WECs are producing a power bigger than P_{avg}, which is the value that we want to provide to the grid, keeping it as constant as possible. Therefore, the negative value of P_{ess}* represents a surplus of power, and it will be used to charge the supercapacitors.

On the other hand, when P_{ess}* is positive ($P_{wec} < P_{avg}$), it means that the power produced by the WECs is less than the reference, and in order to maintain a certain power level in the grid, an additional power has to be released by the supercapacitors. During this phase, thus, the superconductors are partially discharged, as a certain amount of energy is taken from them and injected into the grid.

The power generated by the wave energy converters presents many oscillations, as seen in the previous chapters, so there will be many short cycles of partial charge and discharge of the supercapacitors in order to compensate the fluctuations. However, the power provided to the grid will not be perfectly constant, as the value of the arithmetical average power P_{avg} is not always the same, but it changes with time.

In the next paragraph some simulations will be carried out with this control based on a moving average approach, changing the width of the moving window to see how the system reacts.

5.2 – Simulations with Moving Average approach

Before integrating the autoregressive prediction code in the APOGEO model, some simulations have been made using the control system for the ESS of fig. 5.5 b), based on the MA approach explained in the previous section.

The wave data set used to run the model is the same used in chapter 4, coming from the observations taken from a buoy in the Biscay Marine Energy Platform (BIMEP), in the Cantabrian Sea, at the North coast of Spain. The data are loaded through the file *Wave1.mat*, and they will be used for the calculation of the power generated by the WECs, P_{wec}. The values of power are quite big, and in these

simulations they have been reduced by the multiplication for a scale factor, called *MB*, of 0,02, in order to allow us to compare the results with those obtained in the CIEMAT laboratory test bench, in which it is not possible to work with a too high level of power, without affecting the simulation results.

The values of all the variables needed in the model are fixed in a Matlab code, *Datos_VM.m* (appendix B.11). In this script the electric variables of the components included in the model are defined, together with other parameters required by the model.

The most relevant of them are resumed in the following table.

Wave farm
MB = 0,02 (scale factor)
DC-link
Udc0 = 120 V (initial and rated DC voltage) Cdc = $12*10^{-3}$ F (capacitance)
Supercapacitors
Uuc = 80 V (total operating voltage) Cuc = 90 F (total capacitance)

Table 5.1 – Values of some of the parameters required for the APOGEO model

To check the efficiency of the moving average control system in smoothing the WEC output power we have done multiple simulations of 10 minutes, changing for each of them the width of the moving window. The width of the window is defined in terms of time: a moving window of 10 seconds, for example, means that in every instant of the simulation the control system calculates the average value of the instantaneous power produced by the WECs in the last 10 seconds, and uses this value as a reference for the storage system, as previously explained. The number of values contained in the window depends on the sampling time. According to the resulting value of average power, the supercapacitors used for the energy storage will be charged or discharged.

The first simulation has been done with a moving window of 12 seconds, and then the width has been gradually increased. To have a numerical evaluation of the efficiency of the system in terms of smoothing power, we introduced an index that has been called Smooth Index (*SI*). It is based on the statistic concept of Standard Deviation (*SD*), normally used to quantify the dispersion of a set of data values from the mean.

The standard deviation is calculated as follows:

$$SD = \sqrt{\frac{\sum_{i=1}^{N}(P_{grid,i} - P_{grid,avg})}{N}} \quad [W] \qquad (\mathbf{19})$$

The terms $P_{grid,i}$ and $P_{grid,avg}$ refer respectively to the instantaneous power provided to the grid and to the arithmetic average power supplied in the 10 minutes period of the simulation, while *N* is the total number of discrete values contained in that period of time.

Once calculated the standard deviation *SD*, the smooth index is determined as:

$$SI = \left(1 - \frac{SD}{P_{grid,avg}}\right) \cdot 100 \qquad (\mathbf{20})$$

While *SD* gives a measure in Watts of the mean distance of the values of instantaneous power from the average, the smooth index *SI* is a measure in percentage of how much the profile of power provided to the grid is smoothed. The bigger is the value of *SI*, the more smoothed is the profile. A value of 100% would mean to have a perfectly smoothed profile, which would be the case of a constant value of power.

The results of the simulations are collected in table 5.2. In the table we can find the width of the moving window, the maximum and minimum values of instantaneous power supplied to the grid ($P_{grid,max}$ and $P_{grid,min}$) during ten minutes of simulation time, the average power provided in the same period, the standard deviation, and finally the smooth index.

width of the window	$P_{grid,max}$	$P_{grid,min}$	$P_{grid,avg}$	SD	Smooth Index
[s]	[W]	[W]	[W]	[W]	[%]
12	1191,3	27,5	372,3	236,2	36,57%
16	1003,6	45,1	371,8	207,7	44,06%
20	1020,5	68,2	370,4	189,1	48,94%
24	1010,1	66,2	369,4	176,5	52,22%
28	905,9	63,1	368,1	166,7	54,72%
32	874,1	61,7	366,9	158,1	56,92%
36	831,9	83,6	366,0	150,4	58,91%
40	779,1	100,0	365,2	143,5	60,70%
44	722,8	119,2	364,4	137,5	62,26%
48	684,3	118,1	363,6	132,2	63,64%
52	640,9	120,5	362,5	127,4	64,85%
56	634,3	120,9	361,3	123,4	65,84%
60	617,8	118,3	360,2	119,9	66,70%
64	589,9	147,8	359,2	117,0	67,42%
68	579,0	169,9	358,2	114,4	68,06%
72	577,7	169,3	357,4	112,0	68,66%
76	581,0	167,3	356,5	109,8	69,20%
80	569,2	162,6	355,7	107,9	69,66%
84	570,5	181,7	354,9	106,3	70,04%
88	565,5	190,0	354,0	105,1	70,32%
92	557,5	181,4	352,8	104,1	70,49%
96	544,4	173,8	351,4	103,2	70,63%
100	523,7	166,9	350,1	102,4	70,76%
104	508,2	160,4	348,8	101,8	70,81%
108	514,2	154,5	347,4	101,6	70,75%
112	515,9	148,9	346,1	101,7	70,62%
116	507,3	143,8	344,8	101,8	70,47%
120	504,1	139,0	343,5	102,1	70,27%
150	467,7	111,0	334,7	107,6	67,83%

Table 5.2 – Results of the simulations with different values of the width of the moving window

For increasing values of width, the tendency showed by the results is that also the smooth index increases, reaching a maximum value of 70,81% with a window of 104 s (highlighted in yellow in table 5.2). This seems perfectly reasonable, as a bigger window means that the average power P_{avg} calculated as a reference for the MA control will have a more constant value, implying that also the power provided to the grid is more constant. Coherently with this statement, we can see that the maximum and minimum values of power supplied to the grid respectively

decreases and increases as the width increases. As a consequence, the profile of the instantaneous power absorbed by the grid will be more smoothed.

At the end of each simulation some graphs are also generated to help to the evaluation and analysis of how the system worked. In fig. 5.6 some of these graphs are illustrated, for the case of moving window of 24 seconds. From the top of fig 5.6. to the bottom, we can see the graphs of the DC-link voltage, the WEC output power, the power injected to the grid, the power absorbed or released by the ESS, and the state of charge (SoC) of the supercapacitors.

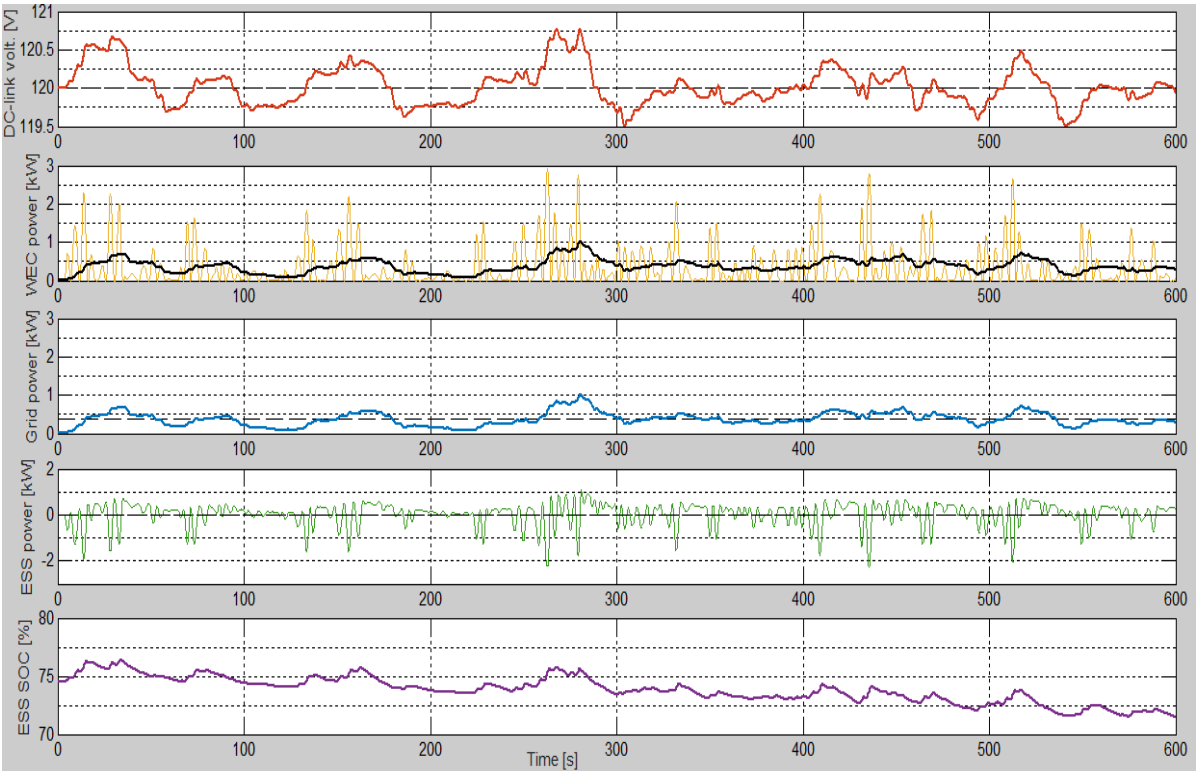

Figure 5.6 – Graphical results in the case of width of the window = 24 s

In the first graph the red line represents the DC-link voltage, controlled to be maintained equal to the reference of 120 V. The voltage presents some fluctuations, but in general it doesn't move too far from the reference. In the second graph, in yellow there is the oscillating power produced by the WECs, while the black line represents the values of the average power P_{avg} of the moving window. As in this case the width of the window is small, the value of P_{avg} changes significantly during the total time of the simulation, increasing strongly when there are peaks of produced power. The third graph, in the center, is the most interesting for the purpose of these simulations, as it shows the profile of the

power supplied to the grid. Without the energy storage, this profile would be identical to the yellow one of the WEC power, but in this case it is evidently more smoothed, and this is exactly what the supercapacitor-based Power Smoothing System is supposed to do. In addition, it is important to notice how the blue curve representing the instantaneous power delivered to the grid has a shape very similar to the black curve of P_{avg}. The reason is that P_{avg} is the reference value of power that we want to provide to the grid, so P_{grid} follows this reference.
To draw a comparison, in figure 5.7 the same graphs are reported for the case of width of the window of 104 seconds, in which the value of the smooth index is the maximum registered among all the simulations carried out.

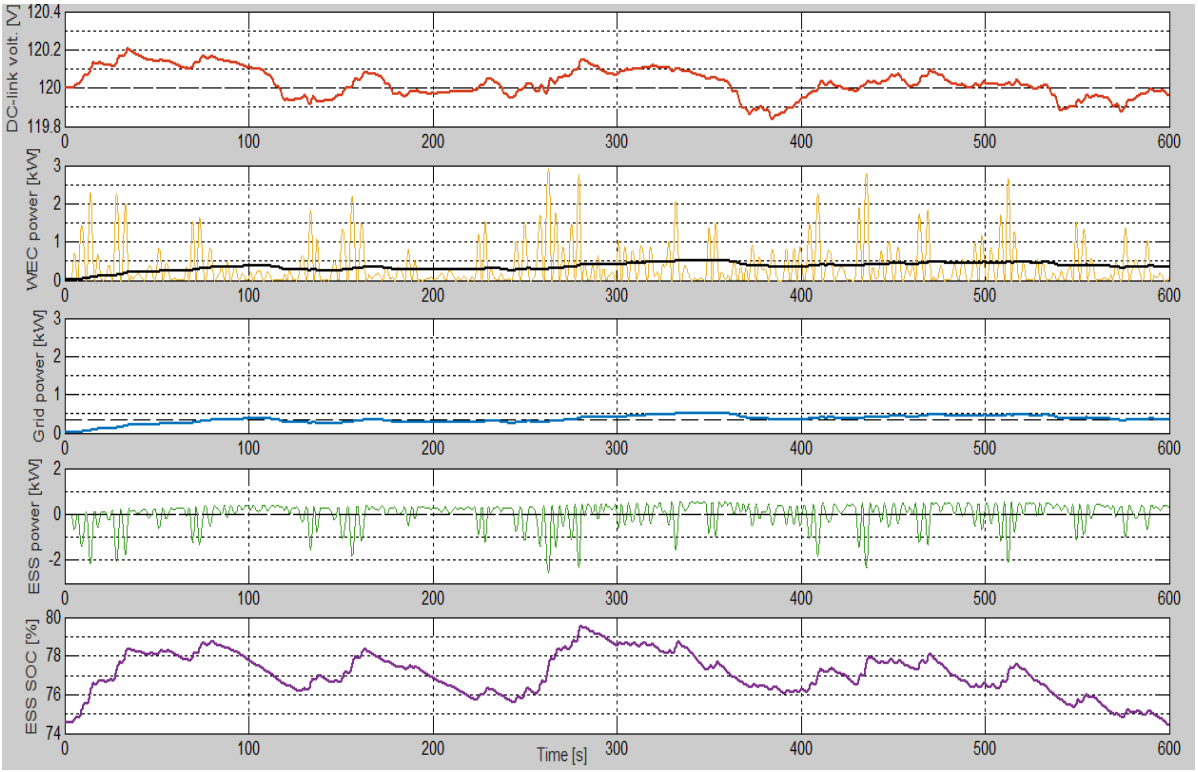

Figure 5.7 – Graphical results in the case of width of the window = 104 s

Looking at the graph of the grid power (blue curve), it looks immediately evident that in this case the power is clearly more smoothed than in the previous one, without any large fluctuation around the mean value. As a consequence, the likelihood of having stability problems or other grid integration issues (discussed in chapter 3) is significantly reduced.

On the other hand, the average value of power delivered to the grid decreases as the width of the moving window increases, as we can see from the results of table 5.2. The reason is that with a larger window, more power is exchanged with the storage system, and hence, the losses are bigger. Moreover, since more energy needs to be stored, the state of charge of the supercapacitors increases with a bigger moving window width. This implies a bigger storage capacity required and therefore a higher cost for the storage system. The best choice for the width, thus, will be a compromise between these considerations and the improvement of the power quality of the grid, as usually happens in engineering's problems.

5.3 – Integration of the AR prediction in the APOGEO model

The purpose here is to replace the control system for the ESS of fig. 5.5, based on the moving average approach, with another one that uses the prediction of WEC power made with an autoregressive model. In chapter 4, two different methods have been assessed for the prediction of power: the direct prediction through AR models, and an indirect forecast obtained from the multiplication of the AR predictions of the power take-off force F_{pto} and the oscillation velocity of the WEC v.

In the APOGEO model we will use the indirect approach, which has shown a higher accuracy in the very short term compared to the direct prediction. The Simulink model for the implementation of the indirect power prediction is shown in figure 5.8, and it will be included as a part of the control system.

To integrate in Simulink the prediction code developed in the previous chapter it is necessary to use a block "S-Function Builder", which works with the programming language C. Therefore, the code written in Matlab language has been translated in C so that it can be read by this type of block. In the model of fig. 5.8 there are two S-Function Builder blocks, one for the prediction of velocity (the upper one) and one for the prediction of force (the one on the bottom). Velocity and force (that in the model are called respectively *vPablo* and *Fm*) are

taken from the hydrodynamic model of the WEC contained in the wave farm block of fig. 5.2, using two “From” blocks.

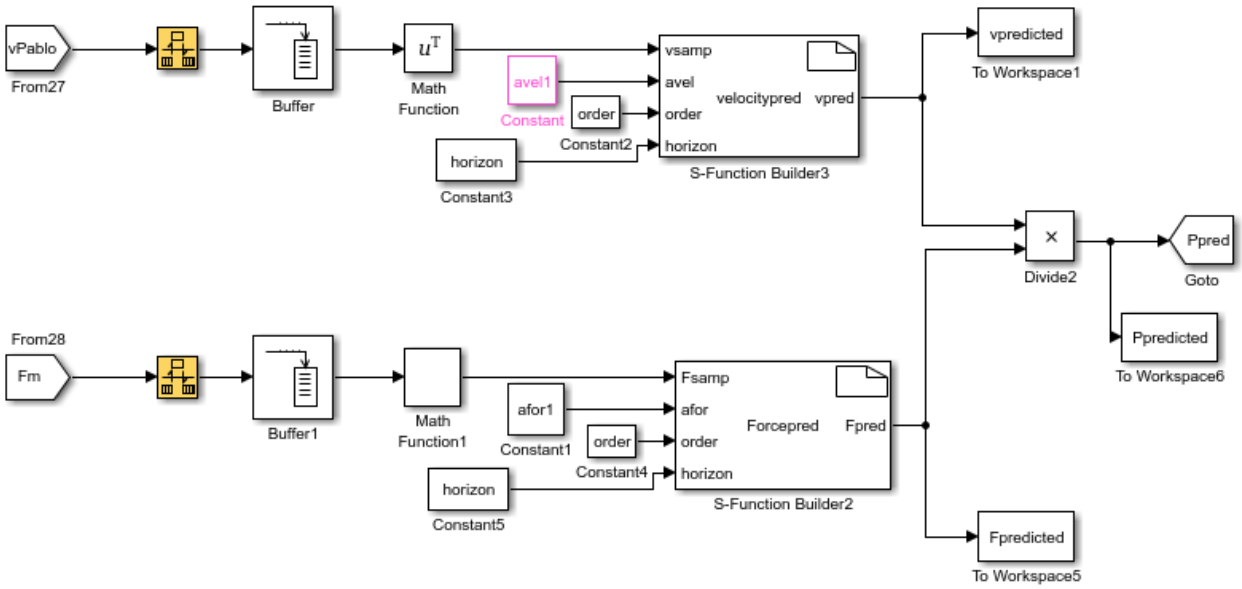

Figure 5.8 – Simulink model of the indirect prediction of WEC power

The two yellow blocks are “Rate Transition” blocks and they are responsible for changing the sampling time. Consistently with what was done so far, for the prediction we will use a sampling time of one second and an order of 30 for the AR process.

The two Buffers collect a fixed number of values of velocity and force, that has been set equal to the order of the AR model. As a consequence, at each step of the simulation the Buffer extracts the last 30 values of the concerned variable, and sends it to the S-function Builder as a first input. The other inputs for this block are the autoregressive coefficients a_i, the order and the *horizon*, defined as the number of steps in the future that we want to predict. The AR coefficients have to be estimated offline before running the APOGEO model, through the optimization procedure presented in chapter 4. As already seen, an online adaptive estimation, extremely more difficult to implement, is not necessary, as it is proved that a static offline AR process keeps its validity for more than two hours [23].

Regarding the horizon, we will repeat the simulation with a 5, 10 and 15 steps-ahead prediction respectively. The outputs of the two S-Function Builder blocks are the predicted force and velocity, in the form of vectors of 5, 10 or 15 values

depending on the chosen forecasting horizon. The two vectors (force and velocity) are then multiplied to each other to finally get the WEC power indirect prediction.

Now that we have a prediction of the power produced by the wave farm, the next issue to deal with is to use it in the control system of the supercapacitors with the aim of smoothing the power provided to the grid. More specifically, the purpose is to use the predicted profile to get a reference average value of power to deliver to the grid, and regulate the cycles of charge and discharge of the storage system according to this reference value.

The adopted solution is to proceed similarly to the case of moving average, calculating the average of *n* past values of instantaneous power and l predicted values, where *n* is now the order of the model and l is the prediction horizon. Thus, the reference value of power will be calculated as the arithmetical mean of $n+l$ values. With a 10 steps-ahead prediction of order 30, for example, the control will calculate the average power P_{avg} of the last 30 values and the 10 predicted values of power. From here on out, the control system works exactly as in the moving average case. P_{avg} is the value of power that has to be supplied to the grid: when the WEC power is bigger than P_{avg}, the surplus of power will be used to charge the supercapacitors, while when P_{wec} is smaller than P_{avg}, the supercapacitors will release an additional amount of power to the grid.

The new control system working with the autoregressive prediction is depicted in fig. 5.9.

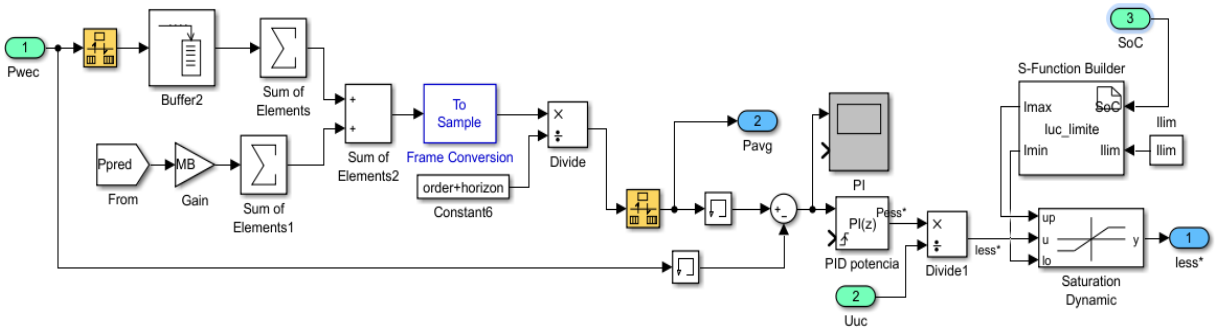

Figure 5.9 – Simulink model of the predictive control system of the energy storage

The control system of the above picture is the only part that has been modified of the APOGEO model presented at the beginning of the chapter. With this new control, three different simulations of 10 minutes each have been made, changing the prediction horizon. It is important to underline that in this case the power level has been also reduced by a scale factor of 0,02, to adapt the power generation levels to the power values later tested in the CIEMAT laboratory during the experimental part of the work. Working always with the same wave profile and maintaining the same values for the functioning parameters of the supercapacitors, the DC-Link and the other components, the results of the three simulations are those collected in table 5.3. The table shows the values of the maximum and minimum instantaneous power delivered to the grid, the average power, the standard deviation, and the Smooth Index, calculated with the use of equation **(20)**.

pred. steps	$P_{grid,max}$	$P_{grid,min}$	$P_{grid,avg}$	standard deviation	smooth index
/	[W]	[W]	[W]	[W]	[%]
5	835,8	75,1	358,7	148,3	58,64%
10	747,7	70,4	330,3	133,1	59,70%
15	667,.4	64,8	298,7	119,3	60,00%

Table 5.3 – Results of the simulations with different prediction horizon for the AR model

The values of the smooth index for the three cases are very similar, around 60%, while with the moving average control a maximum value of approximately 71% was reached. Increasing the prediction horizon, the smooth index improves a little bit, but the average power provided to the grid decreases significantly.

To have also a graphical evaluation of the results, the same graphs already analyzed in the moving average case have been produced. In fig. 5.10 we can see these graphs for the 10 seconds-ahead prediction.

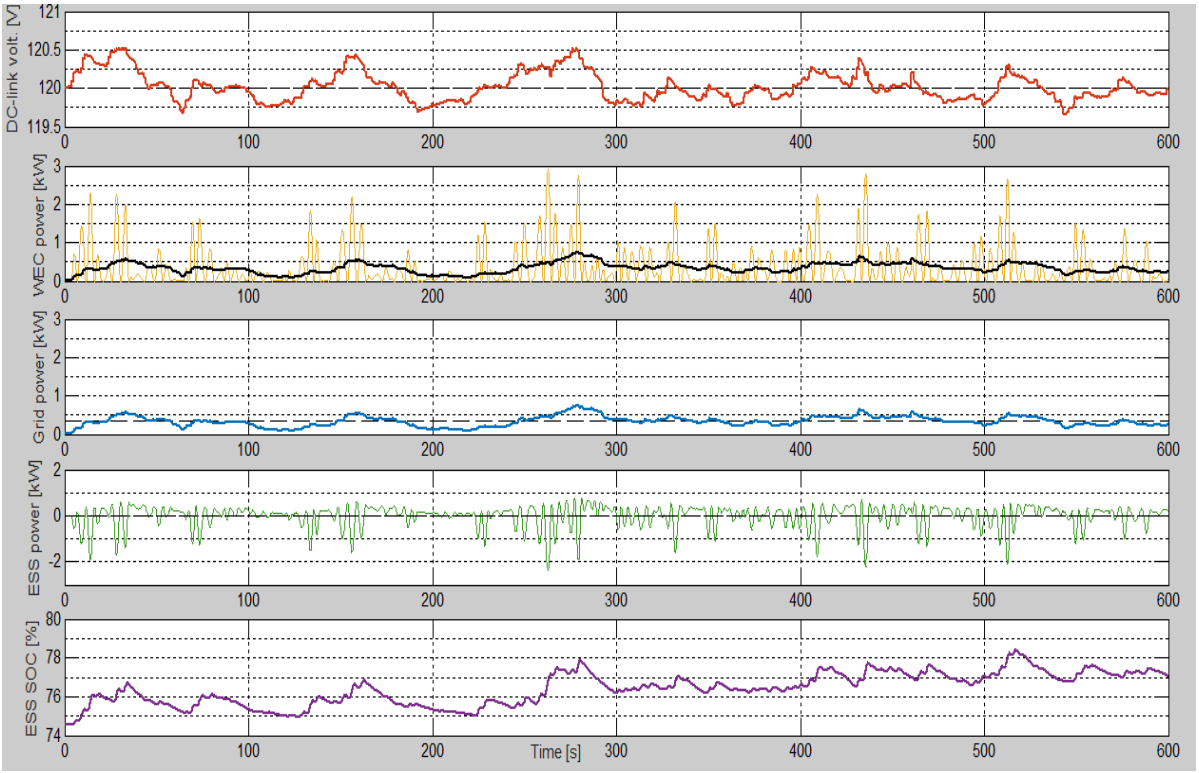

Figure 5.10 – Graphical results in the case of control system based on a 10 steps-ahead prediction

Looking at the third graph, in the middle, it looks clear that this control system works, in the sense that the profile of the power supplied to the grid looks deeply smoothed compared to the WEC power (yellow curve), but it does not improve the control system based on the moving average approach already implemented by the research group of CIEMAT.

In the next chapter, the operation of both the controls will be practically tested in laboratory.

6 – LABORATORY TESTS

In chapter 5 the validity of the supercapacitor-based power smoothing system has been verified through different simulations with the software Matlab-Simulink. In this chapter, the practical operation of the system will be tested in the CIEMAT laboratory, where a test bench is used to emulate wave power oscillations and to partially suppress them by means of an energy storage system before being supplied to a load.

First of all, the laboratory test bench will be presented, with its main components and characteristics. After that, different tests will be carried out with a moving average control system and changing the width of the moving window. Finally, the control based on the autoregressive prediction will be tested, and the results of all these tests will be analyzed and compared.

6.1 – Laboratory Test Bench

The laboratory platform used in the work, whose scheme is depicted in fig. 6.1, consists of three different power subsystems: the wave energy converter (WEC) or the wave farm (WF), the energy storage system based on the use of supercapacitors, and the electrical grid. Each subsystem is circled with a different color in the scheme, to be easily distinguished.

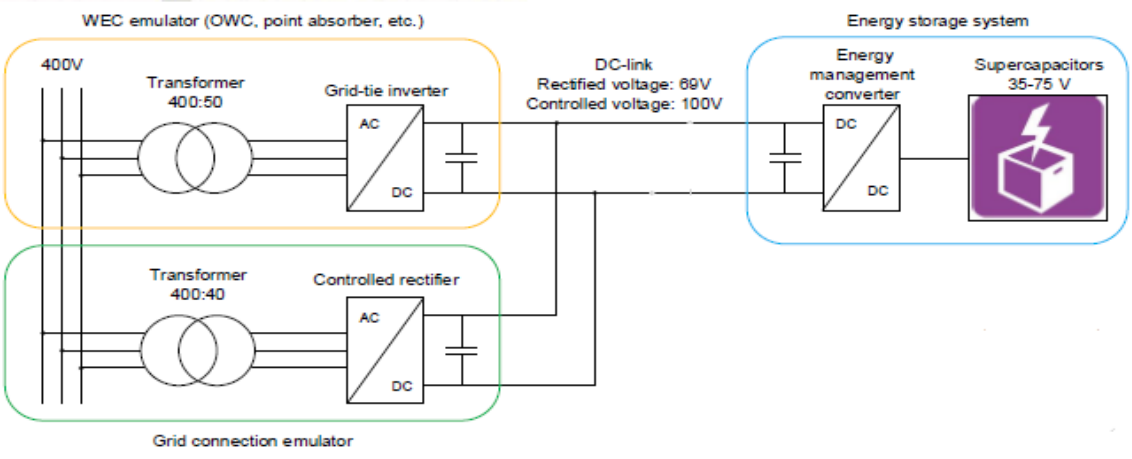

Figure 6.1 – Scheme of the laboratory test bench

In the test bench, some of these subsystems are real, while others are emulated. The WEC/WF part, for example, needs to be emulated so that different sea states, types, number and distribution of WECs, as well as different working conditions can be tested. Conversely, the electrical grid and the ESS are real. In particular, the ESS is a completely real system capable to be installed in a WEC or WF.

All of the aforementioned subsystems are illustrated in the scheme of fig. 6.1, together with the DC-link, referring to the DC connection between the different power electronics converters that represent the system parts. The DC-link, however, is not a physically distinguishable element, but it actually comprises all the capacitors of all the power electronic converters connected together.

The main specifications of the test bench are collected in table 6.1.

Subsystem	***Specifications***		***Subsystem***	***Specifications***	
	Magnitude	***Value [units]***		***Magnitude***	***Value [units]***
DC-link	Capacity	6 mF	ESS	Type	EDLC
	Rated voltage	100 V_{DC}		Rated volt. (1 module)	16 V_{DC}
WEC emulator	Grid voltage	400 V		Rated volt. (total)	80 V_{DC}
	Transf. ratio	400:50		Capacity	430 F
	Transf. power	80 kVA		Inductive link	3 mH

Table 6.1 – Laboratory platform technical specifications

More specifications about the supercapacitors or EDLC (Electrochemical Double-Layer Capacitor) can be found in the manufacturer datasheet (table 6.2).

Item	Performance	
Operating Temperature Range	-40 °C to +65 °C	
Storage Temperature Range	-40 °C to +70 °C	
Rated Voltage	16.2 V DC	
Capacitance Tolerance	+20%	
Resistance Tolerance	Max.	
Temperature Characteristics	Capacitance Change	Within ± 5% of initial measured value at 25 °C (at -40 °C)
	Internal Resistance	Within 150% of initial measured value at 25 °C (at -40 °C)
Endurance	After 1500 hours application of rated voltage at 65 °C	
	Capacitance Change	Within 20% of initial specified value
	Internal Resistance	Within 60% of initial specified value
Shelf Life	After 1500 hours storage at 65 °C without load shall meet specification for endurance	
Life Test	After 10 years at rated voltage and 25 °C	
	Capacitance Change	Within 30% of initial specified value
	Internal Resistance	Within 150% of initial specified value
Cycle Test	Capacitors cycled between specified voltage and half rated voltage under constant current at 25 °C (1 million)	
	Capacitance Change	Within 30% of initial specified value
	Internal Resistance	Within 150% of initial specified value

Table 6.2 – Datasheet of the supercapacitors

Concerning the power electronic converters, as shown in the scheme of fig. 6.1 there are three converters, one for each subsystem. All of the three converters are three-phase IGBT's power converters, but they have different functions in the test bench. The specifications of these converters are contained in table 6.3, taken again from the manufacturer datasheet.

Absolute maximun ratings			$T_{AMBIENT} = T_{AIR\ COOLING}$ = 40°C unless otherwise specified			
Symbol	**Conditions**		**Values**			**Unit**
$I_{OUT\ MAX}$	Maximum continuous output current		**200**			A_{RMS}
$V_{OUT\ MAX}$	Maximum output voltage		**500**			V_{AC}
$V_{BUS\ MAX}$	Maximum DC Bus voltage in operation		**900**			V_{DC}
F_{OUT}	Inverter Output frequency		**500**			Hz
F_{SW}	Maximum switching frequency		**25**			kHz
Electrical characteristics			$T_{AMBIENT} = T_{AIR\ COOLING}$ = 40°C unless otherwise specified			
Symbol	**Conditions**		**min**	**typ**	**max**	**Unit**
AC phase						
$I_{OUT\ RATED}$	Rated output current	V_{BUS}=750Vdc, No overload, Tj<150°C, Power factor PF = 1, Cabinet airflow in operation at 400m3/h Fan airflow through heatsink at 900 m3/h		**200**		A_{RMS}
V_{OUT}	Output voltage			**400**		V_{AC}
P_{OUT}	Rated output power			**140**		kW
F_{SW}	Inverter switching frequency			**3**		kHz
F_{OUT}	Output frequency			**50**		Hz
DC Bus						
V_{BUS}	Rated DC voltage			**750**		V_{DC}
Efficiency						
$P_{LOSS\ INV}$	Total power losses				**1 915**	W
η	Inverter efficiency				**>98**	%
Filtering characteristics						
V_{BUS}	Rated DC voltage applied to the caps bank without switching				**1 100**	V_{DC}
$V_{DC\ CAPACITOR}$	Max DC voltage applied to the caps bank (max 30% of LTE) without switching				**1 100**	V_{DC}
$\tau_{d5\%}$	Discharge time of the capacitors (5%)			**285**		s
CDC	Capacitor bank capacity		**1,43**		**1,68**	mF
LTE	Calculated LTE of the caps with forced air cooling				**> 100**	kH
Stack Insulation						
V_{ISOL}	Frame / Power stage AC/DC (insulation test voltage DC, 60s)				**3 200**	V

Table 6.3 – Datasheet of the power converters

In the following subsections more specific information for all the three subsystems involved will be given. An overall view of the laboratory test bench is illustrated in fig. 6.2, in the next page.

6.1.1 – Wave farm emulator

The WF is emulated using an AC/DC power converter, which is connected to the 400 V grid by means of a transformer with ratio 400:50 V. Thus, the converter works in this case as a controlled rectifier, receiving alternate current from the transformer as an input, and providing direct current as output. The rectifier is

operated with an active power reference given by a certain profile in the time domain. This subsystem could emulate different types of WECs. For the tests presented later in this chapter, however, we will refer only to the case of point absorber WECs, whose reference power profile is taken from the Simulink hydrodynamic model used in chapter 4. This subsystem, therefore, is responsible for generating an oscillating profile of power comparable to the one that would be generated by a real point absorber, and for providing it to the grid or to the ESS.

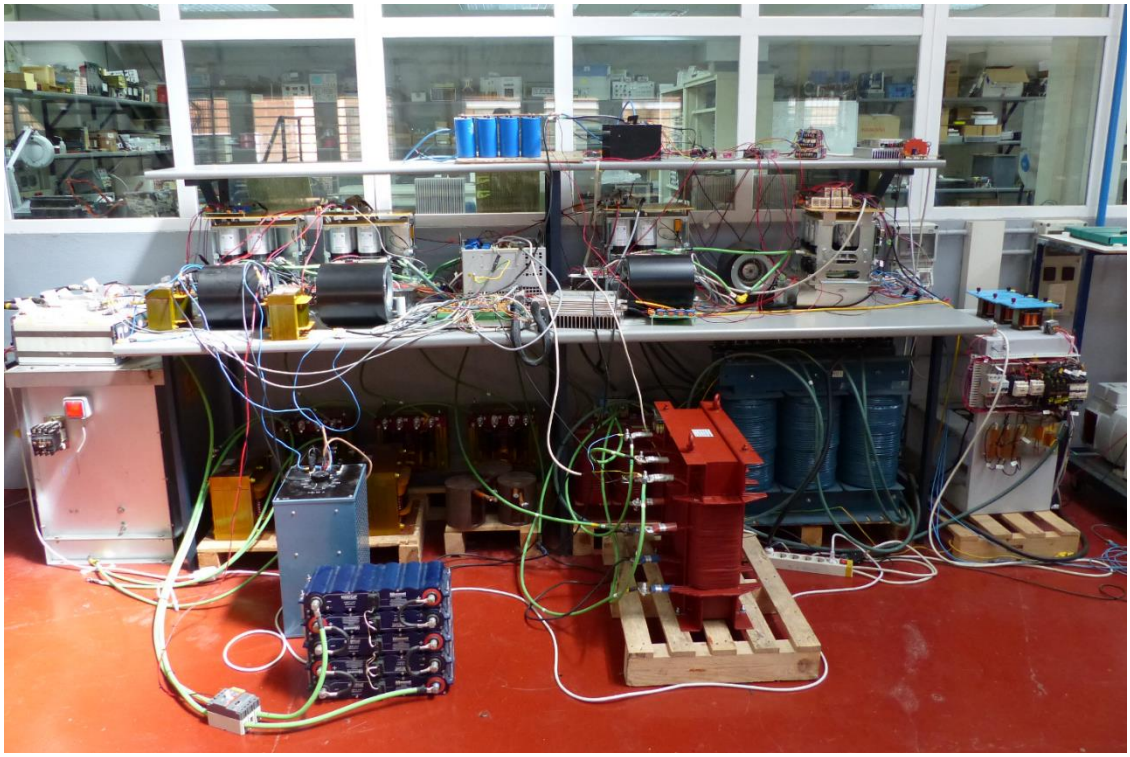

Figure 6.2 – Overall view of the laboratory test bench

6.1.2 – Grid connection emulator

This subsystem comprises also a power electronic converter, connected in DC to the common DC-link and in AC connected to the electric grid, that can withdraw some power from the DC-link and send it to the 400 V electrical grid through a transformer. If the power smoothing system works correctly, the profile of power delivered to the grid by means of this subsystem will not have all the fluctuations that normally characterize a wave power profile. Instead of being transmitted to

the grid, the power oscillations are partially absorbed by the third subsystem, the supercapacitor-based ESS.

6.1.3 – Energy Storage System

This subsystem comprises three elements: the supercapacitors, a DC/DC power converter, and an inductive link with inductance of 3 mH placed between the first two. Consistently with the observations made in chapter 3, the supercapacitors were chosen as storage system for this application because of their power density and energy efficiency, their higher useful life (in terms of number of cycles) compared to batteries, and their easiness of installation.
There are 5 modules of supercapacitors of 16 V each and they are connected in series, for a total rated voltage of 80 V and a capacity of 430 F. Each module is in turn composed by the series of 6 cells with a voltage of 2,7 V each. In fig. 6.3 a photo of the used supercapacitors is shown.

Figure 6.3 – Supercapacitors used in the test bench (5 modules connected in series)

The process of charge and discharge of the supercapacitors is controlled by the bidirectional DC/DC converter. This converter has also the function of controlling

the DC-link voltage and keeping it constant, adapting consequently the ESS voltage.

The control system for the DC/DC converter is depicted in the scheme of fig. 6.4 and it corresponds to the one used also in the simulations of the APOGEO model. The upper part is the power smoothing loop, which calculates a current reference I_{ess}* using a PI controller whose input is the power error, defined as the average power P_{avg} minus the instantaneous power P_{wec}. The average power P_{avg} can be calculated either with the moving average approach or the autoregressive prediction, as seen in the previous chapter.

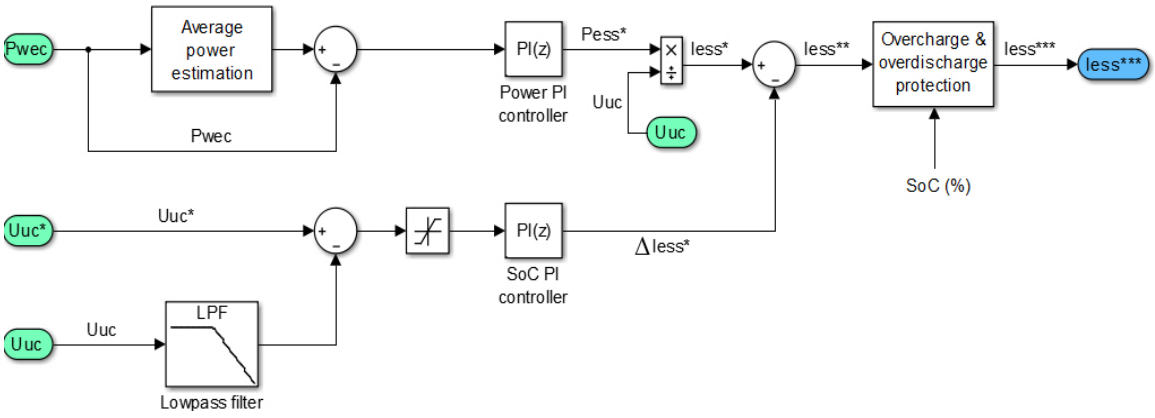

Figure 6.4 – Control scheme for the ESS with SoC compensator

The bottom part, the State of Charge (SoC) compensator, generates a second current reference ΔI_{ess}* so that the supercapacitors voltage does not go below a certain value U_{uc}* in steady state. Ensuring a certain amount of minimum U_{uc} is convenient to keep the power capability without increasing the current over the limits. The resulting current reference I_{ess}** is calculated as the difference between the first two (I_{ess}* minus ΔI_{ess}*). Finally, an overcharge/overdischarge protection block is added at the end of the scheme, which applies some limits to the current reference depending on the state of charge.

6.2 – Laboratory tests and results

In the previous section the main components of the test bench have been described. In addition to them, it is important to underline that also the devices for the electric and thermal measurements have been integrated in the laboratory platform. Moreover, the laboratory is equipped with a refrigeration system as well, that is activated when the temperature of elements as the supercapacitors or the converters, rising during system operation, goes beyond certain limits.

The measures taken with the aforementioned devices are then acquired by the control software, that consists in the control platform dSpace MicroAutoBox II 1401/1503, connected to a personal computer. The control software is responsible for the measurements filtering and postprocessing, and also for the data recording. The computer interface makes it possible to start and stop a test, to regulate and modify the parameters involved, to monitor the operation of the system during the test and to record data and variables in order to be analyzed at a later stage. A screenshot of the mentioned interface is depicted in fig. 6.5.

Figure 6.5 – Screenshot of the control software interface

In this section, five laboratory tests are presented: four with MA and different width of the moving window, and one with the AR prediction. The data of WEC

power are imported as a file .mat, consisting in a matrix of two columns: time and power. The values are taken from the point absorber model used in chapter 4, for a total time of twenty minutes and with a sampling time of 0,1 s. Thus, the wave profile is the same already used in chapters 4 and 5. As already explained, this profile of power in the time domain is used as a reference for the rectifier of the WEC emulator subsystem, and we will refer to this power as P_{ref}, while the measured power effectively provided to the DC-link by the rectifier will be called P_{wec}. If everything works correctly, the curves of P_{ref} and P_{wec} should be very similar, as it will be verified in the analysis of the tests results.

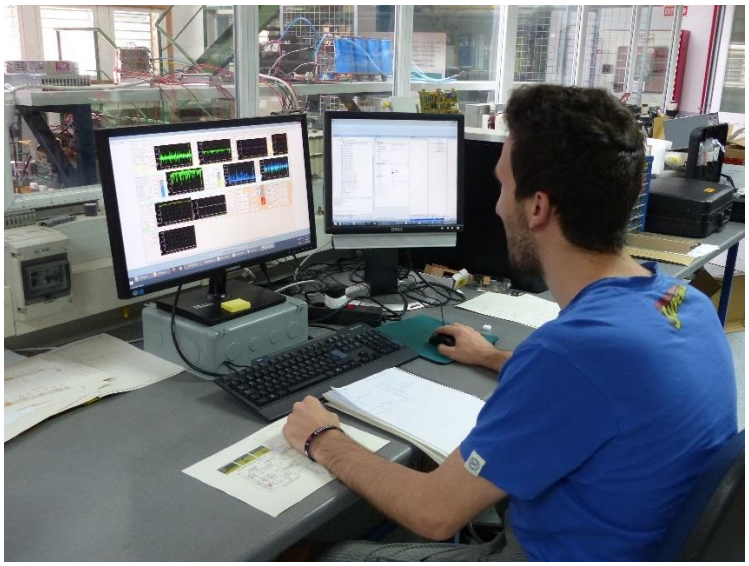

Figure 6.6 – A phase of the laboratory work

6.2.1 – Tests with Moving Average Window

In this case the value of power P_{avg} that is required as a reference for the control scheme of fig. 6.4 is calculated as the mean value of P_{wec} in a moving window of a certain width, as explained in the previous chapters. Four tests are presented here, 900 seconds of duration each, with a moving window of different width, 25, 50, 100 and 150 seconds respectively.

During the tests the control software records all the required data. More specifically, at the end of each test the recorded values of 15 variables are available, listed in table 6.4.

Variable	Description	Unit
Id_{ref}	Current reference in the first converter (WEC emulator subsystem)	A
Id	Real current in the first converter	A
$Id2_{ref}$	Current reference in the second converter (grid connection subsystem)	A
Id2	Real current in the second converter	A
Udc_{ref}	Voltage reference in the DC-link	V
Udc	Real voltage in the DC-link	V
Udc_{filt}	Filtered voltage in the DC-link	V
Pref	WEC power reference	W
Pwec	Effective power provided by the WEC emulator	W
Pavg	Average value of power for the ESS control system	W
Pgrid	Instantaneous power injected to the grid	W
Iuc_{ref}	Current reference in the supercapacitors	A
Iuc	Real current in the supercapacitors	A
Uuc	Voltage in the supercapacitors	V
Puc	Power absorbed or released by the supercapacitors	W

Table 6.4 – Variables recorded by the control software during the tests with MA window

These variables are then analyzed and post-processed with the Matlab code *Postprocesado_MA.m* (appendix B.12). This code generates some graphs to evaluate the behavior of the assessed variables, and also calculates the average power delivered to the grid $P_{grid,avg}$ and the Smooth Index.

As the values of WEC power are too high to operate in this laboratory, they have been reduced by the multiplication by a scale factor (named in this case power gain) of 0,025, in order to not go beyond a few kW as maximum power level in the test bench.

After having verified the correspondence between the reference variables and the measured ones, the results for the first test with a window of 25 seconds are shown in the graphs of figure 6.7.

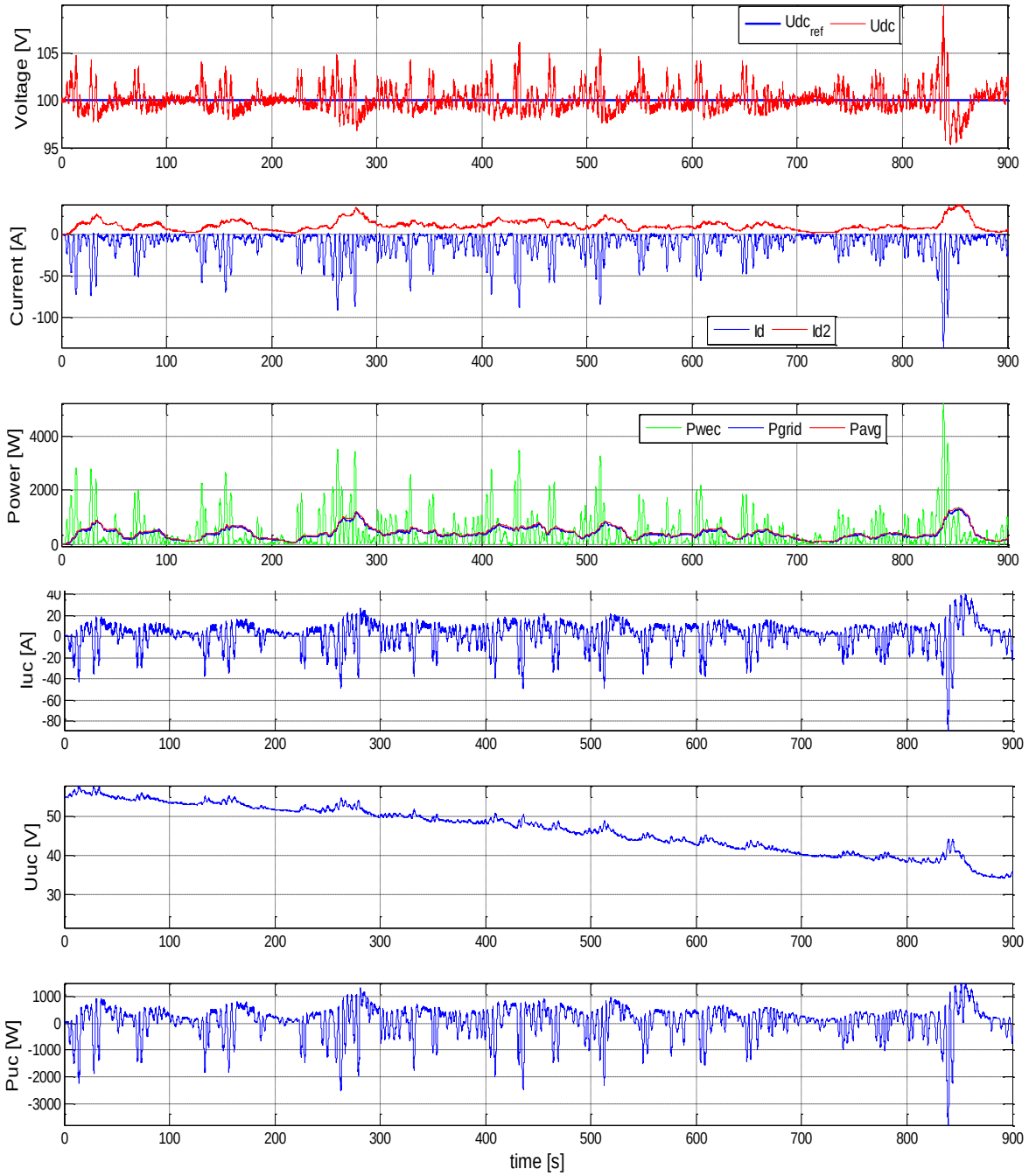

Figure 6.7 – Results of the first test (Moving Average with window of 25 s)

The first graph at the top shows in blue the reference voltage $U_{dc,ref}$ in the DC-link, which is a constant value of 100 V, and in red the measured one U_{dc}. The voltage U_{dc} should be kept constant and equal to the reference by the DC/DC converter, and in fact we can see that, although there are some fluctuations (especially in correspondence with the power peaks), the voltage is kept in a range of a few Volts from the value of 100 V.

In the second graph the currents in the two AC/DC converters are represented. The fact that one of them is positive and the other is negative is because of their opposite direction: from the grid towards the DC-link for the first converter, and from the DC-link back to the grid for the second one.

The third graph shows the oscillating WEC power P_{wec} (in green), the average power in the moving window P_{avg} (in red), and the smoothed power effectively supplied to the grid P_{grid} (in blue). P_{avg} is the reference value for P_{grid}, and it is evident how the two profiles are almost coinciding, with P_{grid} shifted below because of the power losses. We can notice also the very significant difference between the WEC power, which presents very strong oscillations, and the smoothed profile of P_{grid}. The ESS control strategy is responsible for this, as it keeps the power injected to the grid (output power) as constant as possible. As aforementioned, this is done by absorbing power from the DC-link when there is an energy surplus. Reciprocally, energy is supplied to the DC-link when the generated power is below the average.

It is interesting to notice how much the grid converter could be reduced in terms of power considering that the maximum power peaks obtained from the wave converter do not need to be supplied to the grid directly. As we can observe from the third graph of fig. 6.7, the maximum value of power delivered to the grid is less than the half of the maximum power produced by the WEC during the peaks.

The last three graphs show, respectively, the current I_{uc}, the voltage U_{uc} and the power P_{uc} of the supercapacitors. As we can see, P_{uc} can be either positive or negative, depending on whether the supercapacitors are absorbing or releasing energy.

For the other three tests with the MA control only the graphs of power are reported here, as they are the most interesting for the purposes of the tests. In figures 6.8, 6.9 and 6.10 we can find these graphs respectively for the cases of moving window of 50, 100 and 150 seconds.

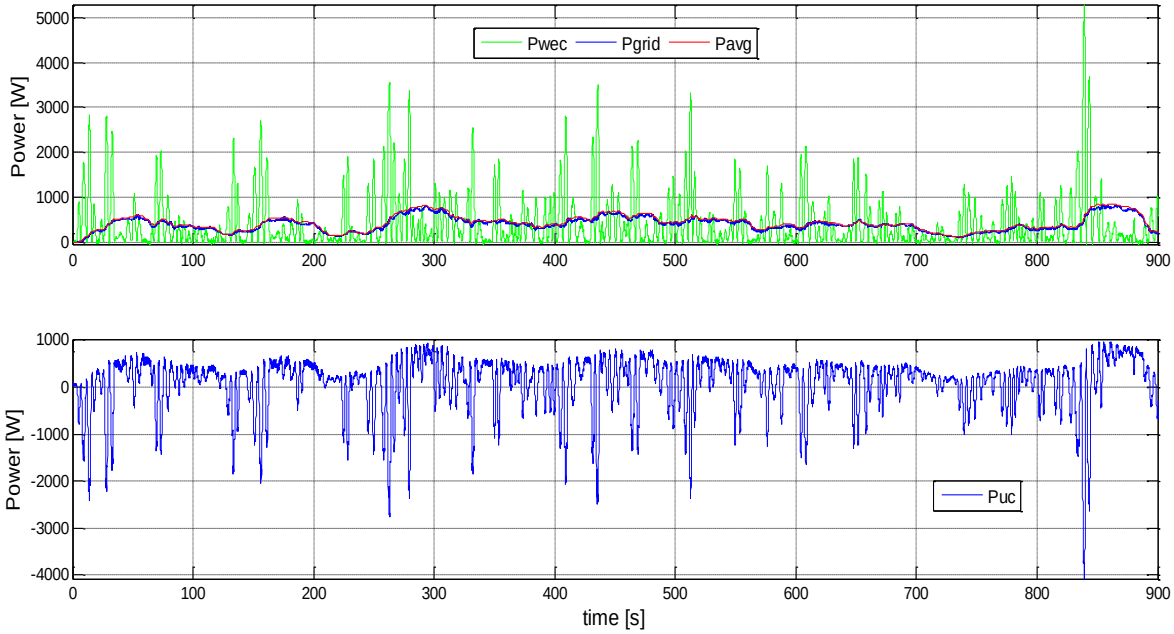

Figure 6.8 – Results of the second test (Moving Average with window of 50 s)

From a visual comparison between the two graphs of fig. 6.8, it is easy to notice that when the WEC produces a lot of power, the power P_{uc} of the supercapacitors assumes negative value. Therefore, a negative sign for the power P_{uc} means that the supercapacitors are charging, absorbing the surplus of energy. On the other side, when P_{uc} is positive, the WEC is producing less power and the supercapacitors are discharging, as they inject energy into the grid providing additional power.

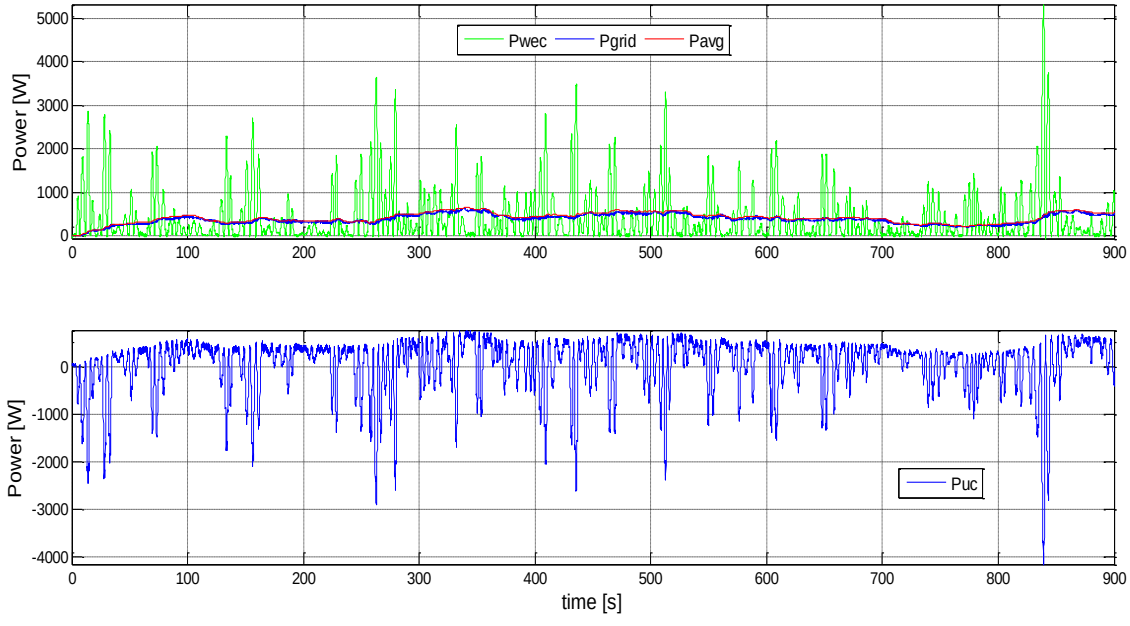

Figure 6.9 – Results of the third test (Moving Average with window of 100 s)

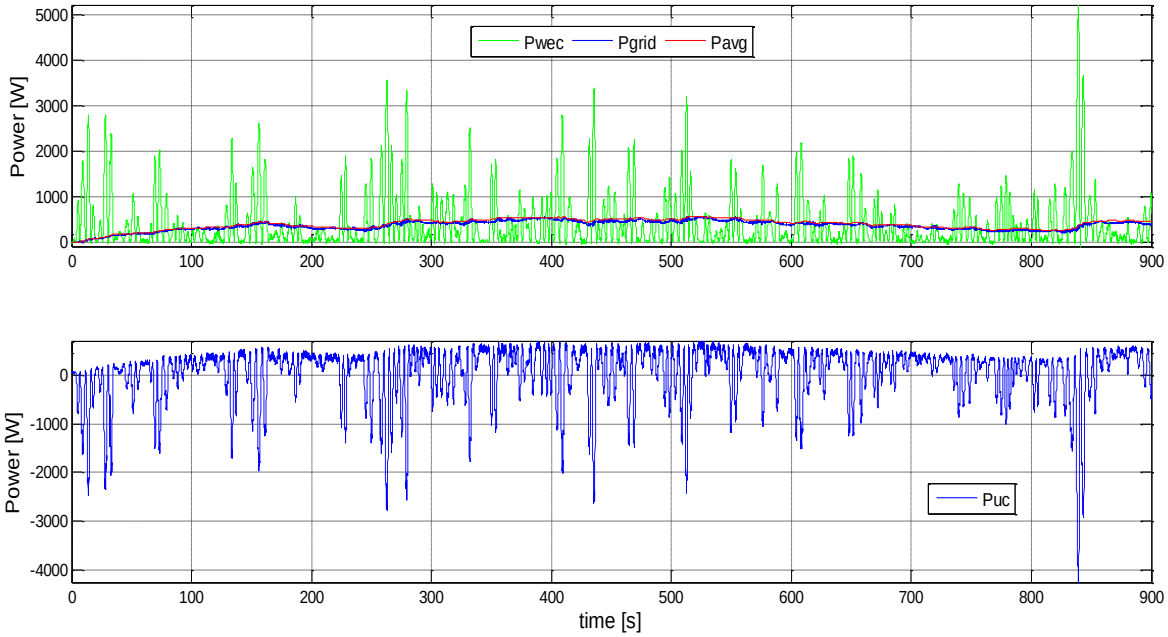

Figure 6.10 – Results of the fourth test (Moving Average with window of 150 s)

Looking at figures 6.7, 6.8, 6.9 and 6.10, and comparing the graphs of power, it is evident that increasing the width of the window the power P_{grid} delivered to the grid becomes more constant, as the profile looks more smoothed. The same fact was observed also in the simulations with the APOGEO model. In table 6.5 some numerical results of the four tests have been collected, including the value of Smooth Index.

Test	Width of the window [s]	Duration [s]	Power gain	Udc_{ref} [V]	$Pgrid_{avg}$ [W]	Smooth Index
1	25	900	0,025	100	407	43,0%
2	50	900	0,025	100	402	58,0%
3	100	900	0,025	100	386	69,6%
4	150	900	0,025	100	372	71,7%

Table 6.5 – Numerical results of the four tests with control based on Moving Average

Coherently with what observed in the graphs, the values of the Smooth Index are increasing with the enlargement of the moving window, meaning that the efficiency of the system in terms of smoothing the output power gets gradually better. The average power supplied to the grid, $P_{grid,avg}$, calculated as the arithmetical mean of the instantaneous power supplied during the test, decreases with larger windows, due to the fact that more power is exchanged with the ESS and consequently the losses are bigger.

The same fact was observed also in the simulations of chapter 5. It is actually interesting to compare the results obtained in those simulations (table 5.2) with the results obtained in the laboratory tests. The values of the smooth index are generally similar, but while in the simulations the maximum value was reached with a window of 104 s (70,8%) and for larger windows it started to decrease, here the maximum value of 71,7% is obtained with the window of 150 s, the largest used. It is important, though, to notice that the power gain used in the simulation (previously named scale factor) was 0,02, while in the tests a value of 0,025 was set.

To have a direct comparison between computer simulations and laboratory tests, in table 6.6 we can find the respective results for the particular case of 50 s window and same evaluation time of 900 seconds and gain factor of 0,025.

Description	Width of the window [s]	Duration [s]	Power gain	Udc_{ref} [V]	$Pgrid_{avg}$ [W]	Smooth Index
Simulation	50	900	0,025	120	439	60,3%
Laboratory	50	900	0,025	100	402	58,0%

Table 6.6 – Comparison between the results obtained in the simulations and in laboratory

The Smooth Index is almost equal, thus there is a good correspondence between simulation and laboratory results. The only appreciable difference regards the average power delivered to the grid, $P_{grid,avg}$: the value calculated in laboratory is lower than in the simulations (402 W instead of 439 W). The reason for this is that the model for the calculation of the losses in the simulations is incomplete.

6.2.2 – Tests with Autoregressive predictive control

The ten seconds-ahead prediction of the WEC power profile, made with an AR model of order 30, is used here to generate a reference value of power for the ESS control, with the same criteria used in chapter 5. Thus, this reference power is calculated as the arithmetical average of the last 30 past values of P_{wec} plus the 10 predicted values. Therefore, the difference is that while here the obtained power, P_{avg}, is calculated as the mean of both past and predicted values, in the case of the moving average (MA) only past values were used.

P_{avg} is used in the same control scheme of fig. 6.4, with the only difference that in this case the SoC compensator (bottom part) has been removed. The approach used for the prediction of power is again the already presented indirect method, based on the multiplication of the predicted PTO force and WEC oscillation velocity.

Only one test is presented in this section, related to the case of AR model of order 30 and 10 steps of prediction. The duration of the test is again 900 seconds. During the test the control software records all the required variables. In addition to the 15 variables contained in table 6.4, now there are five more, listed in table 6.7, for a total of 20 recorded variables.

Variable	**Description**	**Unit**
F	Force applied on the Power Take-Off system	N
v	Oscillation velocity of the WEC	m/s
F_5	5 steps-ahead prediction of the force	N
v_5	5 steps-ahead prediction of the velocity	m/s
P_5	*5-steps-ahead prediction of power*	*W*

Table 6.7 – Additional variables recorded by the control software during the tests with the autoregressive prediction

The recorded data are loaded in the Matlab code *Postprocesado_AR.m* (appendix B.13) in order to be post-processed. The code generates some graphs to evaluate the results and calculates the Smooth Index.

In addition to the ones of fig. 6.7, three more graphs are generated in this case, showing the comparison between the real force, velocity and power and the 5 steps-ahead prediction of the same variables, just to have an idea of how good the prediction is. All the graphs are collected in fig. 6.11. In the last three graphs, related to the prediction, we can see that the predictions of force, velocity and power generally fit quite correctly the real values, but during the biggest peak of power (registered approximately after 840 seconds), the prediction accuracy gets significantly worst. In particular, the prediction of power assumes even negative values in correspondence to this peak.

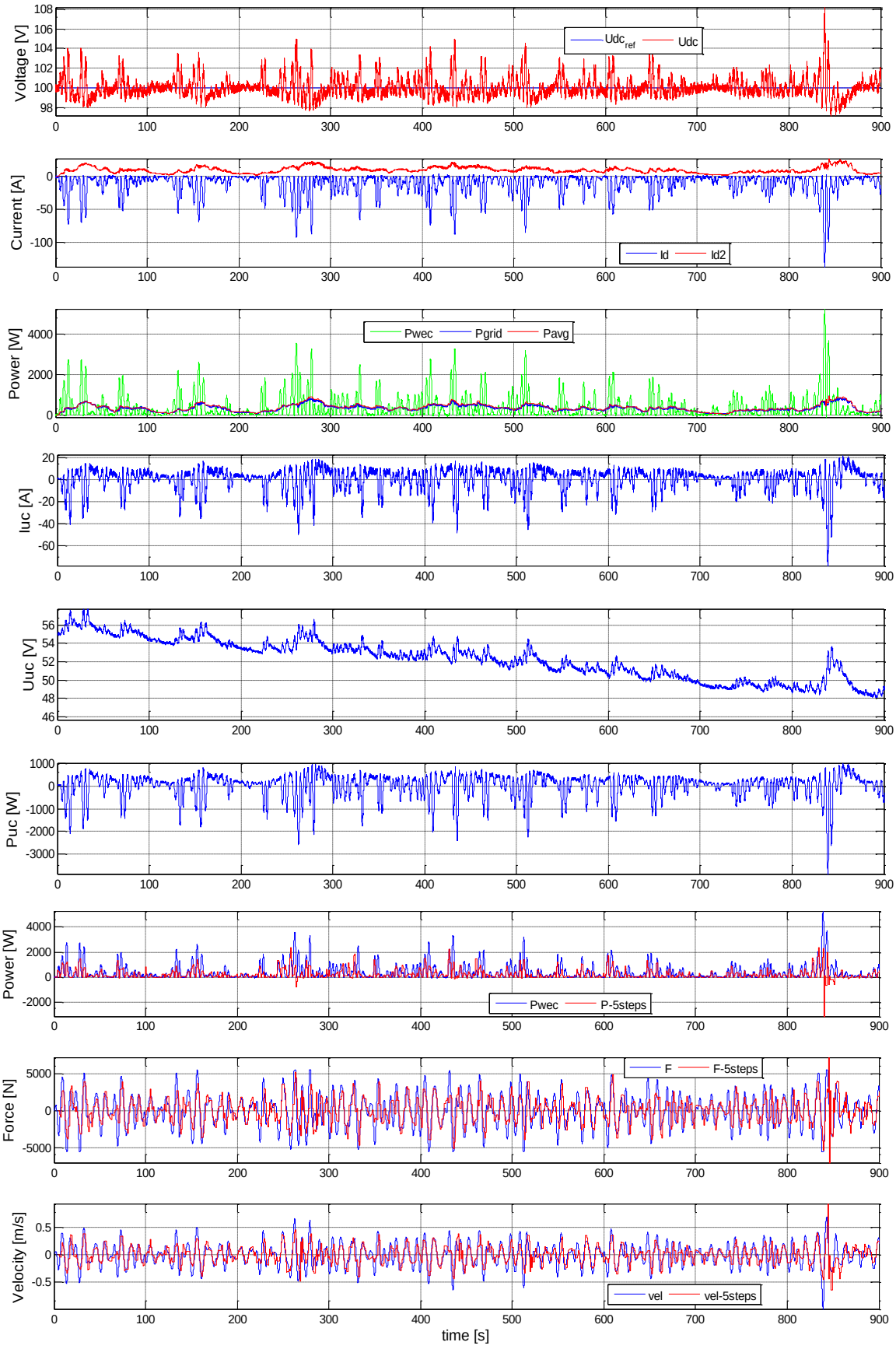

Figure 6.11 – Graphical results of the test with AR prediction

The graph of P_{grid}, the third from the top in fig. 6.11, shows that also with the AR control the output power supplied to the grid is significantly smoothed, as it doesn't present all the wide fluctuations that the WEC power has.
The numerical results of this test, together with the results obtained in the simulation with the same conditions, are collected in table 6.8.

Description	Duration [s]	order of the AR model	steps of prediction	Power gain	Udc_{ref} [V]	$Pgrid_{avg}$ [W]	Smooth Index
Simulation	900	30	10	0,025	120	392	54,1%
Laboratory	900	30	10	0,025	100	352	52,0%

Table 6.8 – Comparison between the results obtained in the simulations and in laboratory for the AR case

The Smooth Index obtained in laboratory is 52%, while in the simulation of the APOGEO model it is 54,1%. The difference is small, also in this case the main discrepancy is in the value of $P_{grid,avg}$, that is lower in the laboratory test due to the aforementioned fact that the model of power losses in the simulations is incomplete.
The results show that the predictive control system for the ESS, based on AR models, satisfies the purpose of smoothing the output power, although it does not improve the control based on the moving window. Only with a window of 25 seconds, indeed, the AR method has a higher value of Smooth Index, while with a larger width the MA control system works better.

7 – CONCLUSIONS AND FURTHER WORKS

One of the first objectives of this thesis was to make a short-term prediction of the power generated by a wave energy converter (WEC), and a lot of effort was put into this. The forecasting method used for this purpose is the one based on autoregressive (AR) models.

The AR prediction method was implemented in the software Matlab and first tested for the prediction of the wave height of a real wave profile, using the observations coming from the Biscay Marine Energy Platform (BIMEP), in the Spanish Cantabrian Sea. The coefficients of the AR model were estimated through the Long Range Predictive Identification (LRPI) optimization process [26]. The prediction of wave elevation offered quite good results in terms of accuracy (measured through the Index of Fitness), at least up to 10 seconds of forecast. It was also shown that low-pass filtering the data can partially improve the accuracy of the prediction, as the low-frequency components of the wave spectra are the most regular and energetic, thus, more predictable as well.

When applied to the prediction of power, however, AR models didn't show equally good results. The reason is that AR models are well suited for profiles like the wave elevation one, made by a combination of sinusoidal waveforms, while the power profile has a very different shape, as it is more similar to a combination of squared sinusoidal waveforms. This is why the WEC output power, instead of being directly predicted by means of an AR model, was derived indirectly from the prediction of the WEC oscillation velocity v and the Power Take-Off (PTO) force F_{pto}. These two variables have a shape more similar to the wave height, so they are more adequate to be predicted through an AR process, and their product gives the value of power absorbed by the WEC. The indirect forecast of power gave significantly better results in the short term when compared to the direct prediction, but it showed also a faster degradation in terms of accuracy.

The next step of the work consisted in the attempt to use the predicted power in the control system of a supercapacitor-based Power Smoothing System (PSS), with the aim of smoothing the WEC output power before supplying it to the grid.

In this way, grid power quality problems such as voltage and frequency fluctuations as well as instability issues are avoided.

More specifically, the indirect prediction of the WEC output power was used to generate an instantaneous reference value P_{avg} of power to be delivered to the grid. This reference value is calculated instant by instant as the arithmetical average of both past and predicted values. When the WEC produces more power than the average, the surplus is used to charge the supercapacitor-based Energy Storage System (ESS). On the other hand, when the WEC produces less power than the average, the required additional power is supplied by the supercapacitors, which are partially discharged as they inject an amount of energy into the grid.

This procedure was at first simulated with the use of the software Simulink, in a model named APOGEO, and then replied in practical laboratory tests. This model represents basically a wave farm that produces oscillating power, an ESS that absorbs and releases energy with the purpose of reducing the power fluctuations, and the electrical grid to which the power is delivered. The APOGEO model was developed by the CIEMAT research group and it was originally working with a Moving Average (MA) criteria for the ESS control system. Here, this control system was replaced with the predictive one, using AR model to predict power and generate the aforementioned reference value P_{avg}.

The results of the simulations showed that the system performs well, in the sense that the proposed PSS based on predictive techniques effectively and significantly reduces the WEC power oscillations, reaching a value of Smooth Index (*SI*) of approximately 60%. On the other side, however, the prediction control system does not improve the already implemented MA-based one, that reached in particular conditions values of *SI* of more than 70%.

Very similar results were obtained in the tests conducted in the CIEMAT laboratory, by means of a test bench that comprises a WEC emulator subsystem, the grid connections and the ESS, consisting in the series of five 16V modules of supercapacitors. Tests were conducted both with the MA and the predictive control logic. Coherently with the simulations results, also in the laboratory tests the proposed predictive control obtained good results in terms of reducing power oscillations, but still worse than the already existent moving average method.

The analysis of the obtained results has led to draw up the following considerations, together with some ideas for further works:

- None of the two methods used for the prediction of power seemed to be optimal for this application. On the one hand, in fact, AR models didn't show a very good accuracy in predicting this kind of profile, especially in comparison with the good results obtained in the prediction of wave height. On the other hand, the indirect method showed better results in the very short term, but a faster decreasing in the accuracy for longer terms prediction. Therefore, other forecasting method could be studied and developed, in order to get a more accurate prediction of the WEC power profile.
- The AR prediction of power was used here to calculate an average value of power to deliver to the grid, and this is the only information that has been used. But the prediction gives much other information apart from an average value of power, it shows the shape and the evolution of the profile of power, the peaks and the troughs. Somehow there could be the possibility to take advantage of this additional information and improve the control system.
- It seems that, for the case of energy storage of big size, even a very accurate short-term prediction of power could not improve the moving average control in the efficiency in smoothing the WEC output power. The point is that the period of the power fluctuations usually ranges from 5 to 25 seconds, thus in a short-term prediction of 15-20 seconds only a few fluctuations are involved. This means that only a couple of cycles of partial charge and discharge of the storage system are predicted, and the amount of energy that needs to be stored or released during this period of time will be a small percentage of the capacity of the ESS. Thus, since enough capacity will be available in wide range storage, no significant benefits in predicting power can be obtained.

  On the other side, the contribution of the power prediction could be very positive when the size of the storage system is limited. In this case, in fact, the amount of energy involved in one period of the predicted WEC power profile becomes clearly more significant in relative terms.

To help understanding the benefits that the prediction could give, in fig. 7.1 it is illustrated a possible application.

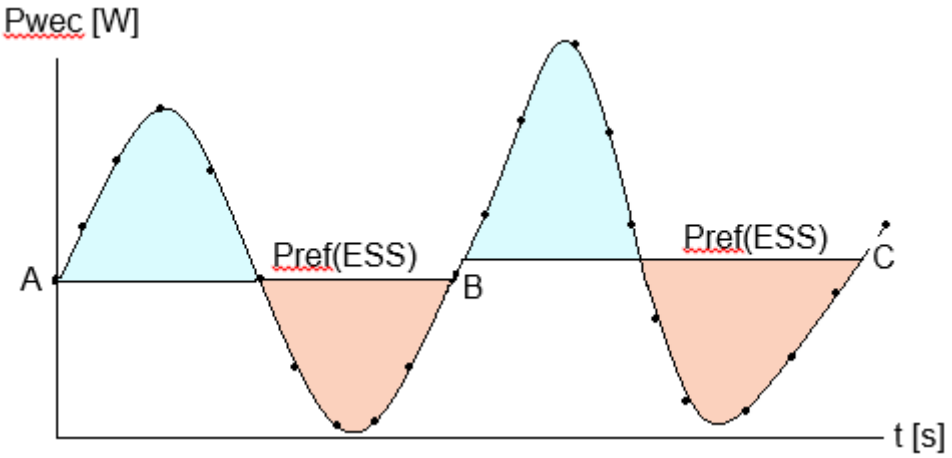

Figure 7.1 – Possible utilization of the power prediction for the dimensioning of the ESS

In fig. 7.1 it is depicted a portion of predicted WEC power profile. Let's imagine that in the instant A we are predicting up to one period (one peak and one trough) of the power profile, finding the curve that goes from A to B. If we calculate the average value of power produced in this period (called Pref in the figure), then we can use this value as the reference power that we want to supply to the grid or to the load. Thus, when the WEC is producing more power than Pref, the surplus will be used to charge the ESS, and when it is producing less power than the reference, the ESS will discharge releasing some additional power. The blue and red areas of the figure represent respectively the amount of energy stored and released in the two stages of charge and discharge of the storage system. It is possible to select the reference value Pref in a way that the two areas are equal, and the process can be repeated now predicting the next cycle of charge and discharge (from B to C), generating another value of Pref. Using the prediction in this way, and assuming that it is accurate enough, it could be possible to dimension or select the storage system according to the amount of energy that needs to be stored only in a few cycles. By doing this, the investment costs for the ESS could be significantly reduced, although the risk of using a smaller storage capacity is not negligible.

According to these considerations, a possible specific application of the short term AR prediction is the case of storage in the DC-link of a back to back power converter, like the one illustrated in fig. 7.2.

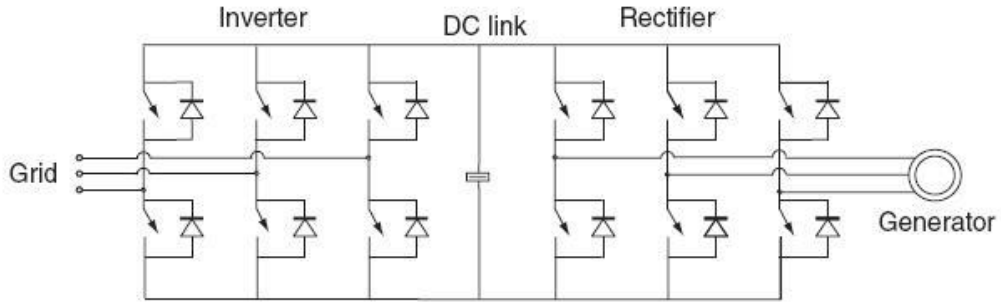

Figure 7.2 – Scheme of a back-to-back power converter

For the small amounts of energy required when the short-term prediction is used as in fig.7.1, it could be possible to store energy directly in the DC-link capacitor of a back-to-back power converter. In this system, the rectifier would convert from AC to DC the power coming from the WEC generator, the DC-link capacitor would act as power smoothing system and the inverter would do the conversion from DC to AC in order to deliver the power to the electric grid. With this application, the significant amount of money required by the installation of an additional storage system could be saved.

APPENDIX A – WAVE DYNAMICS

A.1 – Regular Waves

When the wind blows across a smooth water surface, air particles from the wind grab the water molecules they touch. The friction between air and water stretches the water surface, resulting in small ripples, known as capillary waves. As the wind continues to blow the waves grow bigger. When the waves propagate outside their region of generation, they are called swells, and when the water is deep, swells can travel very large distances with negligible losses of energy.
Although waves can occasionally be formed by other means, such as naval traffic or seismic activity, wind is the main direct source. The indirect source is the sun, that is responsible for creating winds through local heating of the earth surface.
The characteristics of a wind-generated wave depend on:

- the fetch, defined as the distance the wind blows over open water;
- the length of time the wind blows;
- the speed of the wind;
- the water depth.

With the process of conversion of wind energy into waves, below the ocean's water surface there is a concentration of energy flow. Sea waves are, indeed, a form of energy. It is energy, not water, that moves along the ocean's surface, water particles only travel in small circles when a wave passes, as illustrated by fig. A.1.

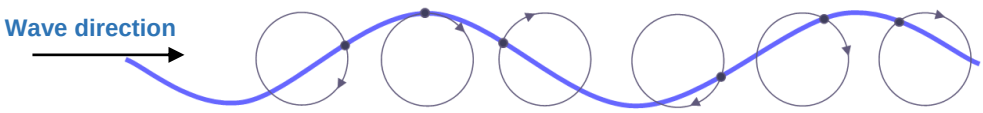

Figure A.1 – Movement of water particles in ocean waves

The dark dots on each circles of fig. A.1 indicate the position of the considered water particle at the snapshot instant. At later instants, as water particles move in the clockwise direction along their circular orbits, wave crests and wave troughs

move from left towards right. The circles representing the orbits of the water particles' movement get smaller as the water depth increase.
In figure A.2 it is shown a simple sinusoidal wave propagating from left to right.

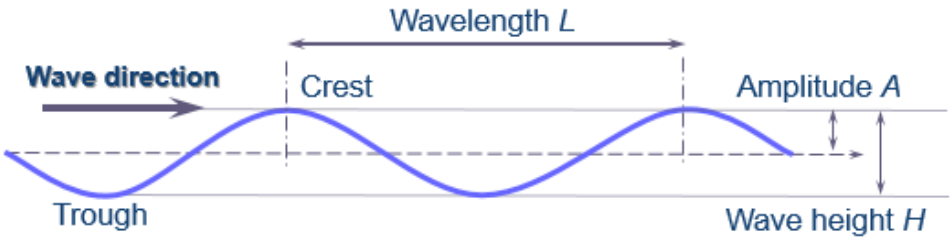

Figure A.2 – Example of simple sinusoidal wave

At a fixed position in space, if we measure the time interval between the arrival of two consecutive crests we get the period *T* of the sinusoidal wave. The frequency *f* is the reciprocal of the period:

$$f = 1/T \quad [Hz] \tag{21}$$

Related to the expression of frequency is also the definition of the angular frequency *ω*:

$$\omega = 2\pi f = 2\pi/T \quad [rad/s] \tag{22}$$

The angular wave number represents the number of wavelengths *L* per unit distance, that is:

$$k = 2\pi/L \quad [m^{-1}] \tag{23}$$

The phase velocity, *c*, is the travel velocity of the individual waves, defined as:

$$c = \frac{\omega}{k} = \frac{L}{T} \quad [m/s] \tag{24}$$

Waves of different wavelengths travel at different phase velocities, and this phenomenon is usually called wave dispersion. Due to dispersion it is not sufficient to characterize the wave velocity by the phase velocity. Therefore, it is necessary to introduce a new concept, called group velocity, that is the velocity

with which the overall shape of the waves' amplitudes (known as the envelope of the wave) propagates through space. The group velocity, c_g, is defined by:

$$c_g = \frac{d\omega}{dk} \quad [m/s] \tag{25}$$

The energy in the waves travel with a velocity equal to c_g. Since the group velocity is proportional to the period, low-frequency waves move faster than high-frequency ones.

As previously seen, the orbit of the movement of water particles depends on the water depth. In deep water the water particles travel in vertical circles, while in shallow water the motion is elliptical.

This motion of water, illustrated in fig. A.3, also happens underwater, but the particles velocity and thereby the circle radius decrease quickly as we go deeper in water.

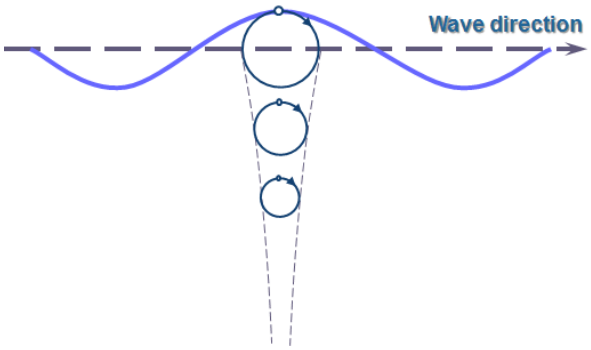

Figure A.3 – Decay of water particles' motion radius with the depth

In deep waters there is almost only oscillating motion, with no mass transport, and most of the motion is closed to the free surface. In these conditions, as already mentioned, waves can travel for long distances with almost no energy losses.

In shallow waters, on the other side, waves have smaller wavelengths and phase velocity, and there is a higher horizontal motion of water. In addition, due to the friction with the sea bed, the rate of energy dissipation is also higher.

For a sinusoidal wave of height H, the average energy E stored on a horizontal square metre of the water surface is:

$$E = E_k + E_p = \frac{\rho g}{8} H^2 \quad [J/m^2] \tag{26}$$

Where ρ is the density of sea water and g the acceleration of gravity. A part of this energy is potential energy (E_p) due to the weight of the water lifted from wave troughs to wave crests. The other part is kinetic energy (E_k), due to the motion of the water.

The energy transport J per meter width of the wave front is:

$$J = c_g E \quad [W/m] \tag{27}$$

A.2 – Irregular waves

The waves on the ocean are more irregular than a sinusoidal wave. Real sea waves contain a mixture of waves with different directions, frequencies and wave heights. Hence, statistical versions of wave parameters are used to describe the waves.

To record the sea wave parameters, appropriate measurement buoys are used in different locations. A typical wave measurement lasts for about twenty minutes, and it is repeated every three hours. The acceleration of the buoy is measured once or twice every second. The data are recorded, and the vertical excursion of the water surface from its mean position can be derived, as well as the direction of wave propagation. An example of measurement buoy is shown in figure A.4.

Figure A.4 – Measurement buoy (photo taken from OCEANOR, Norway)

The main parameter used to describe real ocean waves is the significant wave height (H_s), defined as the average height of the one third highest recorded values of the individual heights H_i, considered from trough to crest. If N is the number of consecutive recorded values of individual wave height, the value of H_s is calculated through the following equation:

$$H_s = \frac{H_{j,1} + H_{j,2} + \ldots + H_{j,N/3}}{N/3} \qquad (\mathbf{28})$$

The index j is used to mark the wave heights contained in the highest one third.
Another significant parameter is the average zero up-cross time T_z, that is the average over a certain time of the individual zero up-cross times T_i, defined as the time interval between two consecutive instants where the wave elevation crosses the zero level in the upward direction. T_z provides a useful measure of the real sea wave period, and its definition is expressed by equation **(29):**

$$T_z = \frac{T_1 + T_2 + \ldots + T_N}{N} \qquad (\mathbf{29})$$

A very important quantity derived from wave measurements is the so-called energy spectrum $S(f)$, which tells us how much energy is carried by the different frequency (f) components in the real sea "mixture" of waves.
With the value of significant wave height (H_s) taken from measurements, the energy spectrum is derived as:

$$\int_0^\infty S(f)df = {H_s}^2/16 \qquad (\mathbf{30})$$

Ant the average energy stored on a horizontal square metre of the water surface is:

$$E = \rho g \int_0^\infty S(f)df \equiv \rho g\, {H_s}^2/16 \qquad (\mathbf{31})$$

Often the buoys also measure the wave direction (angle θ), and then we get the directional wave spectrum $S(f, \theta)$, which gives all the information about wave periods, heights, directions and energy transport.
The energy transport by real sea waves is now calculated by:

$$J = \left(k_J/2\right)T_J {H_s}^2 \qquad (\mathbf{32})$$

The so-called wave energy period T_j, typically 15-25 % longer than T_z, may be derived as well from the wave spectrum $S(f)$, while k_j is a coefficient of proportionality.
The average values of wave energy transport J usually don't vary so much from one year to another, they vary more between seasons. For example, on the northern hemisphere the average values for November and May might differ by a factor of two or more. Generally, the wave energy production is facilitated in winter, because of the stronger winds in comparison with the other seasons. However, as there may be waves (swells) even in the absence of wind, wave energy is more persistent than wind energy.

A.3 – Interaction between waves and a point absorber WEC

The hydrodynamic interaction between wave energy converters (WECs) and ocean waves is a complex high order non-linear process, which might be simplified under particular conditions. Here, the following assumptions will be considered:

- All the external forces acting on the WEC captor are linear;
- The considered WEC is a heaving axisymmetric point absorber oscillating with the frequency of the incident wave;
- The motions of the waves and the device are of small amplitude.

Under these assumptions, the hydrodynamic modeling of the WEC becomes a linear problem, and the equation of motion of the oscillating body of the WEC can be expressed with the use of Newton's second law:

$$F(t) = m \cdot a(t) \qquad (\mathbf{33})$$

Where *m* is the body mass, *a* is the body acceleration, and *F* is the total force acting on the WEC. The total force can be split in two main components: the hydrodynamic forces F_{hd} and the external forces F_{ex}.

$$F(t) = F_{hd}(t) + F_{ex}(t) \quad (34)$$

The hydrodynamic forces, resulting from the interaction between the WEC and the sea, can in turn be decomposed into:

- *Excitation force,* F_{exc}: force induced by the incident waves on the captor.
- *Radiation force,* F_{rd}: force associated with the water moved and the waves generated by the body motions.
- *Hydrostatic force,* F_{hs}: force that acts to restore the initial position of the body.
- *Friction,* F_f: dissipative force due to the viscous effects.

Also the external forces F_{ex}, imposed as constraints to the free floating motion, can be split into different components:

- *Power take-off (PTO) force,* F_{pto}: force induced on the captor by the PTO equipment.
- *Anchoring force,* F_m: force exerted by the mooring system.

The total force is then expressed as:

$$F(t) = F_{exc}(t) + F_{rd}(t) + F_{hs}(t) + F_f(t) + F_{pto}(t) + F_m(t) \quad (35)$$

The average mechanical power absorbed by the WEC during a certain time *T* can be calculated as:

$$\bar{P} = \int_0^T F_{pto}(t)v(t)\ dt \quad (36)$$

where *v* is the oscillation velocity of the WEC body. This equation has been used in this thesis for the indirect prediction of the WEC power.

APPENDIX B - MATLAB CODES

B.1 – AR_example.m

```
%% SCRIPT 1 - AR example: wave with 3 harmonic components
% Michele Pasquotto
% April, 2016

clear all
clc
close all

% Wave
A1=1;   % amplitude [m]
A2=0.5;
A3=0.3;
f1=0.03;  % frequency [Hz]
f2=0.12;
f3=0.015;

t=0:0.01:100;
H=A1*sin(2*pi*f1*t)+A2*sin(2*pi*f2*t)+A3*sin(2*pi*f3*t);
figure('position',[46 363 560 420])
plot(t,H)
hold on, grid on,

t2=1:100;
H2=A1*sin(2*pi*f1*t2)+A2*sin(2*pi*f2*t2)+A3*sin(2*pi*f3*t2);
plot(t2,H2,'.','markersize',8)
hold off

xlabel('time [s]')
ylabel('wave height [m]')
legend('wave','samples')


%% Estimation of coefficients, 1 step prediction (N2=1), Multistart
% Michele Pasquotto

N=100; % number of samples
n=10; % order
npoint=50; % number of starting points
Jlpri= @(a)onepred(a,n,N,H2);


x0=ones(1,n);
options = optimoptions('fminunc','Algorithm','quasi-newton');
problem =
createOptimProblem('fminunc','objective',Jlpri,'x0',x0,'options',optio
ns);
ms = MultiStart;
[a,Jmin,exitflag,output,solutions] = run(ms,problem,npoint)
```

```
% figure;
z=max(size(solutions));
for i=1:z
    plot (solutions(1, i).X0{1, 1}(1),solutions(1, i).X0{1,
1}(2),'bo');
    hold on;
end
grid on;
plot(a(1),a(2),'rx');
title(['order: ',num2str(n),'   start points: ',num2str(npoint),'
Jmin = ',num2str(Jmin)]);
%text(a(1),a(2),['  a1= ',num2str(a(1)),'  a2= ',num2str(a(2))]);
xlabel('a1');
ylabel('a2');


%% 1-step prediction with the parameters estimated

for k=n:N;
    Hp(k+1)=0;
    for q=1:n
        ETA = a(q)*H2(k+1-q);
        Hp(k+1) = Hp(k+1)+ETA;
    end
end

t1=1:101;
figure;
plot(t1,Hp,'r--.')
hold on, grid on,
plot(t,H)
title(['1 STEP PREDICTION OF WAVE HEIGHT','      order:',num2str(n)])
xlabel('time [s]')
ylabel('wave height [m]')
legend('predicted wave','real wave')
```

B.2 – onepred.m

```
% FUNCTION 1 - 1 Step Predictive Identification
%Michele Pasquotto

function f = onepred(a,n,N,H)
f=0;
for k=(n+1):N
    Hp=0; %Wave height predicted
    for i=1:n
        H1=a(i)*H(k-i);
        Hp=Hp+H1;
    end
    r=(H(k)-Hp)^2;
    f=f+r;
end

end
```

B.3 – AR_example_bound.m

```
%% SCRIPT 2 - AR example with bounds
% Michele Pasquotto
% April, 2016

clear all
clc
close all

% Wave
A1=1;
A2=0.5;
A3=0.3;
f1=0.03;
f2=0.12;
f3=0.015;

t=0:0.01:100;
H=A1*sin(2*pi*f1*t)+A2*sin(2*pi*f2*t)+A3*sin(2*pi*f3*t);
%figure('position',[46 363 560 420])
%plot(t,H)
%hold on, grid on,

t2=1:101;
H2=A1*sin(2*pi*f1*t2)+A2*sin(2*pi*f2*t2)+A3*sin(2*pi*f3*t2);
%plot(t2,H2,'.','markersize',8)
%hold off

%% Jlpri, 1 step prediction (N2=1), Multistart
% Michele Pasquotto

N=100; % number of samples
n=10; % order
npoint=50; % number of starting points
Jlpri= @(a)onepred(a,n,N,H2);

x0=ones(1,n);
options = optimoptions('fmincon','Algorithm','interior-point');
l = -100*x0;
u = 100*x0;
problem =
createOptimProblem('fmincon','objective',Jlpri,'x0',x0,'lb',l,'ub',u,'
options',options);
ms = MultiStart('StartPointsToRun','bounds');
[a,Jmin,exitflag,output,solutions] = run(ms,problem,npoint)

z=max(size(solutions));
for i=1:z
```

```
    plot (solutions(1, i).X0{1, 1}(1),solutions(1, i).X0{1,
1}(2),'bo');
    hold on;
end
grid on;
plot(a(1),a(2),'rx');
title(['order: ',num2str(n),' start points: ',num2str(npoint),' Jmin =
',num2str(Jmin)]);
%text(a(1),a(2),['  a1= ',num2str(a(1)),'  a2= ',num2str(a(2))]);
xlabel('a1');
ylabel('a2');
hold on;

%% 1-step prediction with the parameters estimated

for k=n:N;
    Hp(k+1)=0;
    for q=1:n
        ETA = a(q)*H2(k+1-q);
        Hp(k+1) = Hp(k+1)+ETA;
    end
end

figure;
plot(t2,Hp,'r--.')
hold on, grid on,
plot(t,H)
title(['1 STEP PREDICTION OF WAVE HEIGHT','      order:',num2str(n)])
xlabel('time [s]')
ylabel('wave height [m]')
legend('predicted wave','real wave')
```

B.4 – AR_example2.m

```
%% SCRIPT 3 - AR example 2: wave with 9 harmonic components
% Michele Pasquotto
% April, 2016

clear all
clc
%close all

% Wave
A1=0.2;
A2=0.5;
A3=0.3;
A4=0.8;
A5=1;
A6=0.5;
A7=1.3;
A8=0.2;
A9=0.6;
f1=0.05;
f2=0.21;
```

```
f3=0.13;
f4=0.03;
f5=0.15;
f6=0.07;
f7=0.02;
f8=0.3;
f9=0.12;

t=0:0.01:100;
H=A1*sin(2*pi*f1*t)+A2*sin(2*pi*f2*t)+A3*sin(2*pi*f3*t)+A4*sin(2*pi*f4
*t)+A5*sin(2*pi*f5*t)+A6*sin(2*pi*f6*t)+A7*sin(2*pi*f7*t)+A8*sin(2*pi*
f8*t)+A9*sin(2*pi*f9*t);
figure('position',[46 363 560 420])
plot(t,H)
hold on, grid on,

t2=1:100;
H2=A1*sin(2*pi*f1*t2)+A2*sin(2*pi*f2*t2)+A3*sin(2*pi*f3*t2)+A4*sin(2*p
i*f4*t2)+A5*sin(2*pi*f5*t2)+A6*sin(2*pi*f6*t2)+A7*sin(2*pi*f7*t2)+A8*s
in(2*pi*f8*t2)+A9*sin(2*pi*f9*t2);
plot(t2,H2,'.','markersize',8)
hold off

xlabel('time [s]')
ylabel('wave height [m]')
legend('wave','samples')


%% Jlpri, 1 step prediction (N2=1), Multistart
% Michele Pasquotto

N=100; % number of samples
n=10; % order
npoint=50; % number of starting points
Jlpri= @(a)onepred(a,n,N,H2);

x0=ones(1,n);
options = optimoptions('fminunc','Algorithm','quasi-newton');
problem =
createOptimProblem('fminunc','objective',Jlpri,'x0',x0,'options',optio
ns);
ms = MultiStart;
[a,Jmin,exitflag,output,solutions] = run(ms,problem,npoint)

% figure;
z=max(size(solutions));
for i=1:z
    plot (solutions(1, i).X0{1, 1}(1),solutions(1, i).X0{1,
1}(2),'bo');
    hold on;
end
grid on;
plot(a(1),a(2),'rx');
title(['order: ',num2str(n),' start points: ',num2str(npoint),' Jmin =
',num2str(Jmin)]);
text(a(1),a(2),['  a1= ',num2str(a(1)),'  a2= ',num2str(a(2))]);
xlabel('a1');
ylabel('a2');
```

```
%% 1-step prediction with the parameters estimated

for k=n:N;
    Hp(k+1)=0;
    for q=1:n
        ETA = a(q)*H2(k+1-q);
        Hp(k+1) = Hp(k+1)+ETA;
    end
end

t_1=1:101;
figure;
plot(t_1,Hp,'r--.')
hold on, grid on,
plot(t,H)
title(['1 STEP PREDICTION OF WAVE HEIGHT','      order:',num2str(n)])
xlabel('time [s]')
ylabel('wave height [m]')
legend('predicted wave','real wave')
```

B.5 – AR3.m

```
%% SCRIPT 4 - AR3: one-step prediction of a real wave
% Michele Pasquotto
% April, 2016

clear all
clc
%close all

% Wave
load('samples20.mat')
load('wave20.mat')
t=wave.time;
H=wave.signals.values;
t2=samples.time;
H2=samples.signals.values;

figure;
plot(t,H)
hold on, grid on,

plot(t2,H2,'.','markersize',8)
hold off

xlabel('time [s]')
ylabel('wave height [m]')
legend('wave','samples')


%% Jlpri, estimation of parameters (N2=1), Multistart
```

```
% Michele Pasquotto

N=max(size(H2)); % number of samples
n=30; % order
npoint=50; % number of starting points
Jlpri= @(a)onepred(a,n,N,H2);

x0=ones(1,n);
options = optimoptions('fminunc','Algorithm','quasi-
newton','MaxIter',1000,'MaxFunEvals',10000);
problem =
createOptimProblem('fminunc','objective',Jlpri,'x0',x0,'options',optio
ns);
ms = MultiStart;
[a,Jmin,exitflag,output,solutions] = run(ms,problem,npoint)

z=max(size(solutions));
for i=1:z
    plot (solutions(1, i).X0{1, 1}(1),solutions(1, i).X0{1,
1}(2),'bo');
    hold on;
end
grid on;
plot(a(1),a(2),'rx');
title(['order: ',num2str(n),' start points: ',num2str(npoint),' Jmin =
',num2str(Jmin)]);
text(a(1),a(2),['  a1= ',num2str(a(1)),'  a2= ',num2str(a(2))]);
xlabel('a1');
ylabel('a2');


%% 1-step prediction with the parameters estimated

for k=n:N;
    Hp(k+1)=0;
    for q=1:n
        ETA = a(q)*H2(k+1-q);
        Hp(k+1) = Hp(k+1)+ETA;
    end
end

t_1=0:max(size(t2));
figure;
plot(t_1,Hp,'r--.')
hold on, grid on,
plot(t,H)
axis([0 1210 -2 2]);
title(['1 STEP PREDICTION OF WAVE HEIGHT','      order: ',num2str(n)])
xlabel('time [s]')
ylabel('wave height [m]')
legend('wave predicted','real wave')
```

B.6 – AR7.m

```
%% SCRIPT 5 - AR7: Multistep prediction of a real wave
% Michele Pasquotto
% May, 2016

clear all
clc
%close all

% Wave
load('samples20.mat')
load('wave20.mat')
t=wave.time;
H=wave.signals.values;
t2=samples.time;
H2=samples.signals.values;

figure;
plot(t,H)
hold on, grid on,

plot(t2,H2,'.','markersize',8)
hold off

xlabel('time [s]')
ylabel('wave height [m]')
legend('wave','samples')


%% Jlpri, estimation of parameters with regular least squares (N2=1),
Multistart
% Michele Pasquotto

N=max(size(H2)); % number of samples
n=30; % order
npoint=50; % number of starting points
Jlpri= @(a1)onepred(a1,n,N,H2);

x0=ones(1,n);
options = optimoptions('fminunc','Algorithm','quasi-
newton','MaxIter',1000,'MaxFunEvals',10000);
problem =
createOptimProblem('fminunc','objective',Jlpri,'x0',x0,'options',optio
ns);
ms = MultiStart;
[a1,Jmin,exitflag,output,solutions] = run(ms,problem,npoint)


%% Jlpri, estimation of parameters with Long Range Predictive
Identification function (N2=20), Multistart
% Michele Pasquotto

N=max(size(H2)); % number of samples
n=30; % order
N2=20; % maximum prediction horizon
Jlpri= @(a)longpred5(a,n,N,N2,H2);

x0=a1;
```

```
options = optimoptions('fminunc','Algorithm','quasi-
newton','MaxIter',1000,'MaxFunEvals',10000);
problem =
createOptimProblem('fminunc','objective',Jlpri,'x0',x0,'options',optio
ns);
[a,Jmin,exitflag,output] = fminunc(problem)


%% l-step prediction with the parameters estimated

l=15; %range of prediction

% (k+l|k) prediction

for k=n:N;
    for j=1:l
        for q=1:n
            if (k+j-q)<=k
                ETA(q) = a(q)*H2(k+j-q);
            elseif (k+j-q)>k
                   ETA(q) = a(q)*Hp(k+j-q);
            end
        end
        Hp(k+j)=sum(ETA);
    end
    Hstep(k+l)=Hp(k+l);
end

M=max(size(Hstep));


% Index of  fitness

load('samplestot')
H_kl=samplestot.signals.values((n+l):M);
Z=max(size(H_kl));
Htrasp=Hstep';
Hpred=Htrasp((n+l):M);
H_k=samplestot.signals.values(n:(M-l));
FITN = fitness(Z,H_kl,Hpred,H_k)

%Graph

load('nu_time')
treal=nu_time(:,1);
Hreal=nu_time(:,2);
t_1=0:(M-1);
figure;
plot(t_1,Hstep,'r--.','markersize',10)
hold on, grid on
plot(treal(1:((M-1)*10)),Hreal(1:((M-1)*10)))
title(['order: ',num2str(n),'   prediction steps: ',num2str(l),'
FITNESS: ',num2str(FITN),'%']);
xlabel('t[s]');
ylabel('H[m]');
axis([0 1220 -2 2]);
```

B.7 – longpred5.m

```
%FUNCTION 2 - Long Range Predictive Identification
%Michele Pasquotto

function f = longpred5(a,n,N,N2,H)
f=0;
for k=n:(N-N2)
    r=0;
    for j=1:N2
        for i=1:n
            if (k+j-i)<=k
                ETA(i) = a(i)*H(k+j-i);
            elseif (k+j-i)>k
                   ETA(i) = a(i)*Hp(k+j-i);
            end
        end
        Hp(k+j)=sum(ETA);
        J=(H(k+j)-Hp(k+j))^2;
        r=r+J;
    end
    f=f+r;
end

end
```

B.8 – fitness.m

```
%FUNCTION 3 - Index of fitness
%Michele Pasquotto

function f = fitness(Z,Hkl,Hpred,Hk)
NUM=0;
DEN=0;
for k=1:Z
    NUM=NUM+(Hkl(k)-Hpred(k))^2;
    DEN=DEN+(Hk(k))^2;
end
f=(1-(sqrt(NUM)/sqrt(DEN)))*100;
end
```

B.9 – ARfilt.m

```
%% SCRIPT 6 - AR example with filter
% Michele Pasquotto
% June, 2016
```

```
clear all
clc
%close all

% Real wave
load('wave20.mat')
t_int=wave.time;
H_int=wave.signals.values;

% Wave filtered
load('samples20filt1.mat')
load('wave20filt1.mat')
t=wave20filt1.time;
H=wave20filt1.signals.values;
t2=samples20filt1.time;
H2=samples20filt1.signals.values;

figure;
plot(t_int,H_int)
hold on, grid on,
plot(t,H)
hold on, grid on,
plot(t2,H2,'r.','markersize',8)
hold off
xlabel('time [s]')
ylabel('wave height [m]')
legend('real wave','filtered wave','samples')
title('cut-off frequency: 1 rad/s')


%% Jlpri, estimation of parameters with regular least squares (N2=1),
Multistart
% Michele Pasquotto

N=max(size(H2)); % number of samples
n=30; % order
npoint=50; % number of starting points
Jlpri= @(a1)onepred(a1,n,N,H2);

x0=ones(1,n);
options = optimoptions('fminunc','Algorithm','quasi-
newton','MaxIter',1000,'MaxFunEvals',10000);
problem =
createOptimProblem('fminunc','objective',Jlpri,'x0',x0,'options',optio
ns);
ms = MultiStart;
[a1,Jmin,exitflag,output,solutions] = run(ms,problem,npoint)


%% Jlpri, estimation of parameters with Long Range Predictive
Identification function (N2=20), Multistart
% Michele Pasquotto

N=max(size(H2)); % number of samples
n=30; % order
N2=20; % maximum prediction horizon
Jlpri= @(a)longpred5(a,n,N,N2,H2);
```

```
x0=a1;
options = optimoptions('fminunc','Algorithm','quasi-
newton','MaxIter',1000,'MaxFunEvals',10000);
problem =
createOptimProblem('fminunc','objective',Jlpri,'x0',x0,'options',optio
ns);
[a,Jmin,exitflag,output] = fminunc(problem)


%% l-step prediction with the parameters estimated

l=15; %range of prediction

% (k+l|k) prediction

for k=n:N;
    for j=1:l
        for q=1:n
            if (k+j-q)<=k
                ETA(q) = a(q)*H2(k+j-q);
            elseif (k+j-q)>k
                    ETA(q) = a(q)*Hp(k+j-q);
            end
        end
        Hp(k+j)=sum(ETA);
    end
    Hstep(k+l)=Hp(k+l);
end

M=max(size(Hstep));

% Index of  fitness

load('samplestotfilt1.mat')
H_kl=samplestotfilt1.signals.values((n+l):M);
Z=max(size(H_kl));
Htrasp=Hstep';
Hpred=Htrasp((n+l):M);
H_k=samplestotfilt1.signals.values(n:(M-l));
FITN = fitness(Z,H_kl,Hpred,H_k)

%Graph

load('wavetotfilt1.mat')
treal=wavetotfilt1.time;
Hreal=wavetotfilt1.signals.values;
t_1=0:(M-1);
figure;
plot(t_1,Hstep,'r--.','markersize',10)
hold on, grid on
plot(treal(1:((M-1)*10)),Hreal(1:((M-1)*10)))
title(['order: ',num2str(n),'   prediction steps: ',num2str(l),'
FITNESS: ',num2str(FITN),'%']);
xlabel('t[s]');
ylabel('H[m]');
axis([0 1220 -2 2]);
```

B.10 – ARpower.m

```
%% SCRIPT 7- AR prediction of power
% Michele Pasquotto
% June, 2016

clear all
clc
%close all

Ts= 1; %Sampling Time

% Wave
load('Pwec20.mat')
load('Pwec20_s.mat')
t=Pwec20.time;
P=Pwec20.signals.values;
t2=Pwec20_s.time;
P2=Pwec20_s.signals.values;

figure;
plot(t,P)
hold on, grid on,

% plot(t2,P2,'.','markersize',8)
% hold off

xlabel('time [s]')
ylabel('WEC power [W]')
legend('power profile')


%% Jlpri, estimation of parameters with regular least squares (N2=1),
Multistart % Michele Pasquotto

N=max(size(P2)); % number of samples
n=30; % order
npoint=50; % number of starting points
Jlpri= @(a1)onepred(a1,n,N,P2);


x0=ones(1,n);
options = optimoptions('fminunc','Algorithm','quasi-
newton','MaxIter',1000,'MaxFunEvals',10000);
problem =
createOptimProblem('fminunc','objective',Jlpri,'x0',x0,'options',optio
ns);
ms = MultiStart;
[a1,Jmin,exitflag,output,solutions] = run(ms,problem,npoint)


%% Jlpri, estimation of parameters with Long Range Predictive
Identification function (N2=20), Multistart
% Michele Pasquotto
```

```
N=max(size(P2)); % number of samples
n=30; % order
N2=20; % maximum prediction horizon
Jlpri= @(a)longpred5(a,n,N,N2,P2);

x0=a1;
options = optimoptions('fminunc','Algorithm','quasi-
newton','MaxIter',1000,'MaxFunEvals',10000);
problem =
createOptimProblem('fminunc','objective',Jlpri,'x0',x0,'options',optio
ns);
[a,Jmin,exitflag,output] = fminunc(problem)


%% l-step prediction with the parameters estimated

l=10; %range of prediction

% (k+l|k) prediction

for k=n:N;
    for j=1:l
        for q=1:n
            if (k+j-q)<=k
                ETA(q) = a1(q)*P2(k+j-q);
            elseif (k+j-q)>k
                   ETA(q) = a1(q)*Pp(k+j-q);
            end
        end
        Pp(k+j)=sum(ETA);
    end
    Pstep(k+l)=Pp(k+l);
end

M=max(size(Pstep));

% Index of  fitness

load('Pwec_s.mat')
P_kl=Pwec_s.signals.values((n+l):M);
Z=max(size(P_kl));
Ptrasp=Pstep';
Ppred=Ptrasp((n+l):M);
P_k=Pwec_s.signals.values(n:(M-l));
FITN = fitness(Z,P_kl,Ppred,P_k)

%Graph

load('Pwec.mat')
treal=Pwec.time;
Preal=Pwec.signals.values;
t_1=0:Ts:(Ts*(M-1));
figure;
plot(t_1,Pstep,'r--.','markersize',10)
hold on, grid on
plot(treal(1:((M-1)*(Ts/0.1))),Preal(1:((M-1)*(Ts/0.1))))
```

```
title(['order: ',num2str(n),'   prediction steps: ',num2str(l),'
FITNESS: ',num2str(FITN),'%']);
xlabel('t[s]');
ylabel('P[W]');
```

B.11 – Datos_VM.m

```
%% Data for APOGEO model

%% General
fixed=500e-6;
tend=600;
decimation=5; % of the block to workspace

%% Moving Average window
ancho=24;
downsampling=10;
n=ancho/fixed/downsampling;

%% AR model

Ts=1; %sampling time
order=30; %order
horizon=10; %prediction horizon
load('avel1.mat')
load('afor1.mat')

%% Wave farm

% Regular wave
a1=10000;
f1=1/10;
t=0:0.1:ancho;
p=a1*sin(2*pi*f1*t);
% p=p+a2*sin(2*pi*f2*t);
% p=p+a3*sin(2*pi*f3*t);
p=abs(p);
% plot(t,p)

% Irregular Wave
MB=0.02;

%% DC-link
Udc0=120;   % tensión inicial y nominal bus DC [V]
Cdc=12e-3;

%% Supercapacitors
s=1;
p=1;
Uuc=80;     % V totales
Cuc=90;     % F totales
Ruc=18e-3;  % ohm totales
Uuc0=60;    % V inicial
Ilim=200;
```

```
%% Converters
fpwm=5000;
slave= 4e-6*5000/fpwm;
muestras=floor((1/fpwm)/slave/2);

% Interleaving
ram_int = 2;

%%%%%% Pérdidas %%%%%%
p    = 1;    % perdidas ON u OFF
pe   = 1;    % perdidas Eon, Eoff y Err ON u OFF

% Bobinas
Rind = 1e-2*p;% [ohm] a 25°C
Lind = 2e-3;  % [H] a 25°C

% Condiciones nominales para el resto de datos
Ic_nom  = 200;     % [A]
Vcc_nom = 600;     % [V]

% IGBT
Eon  = 21e-3*p*pe; % [J] a 25°C
Eoff = 27e-3*p*pe; % [J] a 25°C
rce  = 5.00e-3*p;  % [ohm] a 25°C
Vce0 = 0.80*p;     % [V] a 25°C
Rsnubber = 1e5;
% tf = [107e-9 2*107e-9];

% Diodo
Err  = 13e-3*p*pe; % [J] a 25°C
rf   = rce;
Vf0  = 1.30*p;     % [V] a 25°C

% Valores medios
Von0 = (Vce0+Vf0)/2;
ron  = (rce+rf)/2;
```

B.12 – Postprocesado_MA.m

```
%% Postprocessing of the results for the laboratory tests with Moving
Average

close all
clear all
clc

figure1 = figure('position',[30 20 1391 800]);
figure2 = figure('position',[30 20 1391 800]);
load('20160901_002.mat')
time=rec.X.Data;
t=time+0.002;
```

```
Id_ref=rec.Y(1).Data;
Id=rec.Y(2).Data;
Pref=rec.Y(3).Data;
Id2_ref=rec.Y(5).Data;
Id2=rec.Y(6).Data;
F=rec.Y(8).Data;
vel=rec.Y(9).Data;
F_5=rec.Y(10).Data;
P_5=rec.Y(11).Data;
vel_5=rec.Y(12).Data;
Pavg=rec.Y(13).Data;
Iuc_ref=rec.Y(14).Data;
Udc_ref=rec.Y(15).Data;
Pwec=rec.Y(16).Data;
Pgrid=rec.Y(17).Data;
Iuc=rec.Y(18).Data;
Puc=rec.Y(19).Data;
Uuc=rec.Y(20).Data;
Udc=rec.Y(22).Data;
Udc_filt=rec.Y(23).Data;

dev_Pgrid;

figure(figure1);

subplot(4,1,1)
plot(t,Udc_ref,t,Udc,t,Udc_filt)
axis ([0 900 -inf inf])
ylabel ('Voltage [V]')
legend('Udc_r_e_f','Udc','Udc_f_i_l_t','Location','eastoutside')
grid on,

subplot(4,1,2)
plot(t,Id_ref,t,Id,t,Id2_ref,t,Id2)
axis ([0 900 -inf inf])
ylabel ('Current [A]')
legend('Id_r_e_f','Id','Id2_r_e_f','Id2','Location','eastoutside')
grid on,

subplot(4,1,3)
plot(t,Pwec,t,Pgrid,t,Pavg)
axis ([0 900 -inf inf])
ylabel ('Power [W]')
xlabel('time [s]')
legend('Pwec','Pgrid','Pavg','Location','eastoutside')
grid on,

subplot(4,1,4)
plot(t,Pwec,t,-Pref)
axis ([0 900 -inf inf])
ylabel ('Power [W]')
legend('Pwec','Pref','Location','eastoutside')
grid on,

figure(figure2);

subplot(3,1,1)
plot(t,Iuc_ref,t,Iuc)
```

```
axis ([0 900 -inf inf])
ylabel ('Current [A]')
legend('Iuc_r_e_f','Iuc','Location','eastoutside')
grid on,

subplot(3,1,2)
plot(t,Uuc)
axis ([0 900 -inf inf])
ylabel ('Voltage [V]')
legend('Uuc','Location','eastoutside')
grid on,

subplot(3,1,3)
plot(t,Puc)
axis ([0 900 -inf inf])
ylabel ('Power [W]')
legend('Puc','Location','eastoutside')
grid on,
```

B.13 – Postprocesado_AR.m

```
%% Postprocessing of the results for the laboratory test with AR
prediction

close all
clear all
clc

figure1 = figure('position',[30 20 1391 800]);
figure2 = figure('position',[30 20 1391 800]);
figure3 = figure('position',[30 20 1391 800]);

load('20160914_pred_001.mat')
time=pred_001.X.Data;
t=time+0.002;
t5=t+5;

Id_ref=pred_001.Y(1).Data;
Id=pred_001.Y(2).Data;
Pref=pred_001.Y(3).Data;
x3=pred_001.Y(4).Data;
Id2_ref=pred_001.Y(5).Data;
Id2=pred_001.Y(6).Data;
x2=pred_001.Y(7).Data;
F=pred_001.Y(8).Data;
vel=pred_001.Y(9).Data;
F_5=pred_001.Y(10).Data;
P_5=pred_001.Y(11).Data;
vel_5=pred_001.Y(12).Data;
Pavg=pred_001.Y(13).Data;
Iuc_ref=pred_001.Y(14).Data;
Udc_ref=pred_001.Y(15).Data;
Pwec=pred_001.Y(16).Data;
Pgrid=pred_001.Y(17).Data;
```

```
Iuc=pred_001.Y(18).Data;
Puc=pred_001.Y(19).Data;
Uuc=pred_001.Y(20).Data;
x1=pred_001.Y(21).Data;
Udc=pred_001.Y(22).Data;
Udc_filt=pred_001.Y(23).Data;

dev_Pgrid;

figure(figure1);

subplot(3,1,1)
plot(t,Udc_ref,t,Udc,t,Udc_filt)
axis ([0 900 -inf inf])
ylabel ('Voltage [V]')
legend('Udc_r_e_f','Udc','Udc_f_i_l_t','Location','eastoutside')
grid on,

subplot(3,1,2)
plot(t,Id_ref,t,Id,t,Id2_ref,t,Id2)
axis ([0 900 -inf inf])
ylabel ('Current [A]')
legend('Id_r_e_f','Id','Id2_r_e_f','Id2','Location','eastoutside')
grid on,

subplot(3,1,3)
plot(t,Pwec,t,Pgrid,t,Pavg)
axis ([0 900 -inf inf])
ylabel ('Power [W]')
xlabel('time [s]')
legend('Pwec','Pgrid','Pavg','Location','eastoutside')
grid on,


figure(figure2);

subplot(3,1,1)
plot(t,Iuc_ref,t,Iuc)
axis ([0 900 -inf inf])
ylabel ('Current [A]')
legend('Iuc_r_e_f','Iuc','Location','eastoutside')
grid on,

subplot(3,1,2)
plot(t,Uuc)
axis ([0 900 -inf inf])
ylabel ('Voltage [V]')
legend('Uuc','Location','eastoutside')
grid on,

subplot(3,1,3)
plot(t,Puc)
axis ([0 900 -inf inf])
ylabel ('Power [W]')
legend('Puc','Location','eastoutside')
grid on,
```

```
figure(figure3);

subplot(3,1,1)
plot(t,Pwec,t,-Pref,t,P_5)
axis ([0 900 -inf inf])
ylabel ('Power [W]')
legend('Pwec','Pref','P-5steps','Location','eastoutside')
grid on,

subplot(3,1,2)
plot(t,F,t5,F_5)
axis ([0 900 -inf inf])
ylabel ('Force [N]')
legend('F','F-5steps','Location','eastoutside')
grid on,

subplot(3,1,3)
plot(t,vel,t5,vel_5)
axis ([0 900 -inf inf])
ylabel ('Velocity [m/s]')
legend('vel','vel-5steps','Location','eastoutside')
grid on,
```

REFERENCES

[1] Ocean Energy Forum, “Draft Ocean Energy Strategic Roadmap”, 2015

[2] K.Burman, A. Walker, “Ocean Energy Technology Overview”, *Prepared for the U.S. Department of Energy - Office of Energy Efficiency and Renewable Energy - Federal Energy Management Program*, July 2009

[3] International Energy Agency, “Implementing Agreement on Ocean Energy Systems”, *IEA-OES Annual Report,* 2007

[4] “Chapter 4 – Wave”, *AquaRET Text Book*, www.aquaret.com

[5] B. Czech, P. Bauer, “Wave Energy Converter Concepts, Design Challenges and Classification’’ *IEEE Industrial Electronics Magazine,* June 2012.

[6] Clément et al., "Wave energy in Europe: current status and perspectives", *Renewable and Sustainable Energy Reviews*, 2002

[7] B. Drew, A. R. Plummer, M. N. Sahinkaya, “A review of wave energy converter technology”, *Department of Mechanical Engineering, University of Bath (UK),* 2009

[8] IRENA, “Wave Energy Technology Brief”, June 2014

[9] R. Henderson, “Design, simulation, and testing of a novel hydraulic power take-off system for the Pelamis wave energy converter”, *Renewable Energy*, 2006, pp 271–283.

[10] R. Pelc, R.M. Fujita, **“**Renewable energy from the ocean” *Marine Policy 26*, 2002, 471–479.

[11] T.W. Thorpe, “A review of wave energy”, *ETSU Report Number R-72*, 1992.

[12] M. Leijon, O. Danielsson, M. Eriksson, K. Thorburn, H. Bernhoff, J. Isberg, J. Sundberg, I. Ivanova, E. Sjöstedt, O. Ågren, K. E. Karlsson, A. Wolfbrandt, “An electrical approach to wave energy conversion”, *Renewable Energy 31*, 2006, pp 1309–1319.

[13] J. Falnes, “Ocean Waves and Oscillating Systems: Linear Interactions Including Wave-Energy Extraction”, 1st ed., *Cambridge University Press*, 2002.

[14] P. Moreno-Torres, M. Blanco, G. Navarro, M. Lafoz, “Power Smoothing System for Wave Energy Converters by means of a Supercapacitor-based Energy Storage System”, *17th European Conference on Power Electronics and Applications*, 2015.

[15] IEEE, “IEEE guide for planning DC links terminating at AC locations having low short-circuit capacities”, *IEEE Std* 1204-1997; 1997.

[16] A. Etxegarai, P. Eguia, E. Torres, A. Iturregi, V. Valverde, “Review of grid connection requirements for generation assets in weak power grids”, *Renewable and Sustainable Energy Reviews 41*, 2015, pp 1501-1514.

[17] R.D. Jaramillo, A. Garcés, “Wave Energy: Modeling and Analysis of Power Grid Integration”, *IEEE Latin America Transactions Vol.13 No.12*, 2015

[18] A. Blavette, D.L. O’Sullivan, A.W. Lewis, M. Egan, “Impact of a wave farm on its local grid: Voltage limits, flicker level and power fluctuations”, *OCEANS 2012 21-24*, 2012, pp 1-9.

[19] M. Lafoz, M. Blanco, D. Ramirez, “Grid connection for wave power Farms”, *Proc. of Power Electronics and Applications (EPE 2011)*, 2011, pp. 1–10.

[20] F. Fusco, “Short-term wave forecasting as a univariate time series problem”, *Research Report for the Department of Electronic Engineering at NUI Maynooth (Ireland)*, 2009.

[21] F. Fusco, J. Ringwood, “A study on short-term sea profile prediction for wave energy applications”, *Proc. of the 8th European Wave and Tidal Energy Conference (EWTEC)*, pp. 756–765, Uppsala, Sweden, 2009.

[22] F. Fusco, J. Ringwood, “Short-Term Wave Forecasting for Real-Time Control of Wave Energy Converters”, *IEEE Transactions on Sustainable Energy*, 2010.

[23] F. Fusco, J. Ringwood, “Short-Term Wave Forecasting with AR models in Real-Time Optimal Control of Wave Energy Converters”, *Department of Electronic Engineering, NUI Maynooth (Ireland)*, 2010.

[24] C. Chatfield, “Time Series Forecasting”, *Chapman & Hall*, 2000.

[25] L. Piroddi, W. Spinelli, “Long-range nonlinear prediction: A case study”, *Proceedings of the 42nd IEEE Conference on Decision and Control, Maui, Hawaii USA*, pp. 3984-3989, 2003.

[26] D.S. Shook, C. Mohtadi, S.L. Shah, “Identification for long-range predictive control”, *IEEE Proceedings D (Control Theory and Applications)*, vol.138, no.1, pp. 75-84, 1991.

[27] H. Akaike, “A new look at the statistical model identification”, *IEEE Transactions on Automatic Control*, vol.19, pp. 716-723, 1974.

[28] G. Schwarz, “Estimating the dimension of a model”, *The Annals of Statistics*, vol.6, no.2, pp. 461-464, 1978.

[29] BIMEP website, http://bimep.com/

[30] www .puertos.es/es-es/oceanografia/PAGINAS/portus.aspx

[31] J. Falnes, A. Kurniawan, “Fundamental formulae for wave-energy conversion”, *Royal Society Open Science*, vol.2, 2015.

Ringraziamenti

Questa tesi segna per me la fine di un percorso di studio ma anche di un importante capitolo della mia vita. Un percorso bellissimo, costellato di persone, luoghi, momenti, ricordi (ed esami, chiaramente) che porterò sempre con me, che mi hanno fatto crescere e diventare la persona che sono.
Se sono giunto fin qui, certamente non è solo per merito mio. Le prime persone che devo ringraziare non possono che essere i miei genitori, che mi hanno sempre sostenuto sia affettivamente che economicamente, ed hanno sempre mantenuto totale fiducia nei miei confronti, anche nei momenti in cui ero io per primo a dubitare di me stesso.
Desidero poi ringraziare nuovamente la professoressa Stoppato, grazie alla quale si è creata l'opportunità di andare a Madrid, e che mi ha seguito pazientemente e con grande disponibilità durante la stesura della tesi.
Un grazie anche a tutti i familiari, vicini e lontani, e agli amici di vecchia data.
Un grazie veramente speciale infine va a tutti i miei compagni di avventura di questi anni a Padova. In particolare voglio spendere due parole per i vari coinquilini con cui ho convissuto nelle mie tre case padovane, sono tanti e non posso citarli tutti, ma ognuno di loro mi ha dato moltissimo, e se sono stato così bene a Padova principalmente lo devo a loro.

Michele